Probabilistic Tsunami Inundation Assessment for the Western Bay of Plenty District

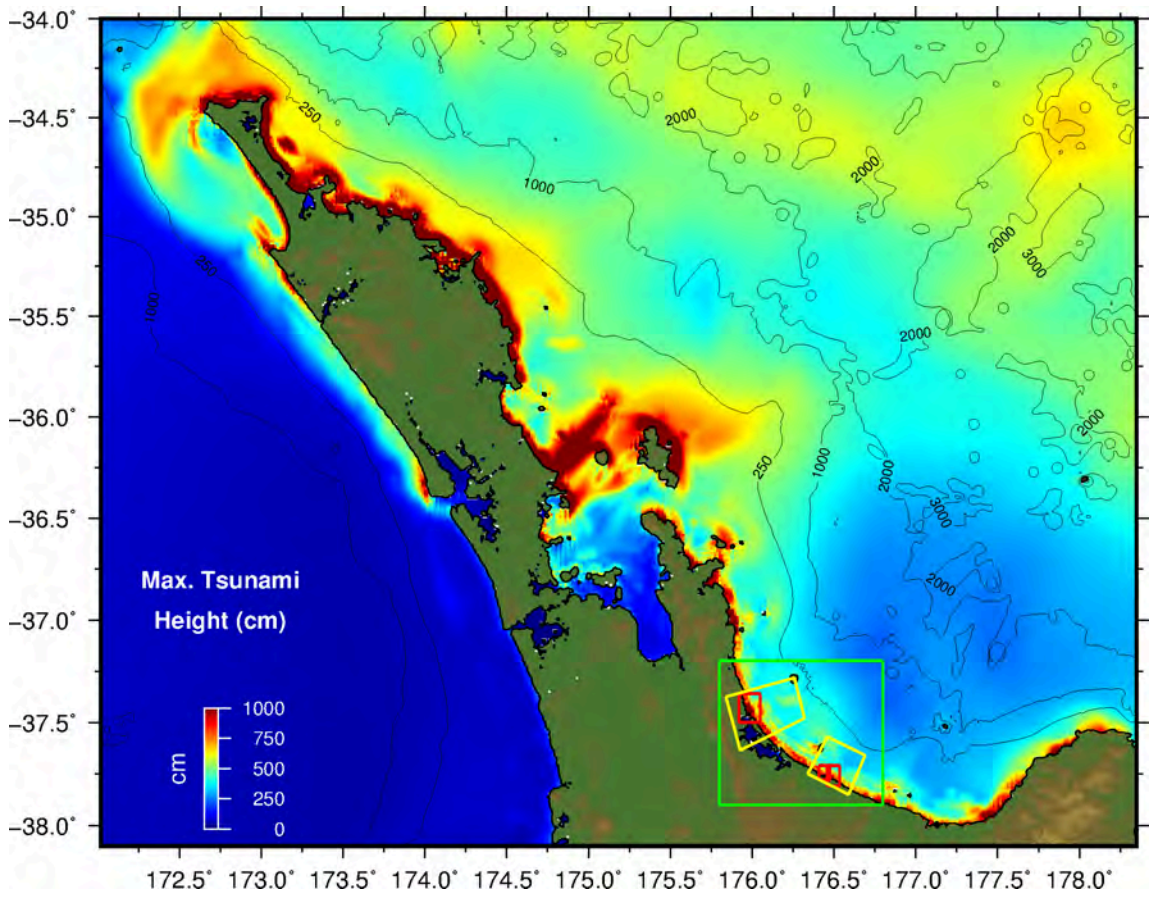

eCoast Limited
Marine Consulting and Research
P.O. Box 151
Raglan, New Zealand

jose@ecoast.co.nz

<BLANK PAGE>

Probabilistic Tsunami Inundation Assessment for the Western Bay of Plenty District

Report Status

Version	Date	Status	Approved By:
V 1	6 June 2017	DRAFT	JCB
V 2	26 June 2017	FINAL	JCB

It is the responsibility of the reader to verify the currency of the version number of this report.

Jose C. Borrero Ph.D.

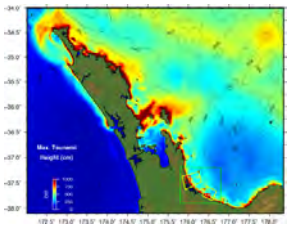

Cover Picture: Maximum computed tsunami height in the A grid for a maximum credible tsunami event in the Bay of Plenty.

<BLANK PAGE>

EXECUTIVE SUMMARY

The objective of this study is to identify areas in the Western Bay of Plenty District susceptible to tsunami inundation hazard and the outputs from this study will be used to set the tsunami hazard context across the Western Bay of Plenty. This study focuses on three areas: Waihī Beach, Maketū and Pukehina Beach and Little Waihī Estuary. For each of these areas we attempt to determine the inundation extents for four different probability levels based on the National Tsunami Hazard Model of Power (2013). Specifically these are the 0.2% AEP (500-year recurrence interval - RI), 0.1% AEP (1000-year RI) 0.04% AEP (2500-year RI) and the Maximum Credible Event (MCE).

The outputs from this study are mapped tsunami overlays of tsunami height, tsunami current speed and tsunami overland flow depth which will be used as input data for future tsunami risk assessments. The model scenarios were assessed at three water levels with allowance for sea level rise. Namely these are current mean sea level (Moturiki Vertical Datum), mean high water spring tide (MHWS) and MHWS + assumed sea level rise in 2130.

The numerical modelling presented in this study was carried out using the Community Model Interface for Tsunamis (ComMIT) numerical modelling tool.

Numerical modelling grids were derived from digitized nautical charts combined with LiDAR data provided by the Bay of Plenty Regional Council. Model grids were set up initially for both mean sea level (MSL) and then the datum was shifted to produce mean high water spring (MHWS) and the sea level rise (SLR) grids.

Models were set up with a 1250 m resolution outer grid and a 200 m middle grid. For the initial determination of the appropriate source models, an inner grid of 50 m resolution was used allowing the model to run very quickly. Once the appropriate sources had been determined, a finer resolution (10 m) inner grid was then used for the detailed inundation assessments.

Due to the low lying nature of the coastal topography, extensive areas are seen to be below sea level a MHWS and would be permanently flooded under the SLR scenarios (Figure 1)

The ComMIT tsunami model was validated against two recent historical tsunami events: the tsunami generated by the March 11, 2011 Japan earthquake and the tsunami generated by the September 2, 2016 East Cape earthquake. In both cases a satisfactory fit was produced between the model results and tsunami heights measured on tide gauges in the region as shown in Figure 2.

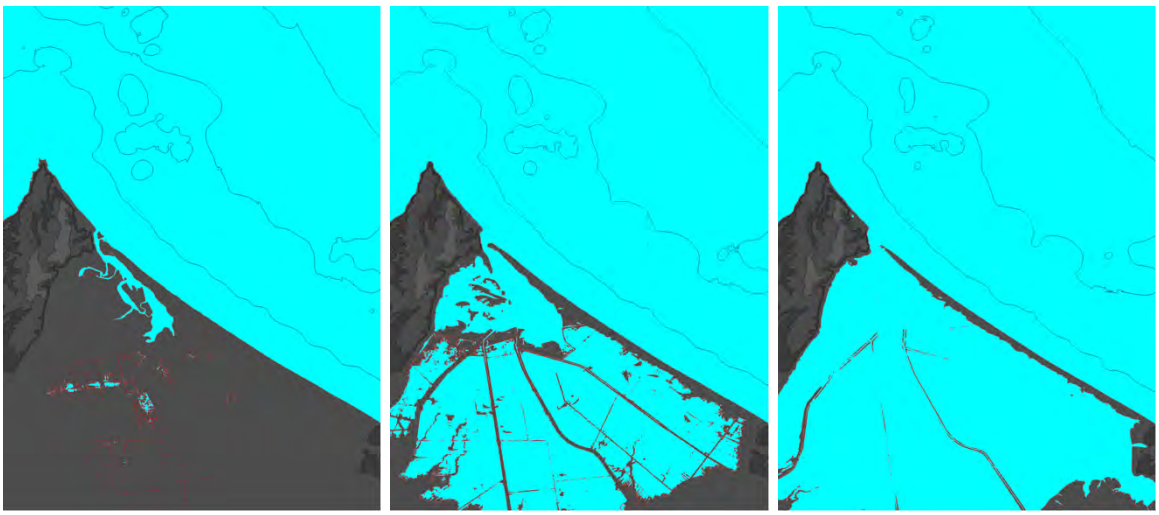

FIGURE 1. The Pukehina model grid under MSL (left) MHWS (mid) and MHWS+SLR (right) water levels.

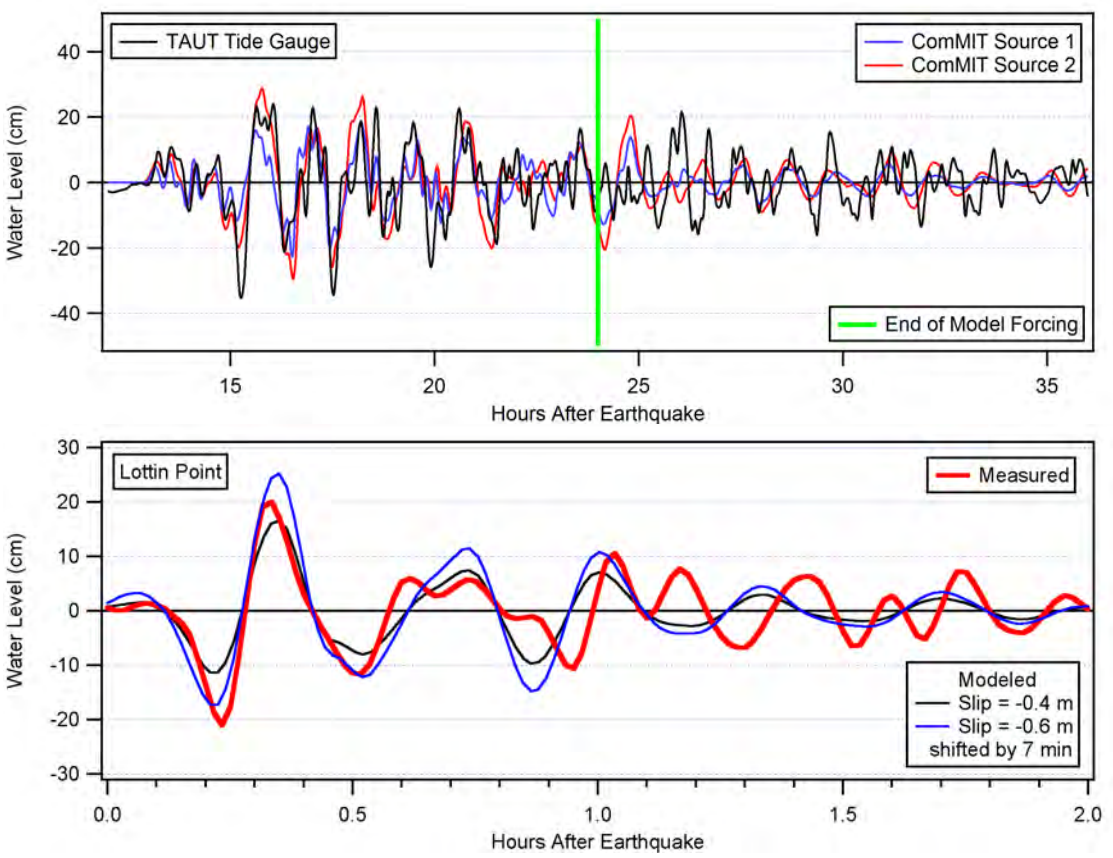

FIGURE 2. Model to measured comparisons at Tauranga for the 2011 Japan tsunami (top) and at Lottin Point for the 2017 East Cape tsunami.

Target tsunami heights for the different recurrence intervals were obtained from the New Zealand National Tsunami Hazard Model (Power 2013, 2104). This model provides hazard curves of tsunami height against recurrence interval in discretised regions along the entire New Zealand coastline. The target tsunami heights were selected according to the 50th percentile tsunami height at each recurrence interval of interest. The Maximum Credible Event (MCE) was assumed to produce 84th percentile tsunami heights at a 2500-year recurrence interval. The target tsunami heights are listed in Table 1.

TABLE 1 Tsunami heights at Waihi Beach and Maketu regions predicted by the New Zealand National Tsunami Hazard Model at the 16th, 50th, and 84th percentile for recurrence intervals of 500, 1000 and 2500-years.

Waihi Beach	Percentile		
RI (yr)	16th	50th	84th
500	4.8	5.8	7.0
1000	5.6	6.9	8.6
2500	7.0	8.4	10.8

Maketu	Percentile		
RI (yr)	16th	50th	84th
500	5.5	6.4	8.0
1000	6.5	7.7	9.9
2500	7.9	9.7	12.5

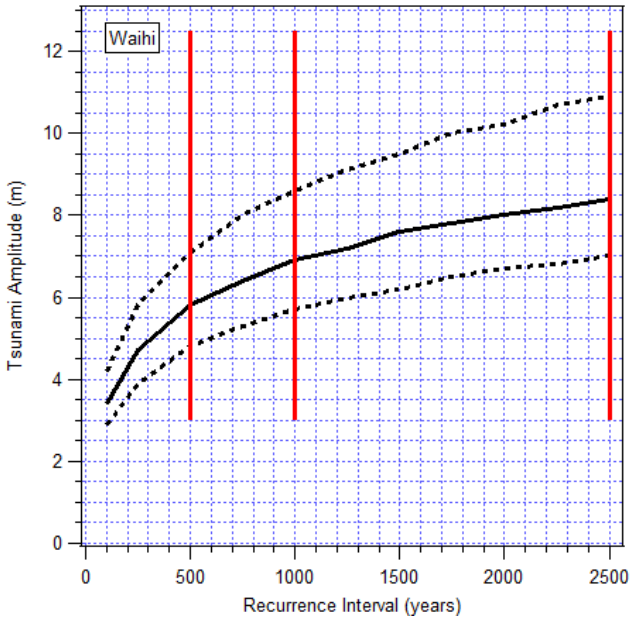

FIGURE 3. (above right) The hazard curve from the National Tsunami Hazard Model of Power (2013, 2014) for offshore of Waihi Beach. The vertical red lines indicate the desired recurrence intervals. The target tsunami amplitudes are determined from where the red line crosses the hazard curve.

Two regions Waihi Beach and Maketu (shown in Figure 4) were used for this study. Candidate tsunami sources were run through the model and a search algorithm was used to determine the modelled maximum tsunami amplitude in each of the coastal regions of interest.

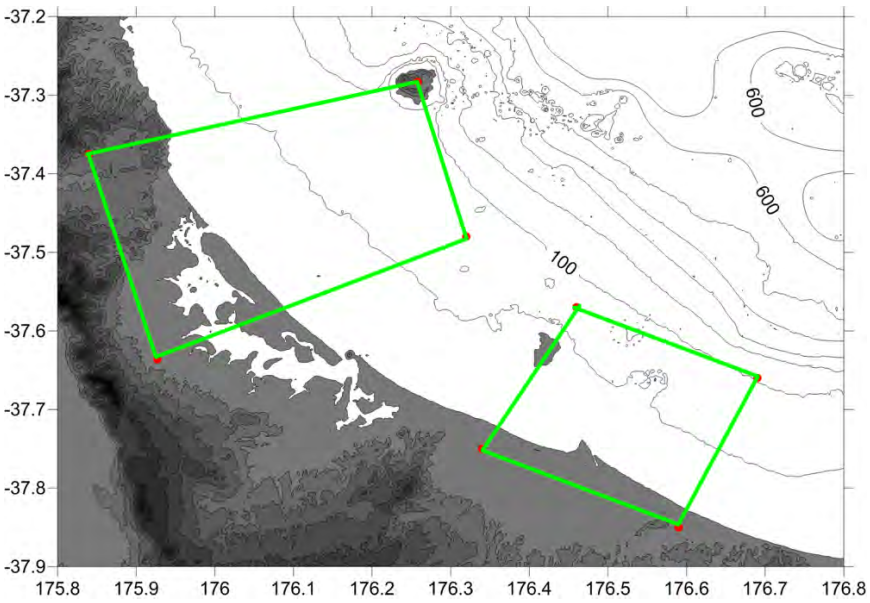

FIGURE 4 Extents of the Waihi Beach and Maketu regions used in determining the tsunami source models.

The model was run repeatedly for tsunami sources of gradually increasing magnitude positioned along segments of the Tonga-Kermadec trench located just north of the East Cape. This region was chosen because sensitivity studies show that this area produces the strongest tsunami effects along Bay of Plenty shores. The candidate source models were assumed to originate from a 400 km x 100 km fault plane with uniform slip (Figure 5). Following each model run, the maximum tsunami amplitude in each coastal polygon (indicated in Figure 4) was determined. If the amplitude matched the target amplitude, then that source was used for that particular recurrence interval.

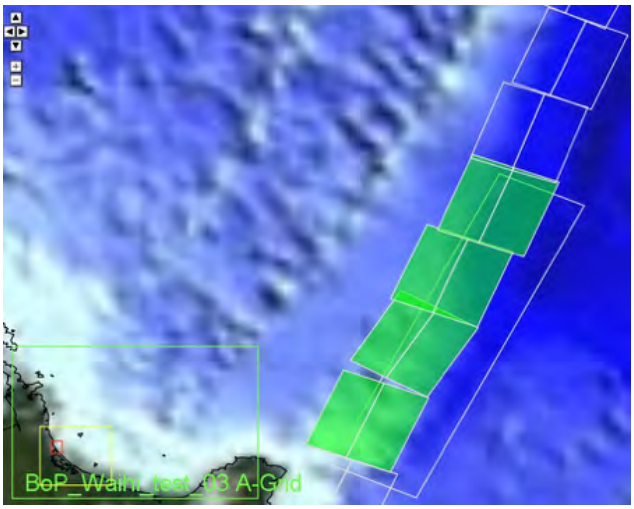

FIGURE 5. Fault segments used to initialise the tsunami model. Each segment is 100 x 50 km.

Ultimately, 8 tsunami sources were chosen corresponding to the 500-year, 1000-year, 2500-year and MCE events in each of the coastal regions of interest (Table 2). These models were run over each of the three bathymetry grids at the MSL, MHWS and MHWS + SLR water levels. Examples of the model output are presented in Figure 6 below.

TABLE 2. Slip amounts and associated earthquake magnitude and modelled nearshore tsunami amplitude for each of the sources used in this study.

Case	M_W	Slip (m)	Max Tsunami Amp. (m)
Waihi Beach 500-year	8.92	17.1	5.7
Waihi Beach 1000-year	8.98	20.4	6.9
Waihi Beach 2500-year	9.03	25	8.5
Waihi Beach MCE	9.13	35	11.7
Maketu/Pukehina 500-year	9.03	25	6.6
Maketu/Pukehina 1000-year	9.09	30	7.8
Maketu/Pukehina 2500-year	9.15	37	9.7
Maketu/Pukehina MCEr	9.20	45	12.5

The results of the study have provided tsunami inundation extents for use by the Bay of Plenty Regional Council in evacuation planning. The digital model output files are being provided to the Council for use in the preparation of maps and information for public dissemination and decision making within the Council.

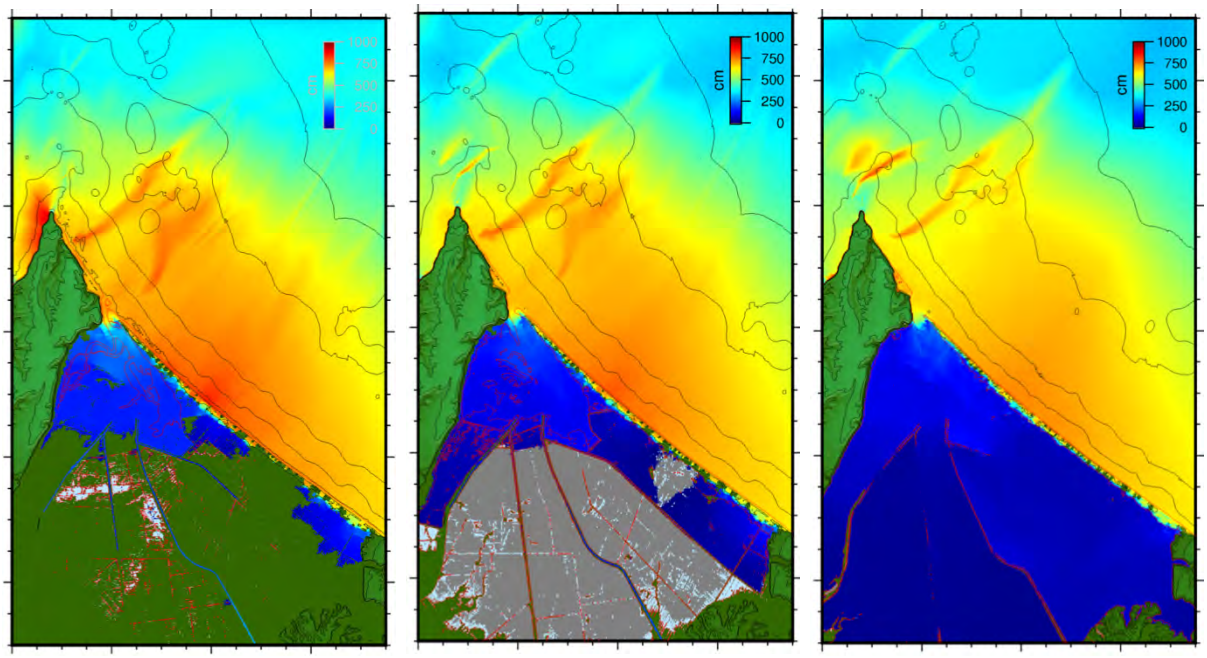

FIGURE 6. Maximum computed tsunami height and inundation extents for the 25-year RI event at Pukehina. Model grids at MSL (left) MHWS (mid) and MHWS+SLR (right).

CONTENTS

TABLE OF FIGURES

TABLE OF TABLES

1 INTRODUCTION

The objective of this study is to identify areas in the western Bay of Plenty District susceptible to tsunami inundation hazard and the outputs from this study will be used to set the tsunami hazard context across the Western Bay of Plenty District. This study focuses on three areas: Waihī Beach, Maketū and Pukehina Beach and Little Waihī Estuary (Figure 1.1). For each of these areas we attempt to determine the inundation extents for four different probability levels based on the National Tsunami Hazard Model of Power (2013). Specifically these are the 0.2% AEP (500-year recurrence), 0.1% AEP (1000-year recurrence) 0.04% AEP (2500-year recurrence) and the Maximum Credible Event (MCE).

The outputs from this study are mapped tsunami overlays of tsunami height, tsunami current speed and tsunami overland flow depth which will be used as input data for future tsunami risk assessments. The model scenarios were assessed at three water levels with allowance for sea level rise. Namely these are current mean sea level (Moturiki Vertical Datum), mean high water spring tide (MHWS) and MHWS + assumed sea level rise in 2130.

Figure 1.1 Location map for study sites and other locations mentioned in the text in the Bay of Plenty, New Zealand.

1.1 Historical Context

The coast of New Zealand, and the Bay of Plenty coast in particular has experienced the effects of many tsunamis over historical and pre-historical times. Several reports and databases now exist that detail these events. Below we summarise some introductory information from the recently developed New Zealand Palaeotsunami Database (2017) and the online Historical Tsunami Database provide by GNS Scince. URL's for these resources are provided in the references.

1.1.1 Prehistoric Tsunami Records

The New Zealand Palaeotsunami Database (2017) was recently established to provide an online resource for investigating existing palaeotsunami records from around New Zealand. In Figure 1.2 below we reproduce the locations and associated inferred tsunami heights from all of the data points in the vicinity of the Bay of Plenty and the Coromandel Peninsula. The data points are also colour coded by the 'validity' assigned to each record; 1 being low validity and 3 being excellent validity. It is important to realize that these records span several thousands of years and do not represent just one tsunami event. This plot is just intended to show some basic location and magnitudes of possible pre-historic tsunami events in the region. We emphasize that the data point corresponding to a 60 m tsunami height shown in Figure 1.2 is also assigned the lowest validity (1) due to the ambiguous nature of this record.

For more details the reader is referred to the New Zealand Palaeotsunami Database (http://ptdb.niwa.co.nz) where detailed reference information for each data record can be found and the raw data downloaded for inspection and/or analysis.

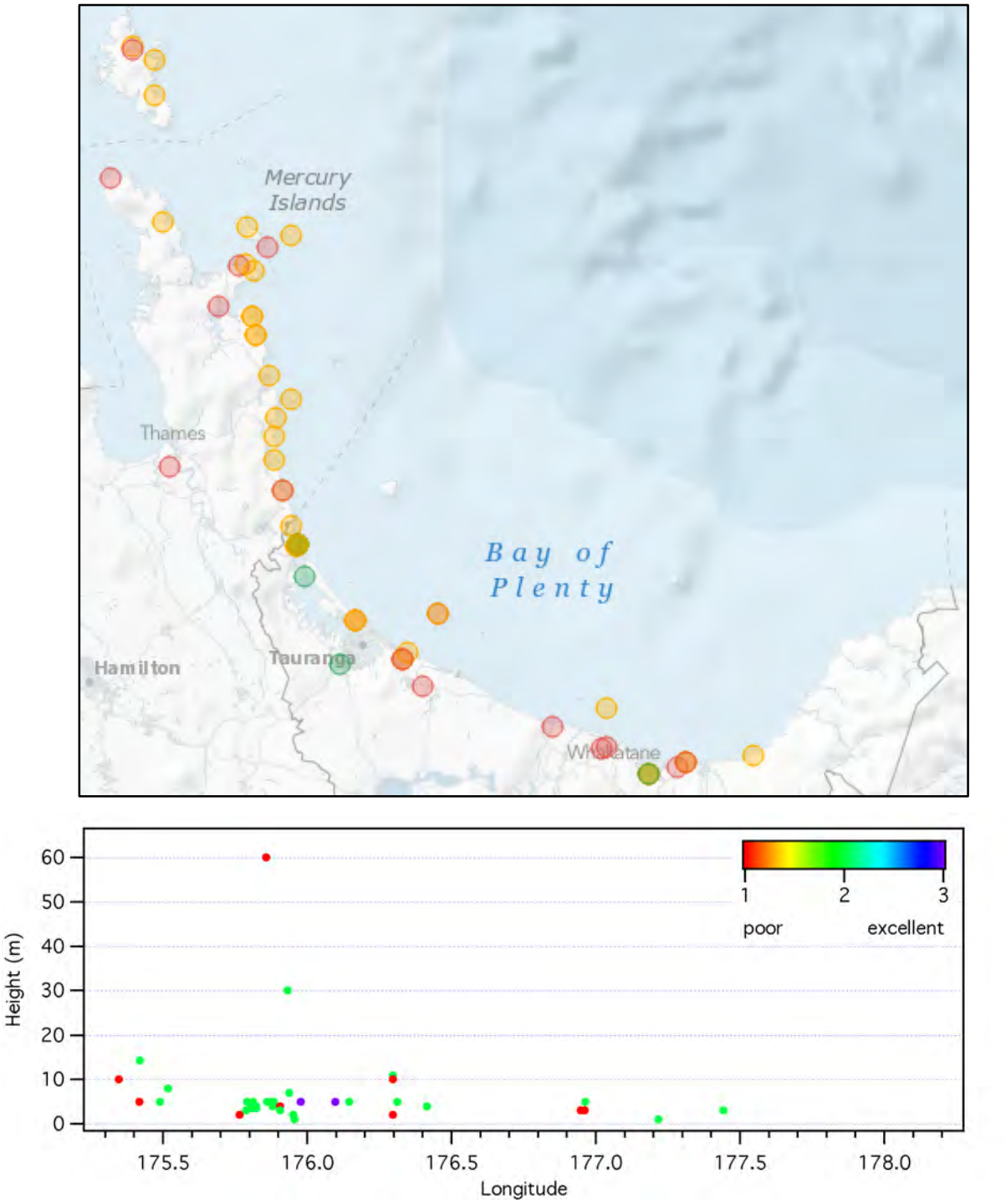

Figure 1.2 Inferred locations (top) and tsunami heights (bottom) of palaeotsunami records along the Coromandel and Bay of Plenty coasts. The validity of the record is indicated by the colour with 1 (red) indicating a poor record and 3 (blue) and excellent record.

1.1.2 Historic Tsunami Records

The Bay of Plenty and Coromandel Peninsula regions have recorded and experienced numerous tsunami events in historical times. A brief search in GNS's online historical tsunami database (http://data.gns.cri.nz/tsunami/) provides a number of records (see Figure 1.3). These include tsunami observations from the south American events of the late 1800's (1868 and 1877 in northern Chile) through to the recent events such as the 2010 Chile and 2011 Japan tsunamis. The reader is referred to this database for more information these specific events and records. Additionally the report of deLange and Healy (1986) also contains a wealth of historic information on tsunamis affecting New Zealand.

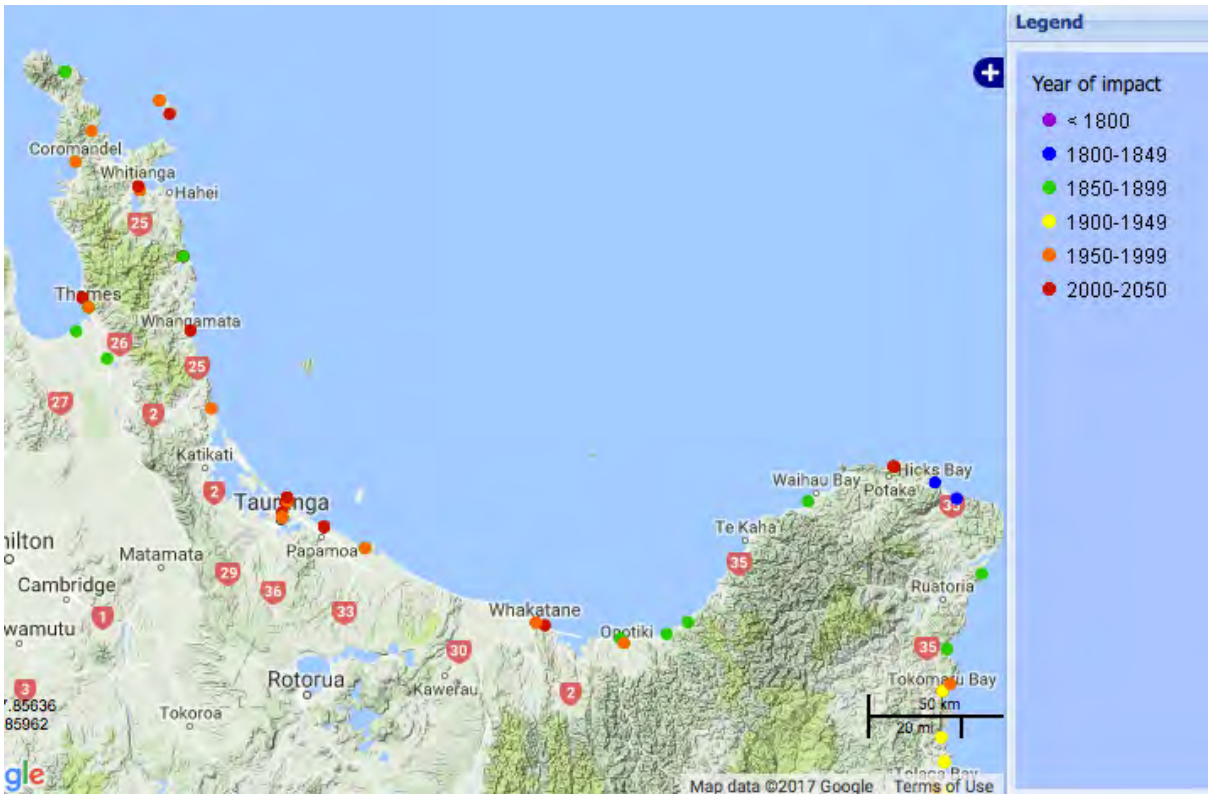

Figure 1.3 Locations of historical tsunami records in the GNS online tsunami database.

1.2 Modelling Approach

The numerical modelling presented in this study was carried out using the Community Model Interface for Tsunamis (ComMIT) numerical modelling tool. The ComMIT model interface was developed by the United States Government National Oceanic and Atmospheric Administration's (NOAA) Centre for Tsunami Research (NCTR) at the Pacific Marine Environmental Laboratory (PMEL) following the December 26, 2004 Indian Ocean tsunami as a way to efficiently distribute assessment capabilities amongst tsunami prone countries.

The backbone of the ComMIT system is a database of pre-computed deep water propagation results for tsunamis generated by unit displacements on fault plane segments (100 x 50 km) positioned along the world's subduction zones. Currently, there are 1,691 pre-computed unit source propagation model runs covering the world's oceans included in the propagation database. Using linear superposition, the

deep ocean tsunami propagation results from more complex faulting scenarios can be created by scaling and/or combining the pre-computed propagation results from a number of unit sources (Titov et al., 2011). The resulting trans-oceanic tsunami propagation results are then used as boundary inputs for a series of nested near shore grids covering a coastline of interest. The nested model propagates the tsunami to shore computing wave height, velocity and overland inundation. The hydrodynamic calculations contained within ComMIT are based on the MOST (Method Of Splitting Tsunami) algorithm described in Titov and Synolakis (1995, 1997) and Titov and Gonzalez (1997). The ComMIT tool can also be used in conjunction with real time recordings of tsunami waveforms on one or more of the deep ocean tsunameter (DART) stations deployed throughout the oceans to fine tune details of an earthquake source mechanism in real time. An iterative algorithm that selects and scales the unit source segments is used until an acceptable fit to the observed DART data is met.

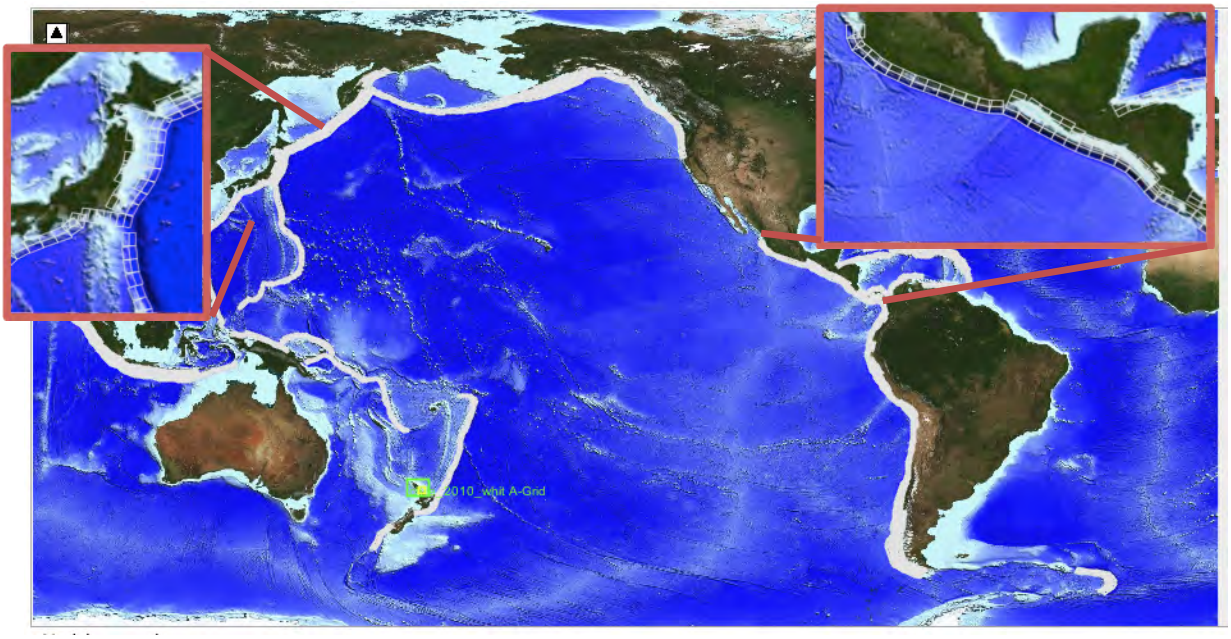

Figure 1.4 The ComMIT propagation model database for tsunamis in the world's oceans. Insets show the details of the source zone discretization in to rectangular sub-faults.

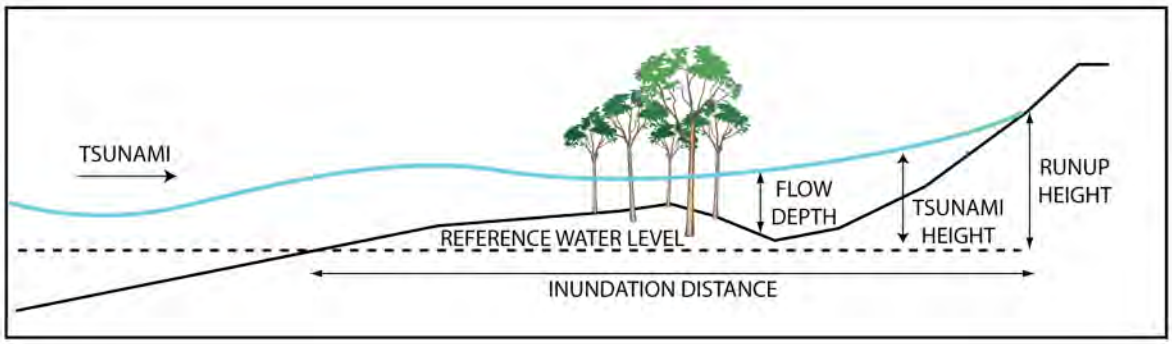

Figure 1.5 Definition sketch for tsunami height, flow depth, runup and inundation distance.

1.2.1 A Note On Terminology

There is often some ambiguity in the terminology used to describe the size of a tsunami. Generally the term 'height' is used as defined in the figure above, i.e. the measure of a distance above a particular datum. However, since tsunamis are waves, it is also common to use the term 'amplitude' which is the distance (height?) above or below a particular datum. For a perfectly symmetrical sine wave, the 'height' is twice the 'amplitude'.

In Power (2013) he writes:

"TSUNAMI HEIGHT (m) is the vertical height of waves above the tide level at the time of the tsunami (offshore it is approximately the same as the AMPLITUDE). It is far from constant, and increases substantially as the wave approaches the shoreline, and as the tsunami travels onshore. The term "WAVE HEIGHT" is also often used, but there is a potential ambiguity as many scientists define WAVE HEIGHT as the peak-to-trough height of a wave (approximately twice the amplitude). Note that this is a change in terminology from the 2005 Tsunami Hazard and Risk Review, intended to bring greater consistency with international usage of these terms.

And with regards to runup he says:

"TSUNAMI RUN-UP (m), a measure much used in tsunami-hazard assessment, is the elevation of inundation above the instantaneous sea level at the time of impact at the farthest inland limit of inundation. This measure has a drawback in that its relationship with the amplitude of the waves at the shore depends markedly on the characteristics of waves and on the local slopes, vegetation, and buildings on the beach and foreshore areas, so it is highly site-specific."

And finally with regards to the hazard curves for the National Tsunami Hazard Model he writes:

"in the curves shown here the 'maximum amplitude' should be interpreted as the tsunami height measured at the location within the section where it is highest"

Hence there is a degree of interchangeability in the use of 'height' and 'amplitude'. In this report we use 'height' for the elevation of the water surface above the sea level datum at the start of a model run. When discussing the hazard curves, we use the term 'amplitude' in line with Power (2013), which, as we see above, is used interchangeably with 'height'.

1.3 Numerical Modelling Grids

The Bay of Plenty Regional Council provided LiDAR topography data for construction of the numerical modelling grids. The data were provided with a reference datum of Moturiki Vertical Datum and a WGS84 projection. The data were combined with additional data sets covering the regional offshore bathymetry and on land topography. This included the Shuttle Radar Topography Mission (SRTM) 90 m resolution topography, 200 m resolution bathymetry from NIWA, as well as nautical chart data from Land Information New Zealand (LINZ). The coverage areas of the various data sets are shown in Figure 1.6. The data were combined in to a master set of (x, y, z) triplets and then gridded in to different resolutions and coverage areas using a Kriging algorithm. Model grids were set up initially for both mean sea level

(MSL) and then the datum was shifted to produce mean high water spring (MHWS) and the sea level rise (SLR) grids.

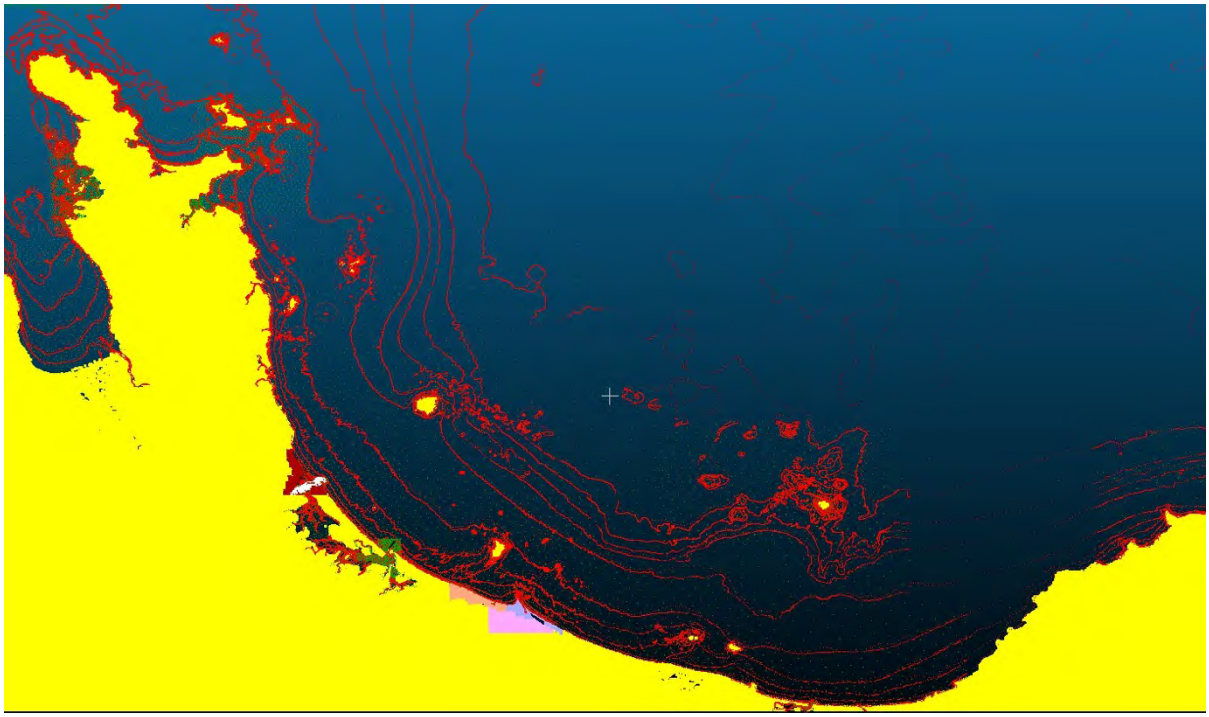

Figure 1.6 coverage area of the different bathymetry data sets. Yellow: SRTM topography, Dark Red, Orange, Blue and Pink: BoP-RC supplied LiDAR, RED: LINZ digitised charts contours and sounding points.

Details on each of the model grids used in this study are presented in Table 1.1 with plots of the different grids presented in Figure 1.7 through Figure 1.11. In Figure 1.9 through Figure 1.11 we present each of the three C-Level modelling grids at the three different water levels: mean sea level (MSL), mean high water spring (MHWS) and MHWS + 1.25 m of sea level rise (SLR). From these plots it is clear that in the Maketu region, there are large expanses of land that lie at or below sea level during the resent-day high tide. At high tide under sea level rise conditions, the wetted area is even greater.

In the MHWS scenarios, although there are regions that lie below sea level, they remain ‘dry’ due to the presence of elevated dykes, road embankments and canals that keep these mostly agricultural fields from being flooded during high tide. Regions lying landward of these embankments would only be flooded if the tsunami surge were large enough to overtop the embankment. These effects are apparent in the modelling results presented in Section 4 below.

Table 1.1 Model grid information.

Grid	nx	ny	dx	dt	Run time
	(nodes)	(nodes)	(m)	(sec)	(min)
A	458	365	1254.8	6.71	n/a
B	443	389	199.7	2.27	n/a
Waihi					
C: 50 m	222	312	50.0	2.49	26
C: 20 m	554	778	20.1	1.0	86
C: 10 m	1107	1555	10.0	0.5	534
Maketu West					
C: 10 m	574	778	10	0.68	139
Maketu East					
C: 10 m	662	1111	10	0.52	291

Table 1.2 Datum shift used for the various model runs.

Water Level	Reference Level
MSL	0.0 m
MHWS	MSL + 0.9 m
MHWS+SLR	MHWS + 1.25 m

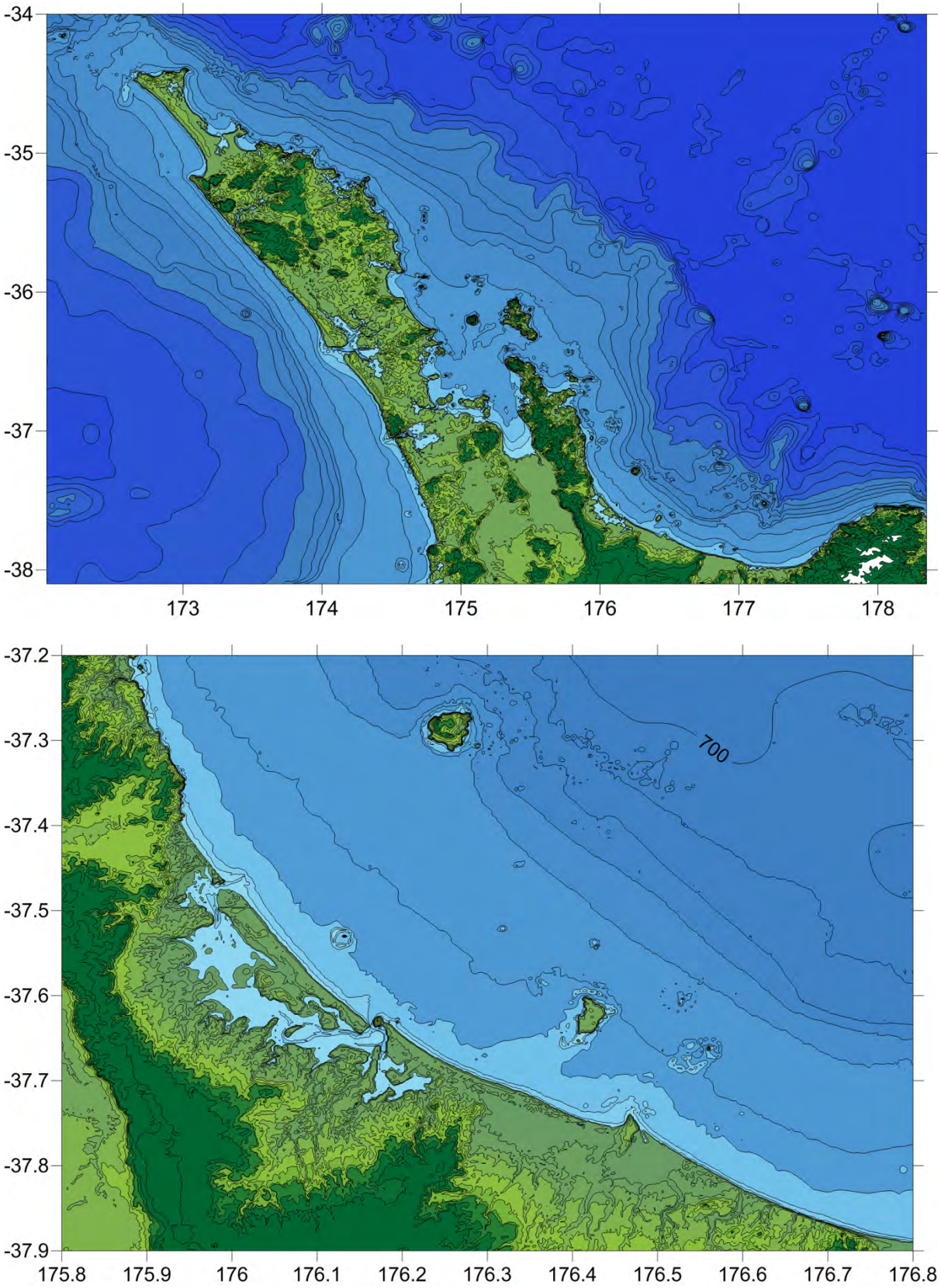

Figure 1.7 The A (top) and B (bottom) level modelling grids.

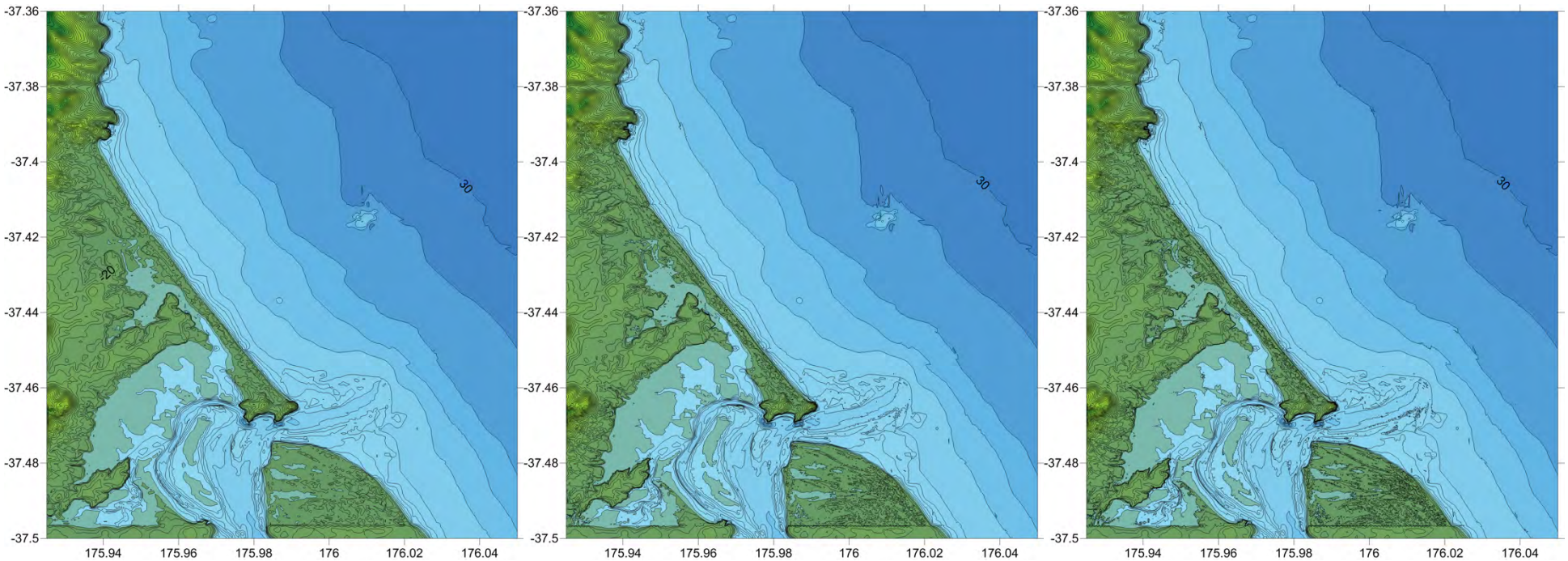

Figure 1.8 The C level numerical modelling grids for Mean Sea Level (MSL) for Waihi Beach at 50, 20 and 10 m resolution (left to right).

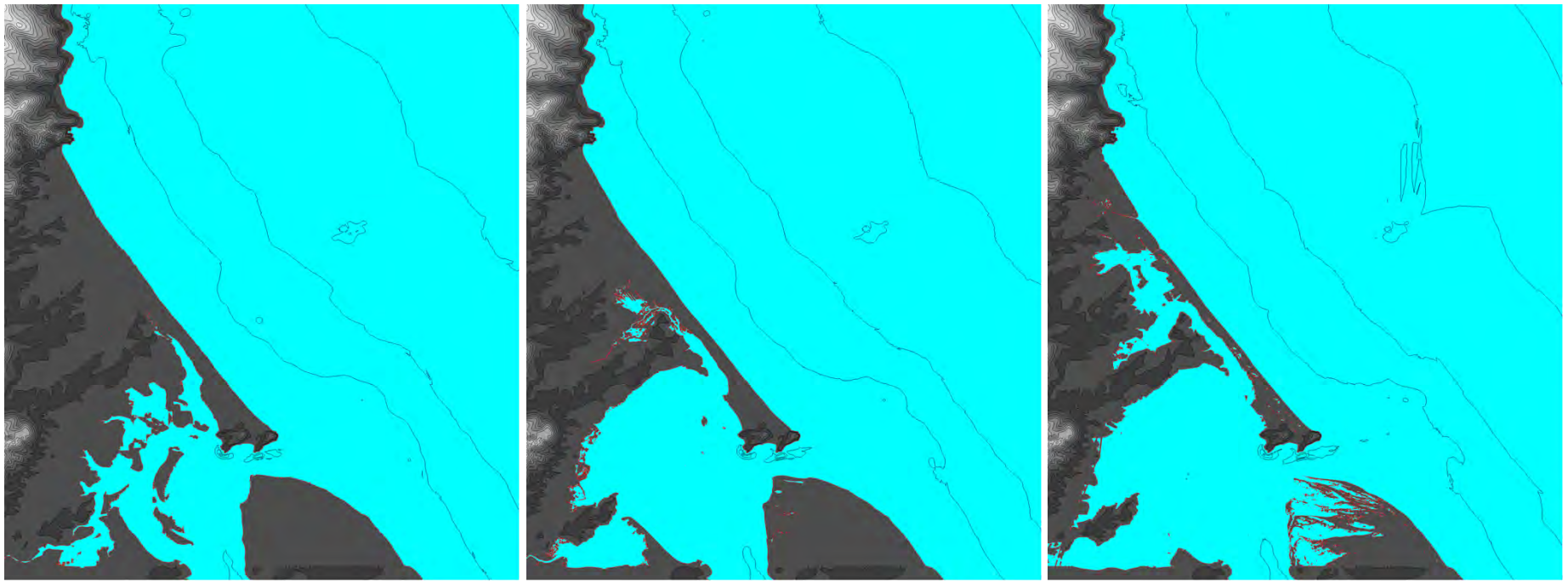

Figure 1.9 The Waihi Beach area at MSL (left), MHWS (mid) and MHWS + 1.25 m SLR (right).

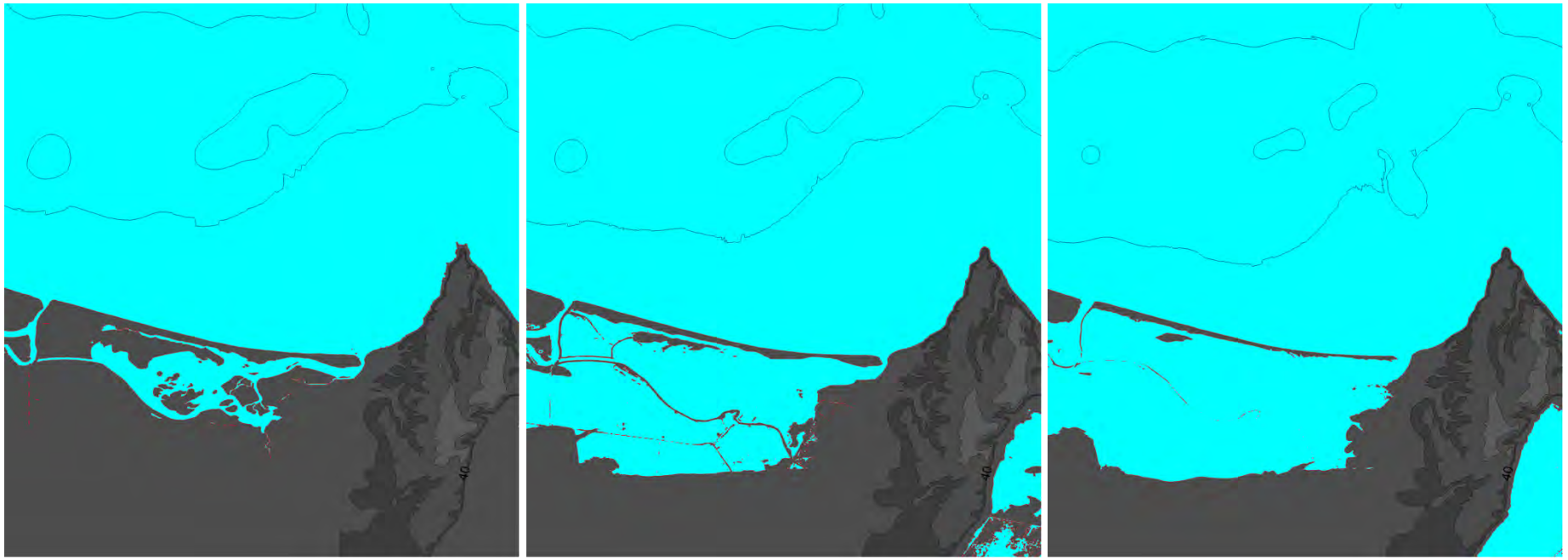

Figure 1.10 The Maketu area at MSL (left), MHWS (mid) and MHWS + 1.25 m SLR (right).

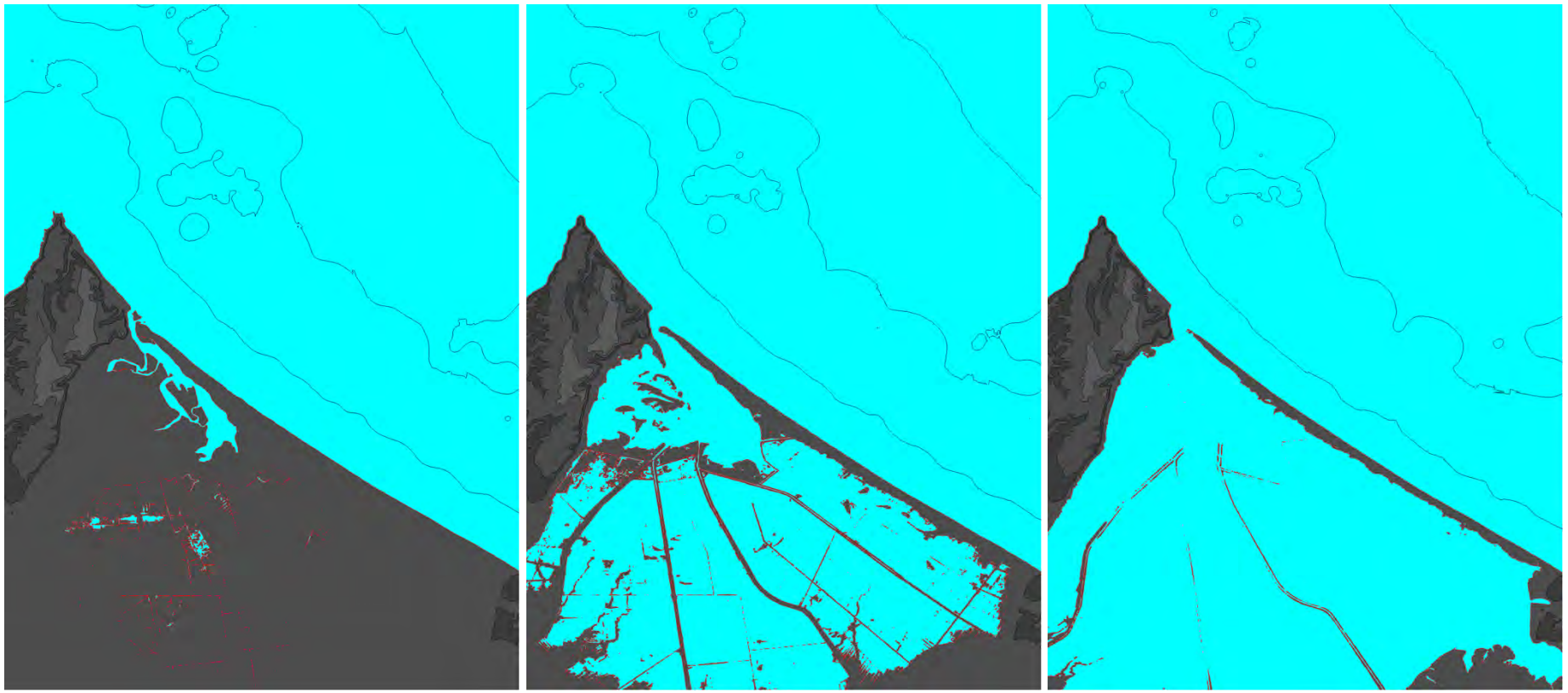

Figure 1.11 The Pukehina area a t MSL (left), MHWS (mid) and MHWS + 1.25 m SLR (right).

2 VALIDATION OF THE COMMIT TSUNAMI MODEL

The ComMIT model was validated for both a distant source and a near source event.

2.1 Case 1: The March 11, 2011 Tohoku Earthquake and Tsunami

The March 11, 2011 Tohoku earthquake and tsunami presents an excellent case study for the validation of the ComMIT model. The tsunami event was recorded on tide gauges throughout New Zealand with a wealth of data recorded on 5 water level gauges and one current meter in Tauranga Harbour (Lynett et al., 2012, Borrero et al., 2012, Borrero and Greer 2013). A full discussion of the modelling and validation of MOST/ComMIT is presented in Borrero et al. (2015).

For the validation, the MOST/ComMIT model was initialised using the tsunami source model derived during the Tohoku event using measured tsunami data. The source model is based on 100 x 50 km fault segments with different slip amounts applied to each segment (see Figure 2.1). The use of real-time data from the DART tsunameters, enabled the development and distribution of this source model approximately 1.5 hours after the earthquake. This source was used to make timely threat assessments for communities on the US West Coast (Wei et al., 2012, 2014) and in New Zealand (Borrero et al., 2012). More details on the inversion process and tsunami source can be found in (Percival et al., 2010).

Several months following the event, another tsunami source was developed for the Tohoku tsunami. This featured a different slip distribution and is shown in the right hand panel of Figure 2.1. Both source models are used to initialise the tsunami model. The far-field propagation patterns are shown in Figure 2.2 and the modelled water level time series inside Tauranga Harbour is presented in Figure 2.3. The results show that both sources do a relatively good job at modelling the tsunami heights with source developed in near real-time (Source 1) slightly underestimating the measured tsunami heights while the source developed later slightly over-predicts the measured data.

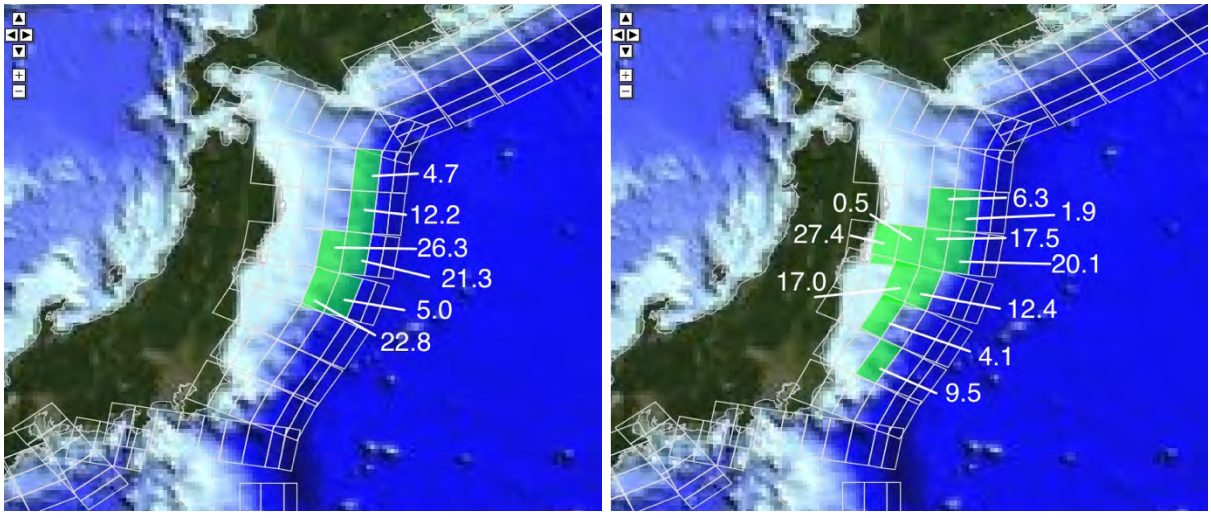

Figure 2.1 Tsunami source models used for the 2011 Tohoku tsunami. The amount of slip on each segment is indicated in white. The left panel is the slip distribution developed in near real-time in the hours following the earthquake and used for real-time forecasting (Wei et al. 2012) while the right panel is the slip distribution developed months after the event.

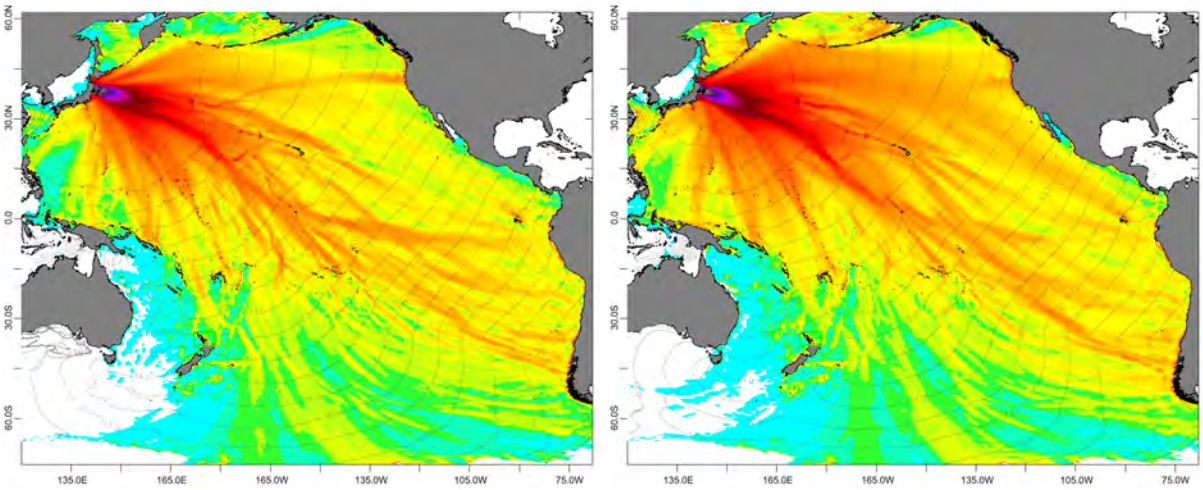

Figure 2.2 Far field propagation patterns for the two tsunami source models shown in Figure 2.1.

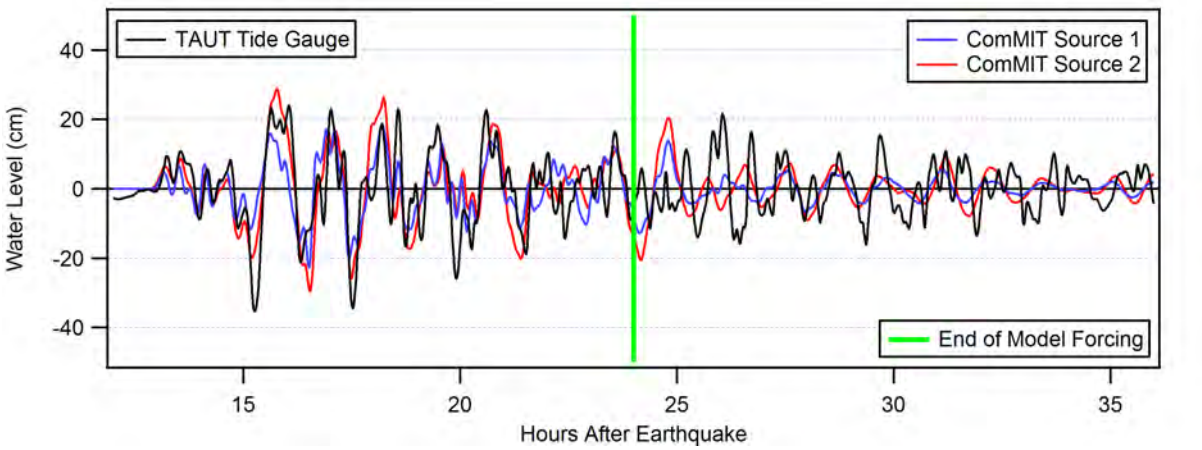

Figure 2.3 Modelled water level time series compared to measured data inside Tauranga Harbour.

2.2 Case 2: The September 2, 2016 East Cape Earthquake and Tsunami

On 2 September, 2016 at 4:37 am NZST (1 September 16:37 UTC), a Magnitude 7.1 (GeoNet) earthquake struck just north-east of the East Cape of New Zealand. The event was felt throughout the North Island. More that 4,000 people filed felt earthquake reports with GeoNet with reports coming in from as far away as Chatham Island and Christchurch (GeoNet, 2017). The event created a small tsunami that was recorded on tide gauges in Gisborne and across the Bay of Plenty.

This event is important in that it was relatively strong and occurred along the Tonga-Kermadec subduction zone and in an area considered as the 'worst-case' source region for generating tsunamis affecting the East Cape, Bay of Plenty, Coromandel and Northland coasts – this due to its proximity and associated short travel times to these regions.

The source mechanism for this event however, was not a straightforward subduction zone event. The strike of the fault plane was oblique to and the source region was displaced west of the trench axis, suggesting a seismic rupture within the overriding Australian plate (Figure 2.5, top panel). Additionally, the sense of the rupture was that of a 'normal' fault - rather than a thrust or 'reverse' fault commonly associated with ruptures on a subduction zone interface. This means that the seafloor displacement above the source area was downward (i.e. negative) rather than upward (uplift). This is indicated by the direction of the slip vector arrows in the bottom panel of Figure 2.5.

To model this event using the pre-computed sources in the ComMIT database, some assumptions and approximations were necessary. Firstly, it was necessary to use a fault segment located to the east of the actual source region. Next, a negative average displacement was applied to the fault plane to produce a negative initial seafloor displacement. Two slip amounts were trialled, -0.4 m and -0.6 m.

The result of the modelling are compared to measured tide gauge data at Lottin Point and Tauranga Harbour in Figure 2.6. The comparison of the waveform at Lottin Point is remarkably good - given the approximations - with the results from the two source models neatly bracketing the measured data. Note that the modelled time series had to be shifted 7 minutes earlier to match the timing of the measured data. This accounts for the fact that the source region used in the model is located further away to the west of the actual source region, thus requiring more time for the wave to reach the tide gauge.

The results for Tauranga are not as good with the model over predicting the measured wave heights and requiring a 14 minute time shift to match the timing of the peaks and troughs. However this is understandable given the very small size of the tsunami and the degree of attenuation that likely occurred as this small signal passed through the narrow entrance of Tauranga Harbour.

Given the limitations of the ComMIT model, the results are good and show that it can be used to accurately predict tsunami heights along the New Zealand coast from near-field tsunami sources

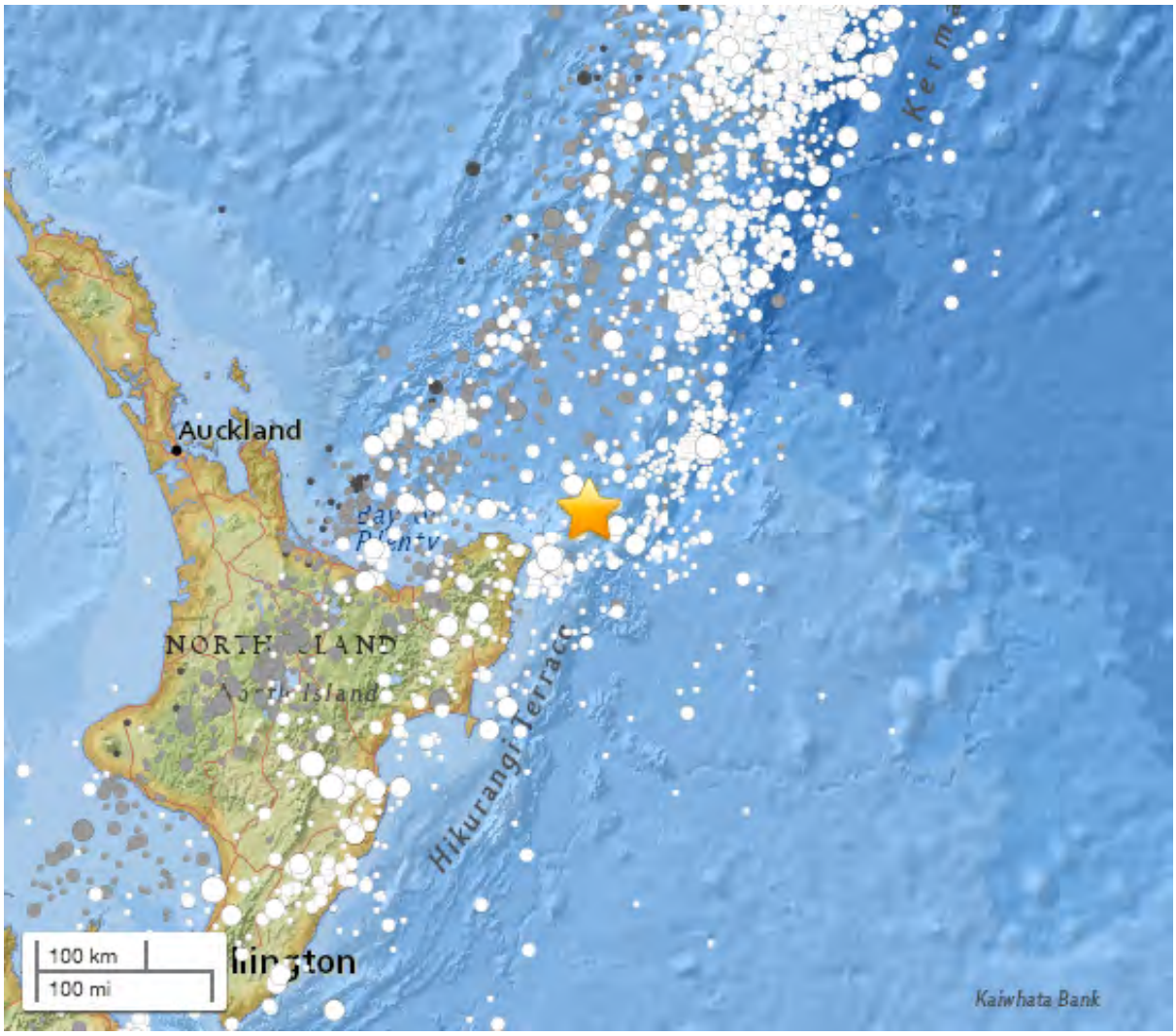

Figure 2.4 Source location of the September 2nd East Cape Earthquake (USGS, 2017).

Figure 2.5 (following page) Top panel: Earthquake source model for the September 2, 2017 East Cape earthquake (reproduced from USGS, 2017). The top panel shows the location of the fault plane (white region). Epicentre of the mains shock is indicated by a star with aftershocks indicated by black circles. Coloured patches indicate coseismic slip amounts according to the colour scale. The thin red line is the top of the fault plane. The white line is the axis of the Tonga-Kermadec Trench. The purple rectangle shows the location of a 100x50 km fault plane source available in the ComMIT tsunami modelling database. Bottom panel: A detail of the slip distribution along the fault plane with the amount of slip indicated by the colour scale. The location of the earthquake hypocentre is indicated by the star with the arrows indicating the direction of the rupture displacement. The contour lines are the timing (in seconds) of the rupture. The red arrow at the top of the fault plane corresponds to the red arrow in the upper panel. The purple box shows the dimensions of a 100x50 km fault plane.

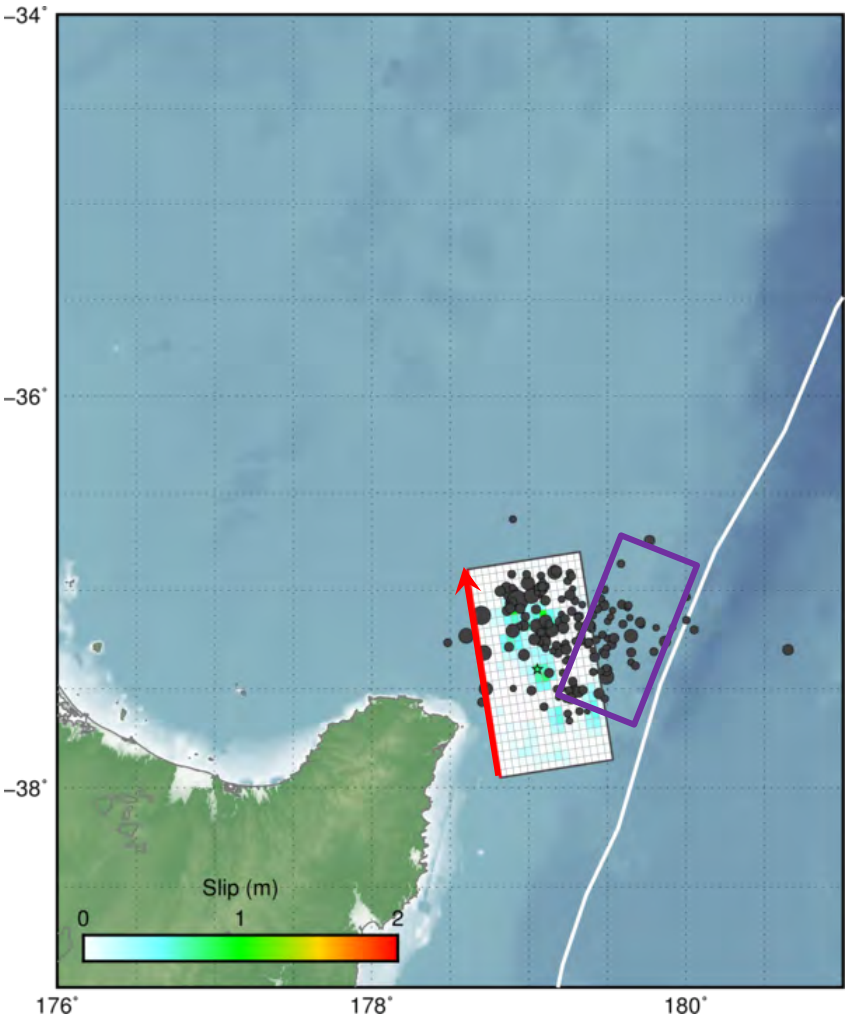
-34°
-36°
-38°
Slip (m)
0
1
2
176°
178°
180°

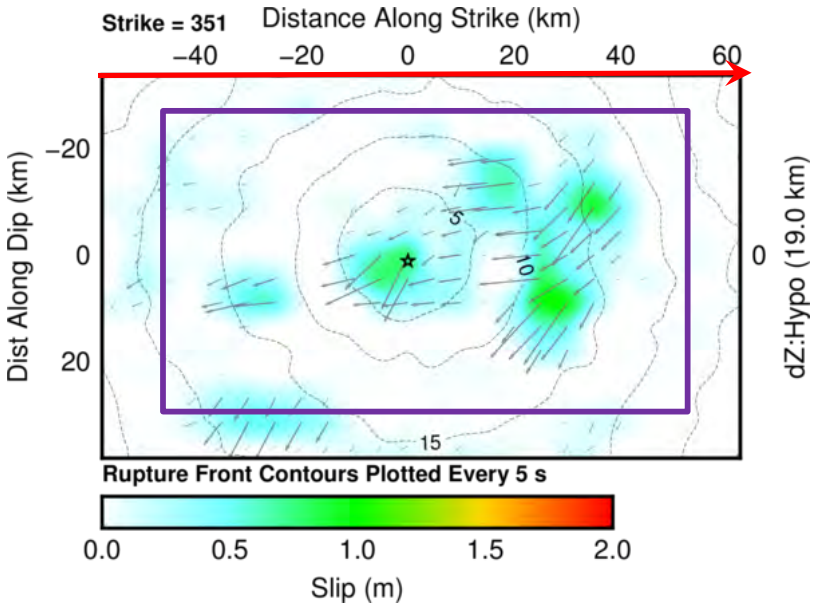
Strike = 351
Distance Along Strike (km)
-40
-20
0
20
40
60
Dist Along Dip (km)
-20
0
20
dZ:Hypo (19.0 km)
0
5
10
15
Rupture Front Contours Plotted Every 5 s
0.0
0.5
1.0
1.5
2.0
Slip (m)

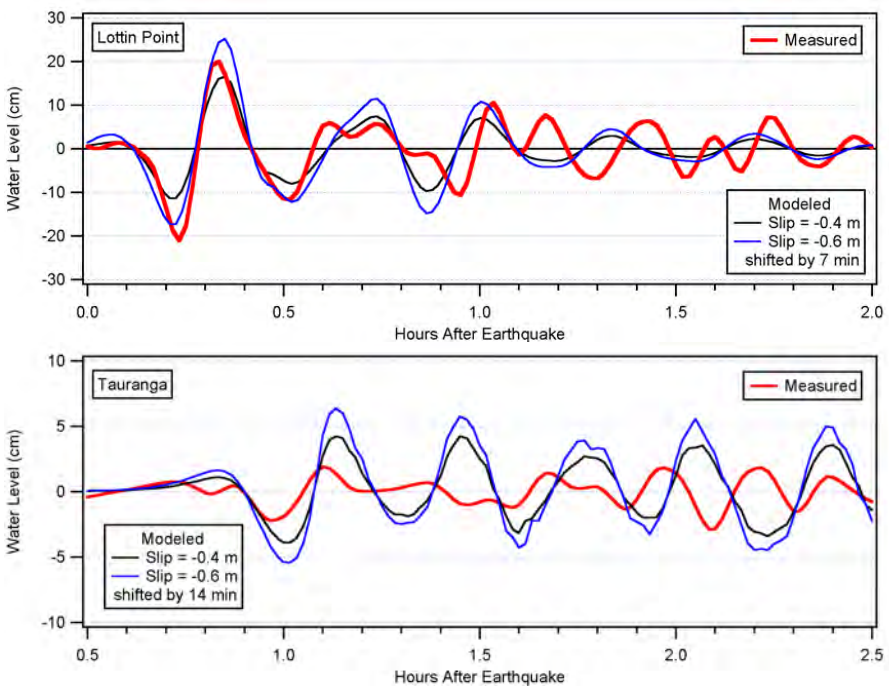

Figure 2.6 Modelled (blue and black traces) versus measured (red trace) water levels at Lottin Point (top) and Tauranga (bottom) for the 1 September tsunami.

3 RECURRENCE INTERVAL ANALYSIS

The GNS (Power 2013, 2014) probabilistic model was run on a numerical grid of approximately 200 m resolution. From this grid, polygons were defined for different coastal areas (Figure 3.1). The maximum computed tsunami amplitudes from within each polygon for each model run in the probabilistic analysis were then used to produce the hazard curves. The hazard curves from the Power (2013, 2014) report were digitized and reproduced in Figure 3.2 below. By selecting a recurrence interval (RI) of interest, one can draw a vertical line to determine the corresponding 16th, 50th and 84th percentile tsunami amplitudes for that hazard level. The Maximum Credible Event (MCE) is taken to be a source capable of generating the 84th percentile tsunami heights for the 2500-year RI. The target tsunami amplitudes for the recurrence intervals used in this study are presented in Table 3.1.

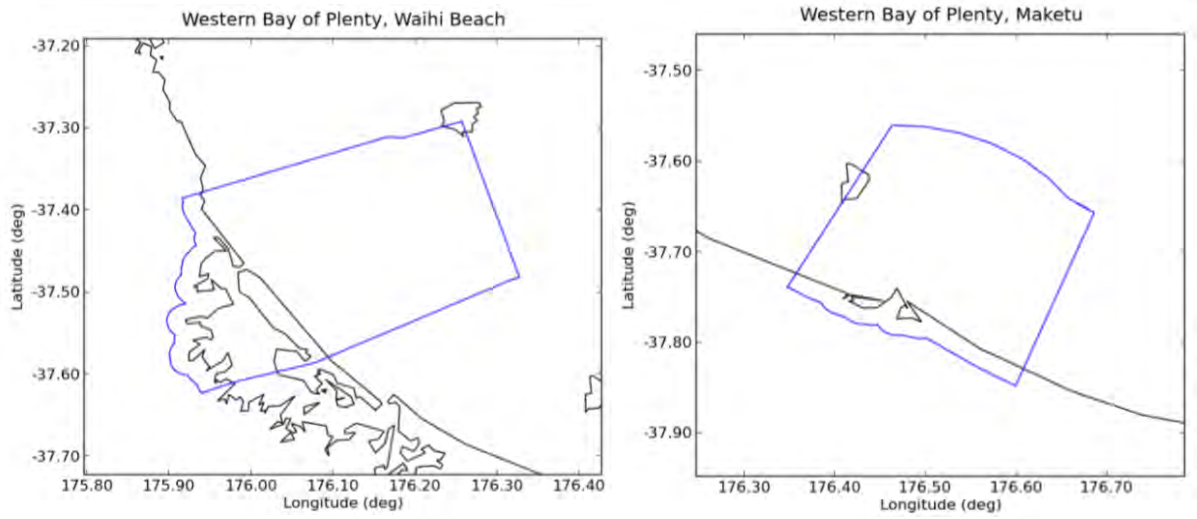

Figure 3.1 The Waihi Beach (left) and Maketu (right) regions used in the GNS (Power, 2013, 2014) probabilistic analysis.

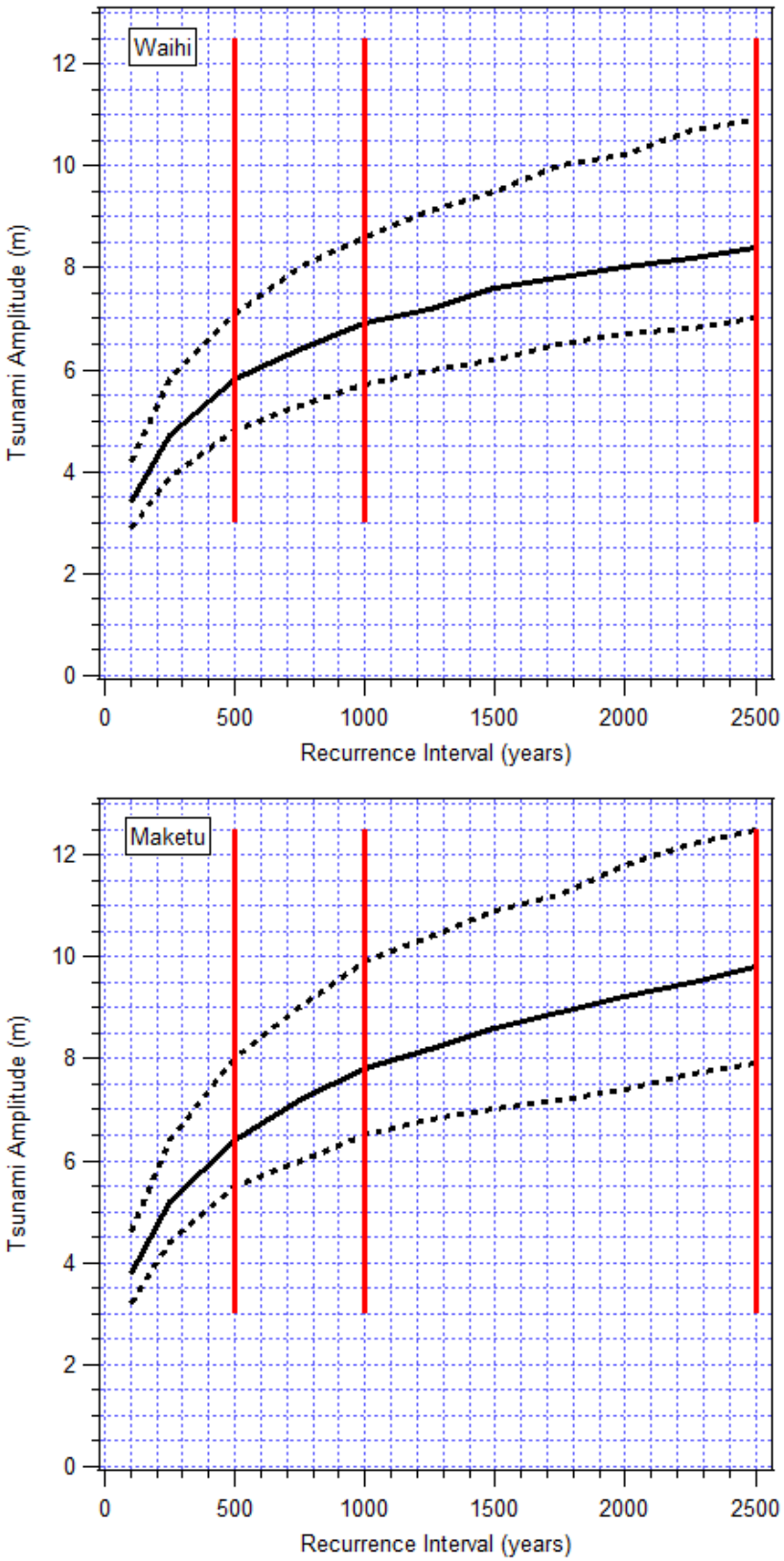

Figure 3.2 The GNS (Power 2013, 2014) hazard curves for Waihi (top) and Maketu (bottom). Tsunami amplitudes at 500, 1000 and 2500 year RI are indicated with the vertical red line.

Table 3.1 Target tsunami amplitudes (in meters) for different recurrence intervals and percentiles.

Waihi Beach	Percentile		
RI (yr)	16th	50th	84th
500	4.8	5.8	7.0
1000	5.6	6.9	8.6
2500	7.0	8.4	10.8

Maketu	Percentile		
RI (yr)	16th	50th	84th
500	5.5	6.4	8.0
1000	6.5	7.7	9.9
2500	7.9	9.7	12.5

3.1 Tsunami Sources

To determine the appropriate source models for the analysis, we trialled a number of different tsunami sources of varying magnitude in an effort to best match the 50th percentile tsunami amplitude at each recurrence interval (i.e. the 500, 1000 and 2500-year RI). For the maximum credible event (MCE) we sought a source producing a tsunami amplitude corresponding to the 84th percentile wave height at the 2500-year RI (see Table 3.1 and Figure 3.2 above).

To accomplish this, we initially trialled 10 source models. Nine these source models was positioned on the southernmost segments of the Tonga-Kermadec trench just north of East Cape (Figure 3.3). This region was chosen since it has been shown to produce the largest and most extreme tsunami heights along the Bay of Plenty coastline (Figure 3.4 and Figure 3.5). To show the relative effect of a far field tsunami, one scenario (Case 7) represented a large magnitude event occurring off the coast of Central Peru.

Cases 1 and 2 were variants of the source model used to reproduce the near field effects of the 2011 Tohoku tsunami in Japan (Wei et al., 2012). Case 1 was positioned 200 km north of East Cape, while Case 2 was positioned further south. The remainder of the sources featured uniform slip over a 400x100 km fault plane positioned just north of East Cape.

The model was run for each of these sources using the A and B level modelling grids described above. The innermost grid was a 50-m resolution grid covering the Waihi Beach area. Since the objective was to match tsunami amplitudes to the 2013 GNS study, only model results from the intermediate B level grid were considered. After each model run, we determined the maximum tsunami amplitude within polygons corresponding to the regions used in the GNS study (see Figure 3.1 and Figure 3.6). The maximum tsunami amplitudes were then compared to the target amplitudes for each recurrence interval for each region. An example of the model output for Case 2 is presented in Figure 3.7.

The model results were tabulated and are presented in Table 3.3 and Table 3.4. In some instances additional cases were added to better match the target tsunami height for each region. Hence, a total of 14 scenarios were run the determine the eight tsunami sources. From this analysis the tsunami sources for the 500, 1000 and 2500-year RI events as well as the maximum credible event were determined.

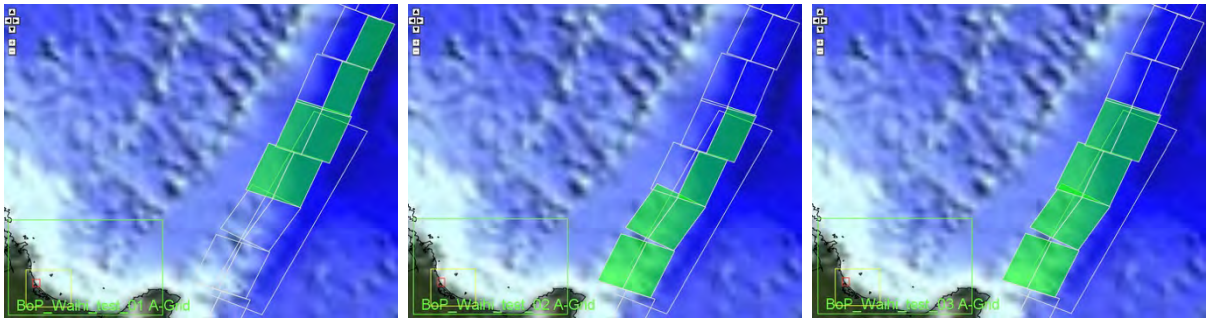

Case 1 Case 2 Cases 3-6 and 8-10

Figure 3.3 Fault segments used for the different near field tsunami sources.

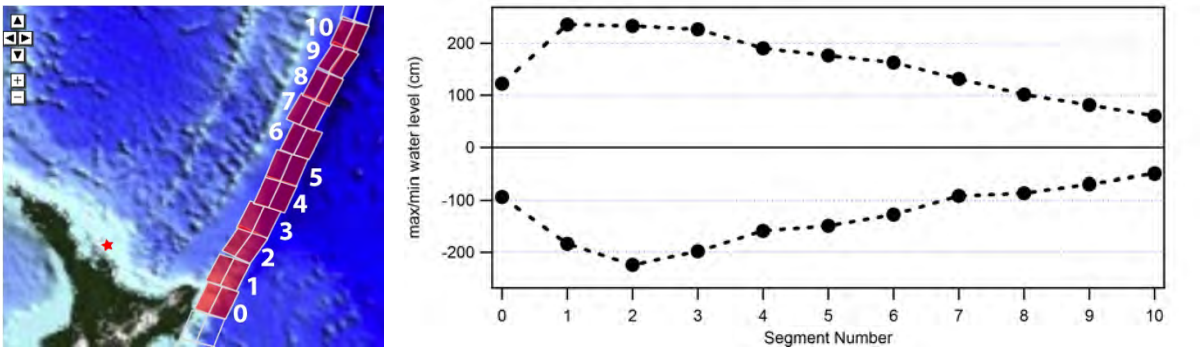

Figure 3.4 Maximum and minimum tsunami amplitudes produced offshore of the Coromandel Peninsula (red star) by identical tsunami sources positioned on each of the fault segments indicated in the panel on the left. Note that the strongest effects are the result of ruptures in the first 400 km north of the East Cape (segments 1, 2, 3 and 4).

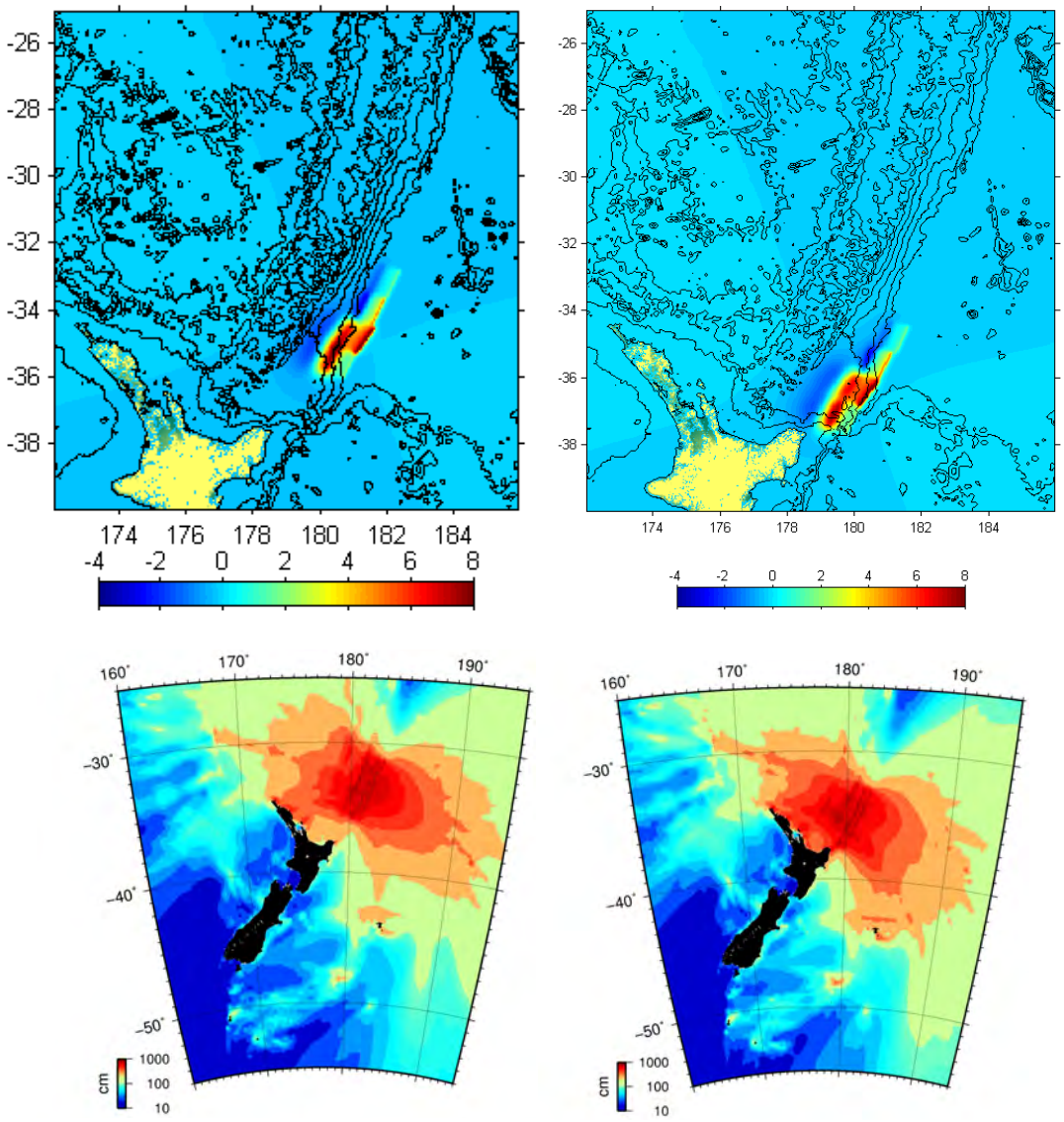

Figure 3.5 (top row) Tsunami initial condition (sea floor deformation) for Case 1 (left) and Case 2 (right). (bottom row) Maximum computed tsunami heights from each of these sources. Note how the source positioned further to the north results in significantly smaller wave heights along the Bay of Plenty coast.

Table 3.2 Tsunami source models for the seven preliminary cases.

Case Number	Magnitude	Slip amount (m)	Source
01	8.81	var	Variable slip model, equivalent to 2011 Tohoku tsunami source positioned 200 km north of East Cape
02	8.81	var	Variable slip model, equivalent to 2011 Tohoku tsunami source positioned 0 km north of East Cape
03	8.89	15	400x100 km fault, 0 km north of East Cape
04	8.97	20	400x100 km fault, 0 km north of East Cape
05	9.03	25	400x100 km fault, 0 km north of East Cape
06	9.09	30	400x100 km fault, 0 km north of East Cape
07	9.53	35	Central Peru
08	9.13	35	400x100 km fault, 0 km north of East Cape
09	9.17	40	400x100 km fault, 0 km north of East Cape
10	9.20	45	400x100 km fault, 0 km north of East Cape

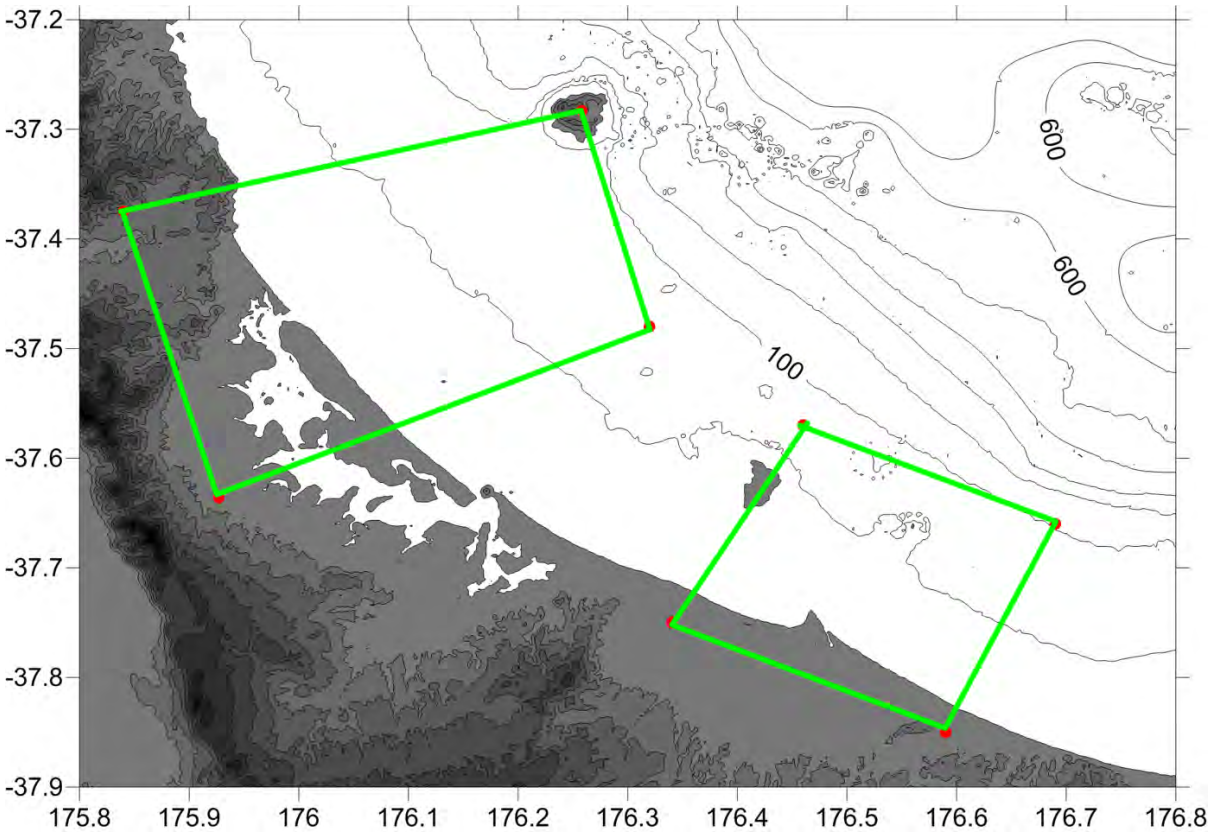

Figure 3.6 The search areas (green boundaries) used to determine the maximum offshore tsunami height for the hazard curves/return period analysis.

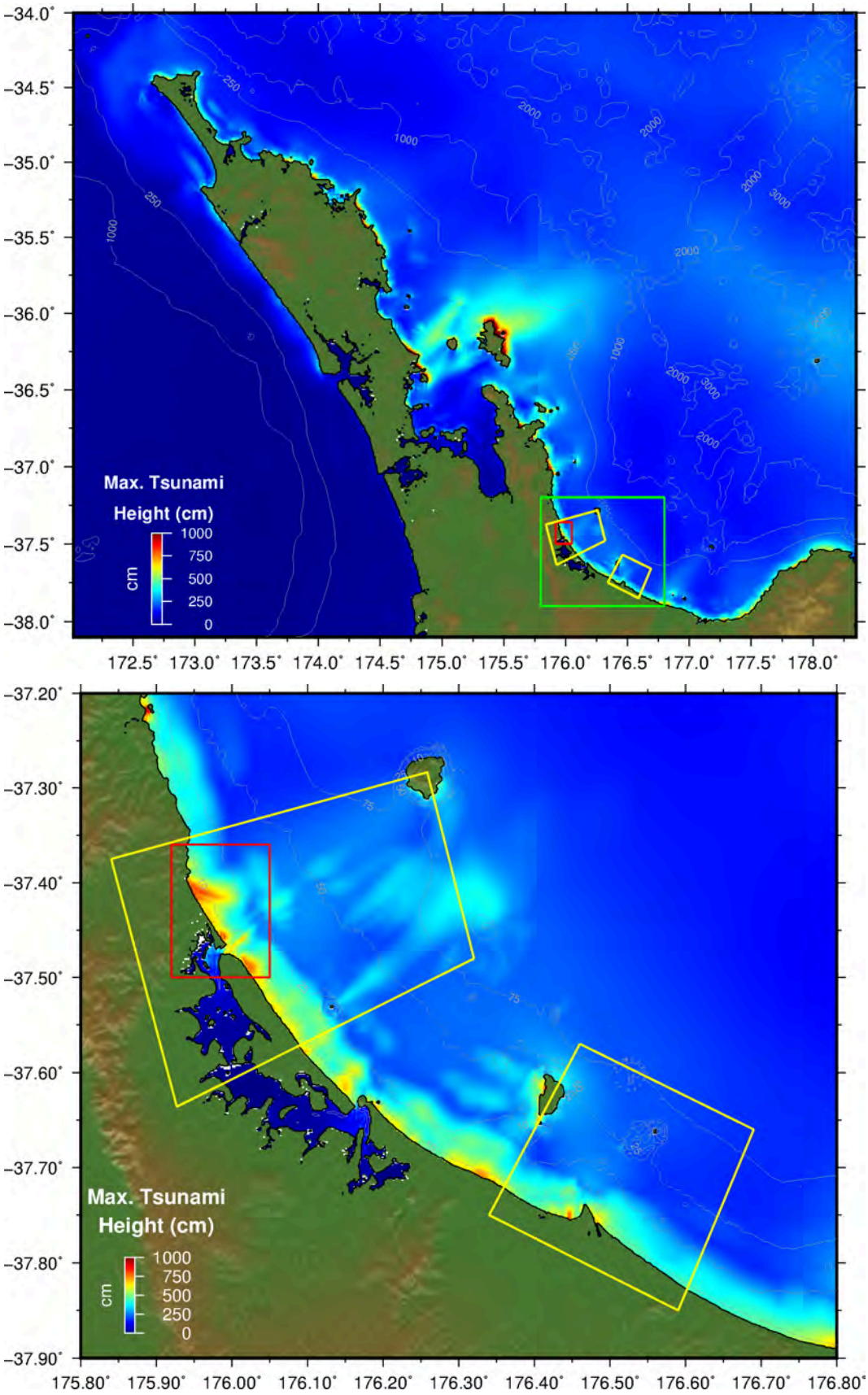

Figure 3.7 Maximum computed tsunami amplitude in the A grid (top) and B grid (bottom) for Case 02. The maxima for the return period analysis are determined from the Waihi Beach and Maketu regions indicated in yellow.

Table 3.3 Recurrence intervals (in blue) for maximum computed tsunami amplitudes (in red) in the Waihi Beach area in the B level model grids (200 m resolution). The

			B Grid	Recurrence Interval (Years)		
Case	M_W	Slip (m)	Max Tsunami Amp. (m)	84th %-ile	50th %-ile	16th %-ile
01	8.81	var	4.56	220	220	410
02	8.81	var	8.36	860	2500	>2500
03	8.89	15	5.04	180	310	600
03a	8.9241	17.06	5.74	250	500	1000
04	8.97	20	6.75	420	910	2200
04a	8.9761	20.42	6.88	480	1000	2500
05	9.03	25	8.48	900	2500	>2500
06	9.09	30	10.10	1900	>2500	>2500
07	9.53	35	2.65	<100	<100	100
08	9.13	35	11.71	>2500	>2500	>2500
08a	9.1441	36.48	12.14	>2500	>2500	>2500
08b	9.1482	37.0	12.31	>2500	>2500	>2500
09	9.17	40	13.30	>2500	>2500	>2500
10	9.20	45	14.89	>2500	>2500	>2500

Table 3.4 Recurrence intervals (in blue) for maximum computed tsunami amplitudes (in red) in the Maketu area in the B level model grids (200 m resolution).

			B Grid	Recurrence Interval (Years)		
Case	M_W	Slip (m)	Max Tsunami Amp. (m)	84th %-ile	50th %-ile	16th %-ile
01	8.81	var	4.05	<100	120	200
02	8.81	var	9.34	820	2100	>2500
03	8.89	15	4.10	<100	130	210
03a	8.9241	17.06	4.54	100	190	300
04	8.97	20	5.24	150	250	450
04a	8.9761	20.42	5.37	180	290	480
05	9.03	25	6.55	250	500	1000
06	9.09	30	7.83	490	1000	2500
07	9.53	35	3.74	<100	100	180
08	9.13	35	9.18	800	2000	>2500
08a	9.1441	36.48	9.58	930	2400	>2500
08b	9.1482	37.0	9.73	970	2500	>2500
09	9.17	40	10.26	1150	>2500	>2500
10	9.20	45	12.48	2500	>2500	>2500

4 DETAILED INUNDATION ASSESSMENT

Using the source models described above, we ran the full propagation and inundation model over each of the three model bathymetries (Waihi Beach, Maketu and Pukehina) for the MHWS and the MHWS + SLR scenarios. Additionally, for the purposes of comparison, we also ran the 2500-year RI and the MCE scenarios over the mean sea level bathymetry. The results are presented in Figure 4.1 through Figure 4.13 below. For the Waihi Beach area, we also conducted a sensitivity study detailing the effect of grid size on the inundation predicted by the model. The results of this sensitivity study are presented in Appendix 1.

Additionally, we conducted a sensitivity study of the inundation patterns occurring over the extensive wetted areas that arise under the MHWS and MHWS+SLR bathymetries for the Pukehina bathymetry. This sensitivity study is discussed in Appendix 2.

In the figures below we present primarily the model results for total tsunami height above sea level. Overland flow depth plots are also presented for the mean sea level cases (2500-year RI and MCE). Figures for tsunami currents, overland flow depths and overland flow speeds are presented in the accompanying Figures Appendix. The digital data corresponding to this model output will be provided to the Bay of Plenty regional council for use in further tsunami hazard assessments.

4.1 Organization of Model Results Figures

The results for each modelling region are presented in the following order: first we show the regional tsunami heights at each of the recurrence intervals over the A-level and B-level grids. These show that the tsunami wave height patterns over the wider area and highlight broad areas of wave focussing. In each of these plots (Figure 4.1, Figure 4.2, Figure 4.6 and Figure 4.7) the extents of the B and C-level modelling grids are indicated as green and red coloured rectangles. The yellow polygons indicate the regions used to search for maximum tsunami heights for use in the Recurrence Interval analysis described above.

The next set of plots (Figure 4.3, Figure 4.8 and Figure 4.11) presents the tsunami height and overland flow depth for the 2500-year RI and MCE scenarios on the mean sea level (MSL) bathymetry.

This is then followed by figures comprised of sets of four plots with each plot showing the maximum tsunami height for each of the four recurrence intervals. The first set is over the mean high water spring (MHWS) water level bathymetry (Figure 4.4, Figure 4.9 and Figure 4.12) and followed by model results over the MHWS + SLR water level bathymetry (Figure 4.5, Figure 4.10, Figure 4.13).

In some plots, particularly Figure 4.9 and Figure 4.12, there are regions with a grey shading. These are areas that are below sea level but not ‘wet’ at the start of the model run and they remain ‘dry’ i.e. are not inundated during the simulation.

A full set of model results is presented in the Figures Appendix supplied with this report.

4.2 Discussion of Inundation Results: Waihi Beach

Starting with the Waihi Beach grid, significant overland inundation is predicted by the model for the 500-year RI event at MHWS, particularly along the northern end of the beach. This effect increases for the larger events. On the largest event, significant inundation is seen all along and across the peninsula with flow reaching well inland in places. In the MHWS+SLR scenarios, the inundation is the most extensive. The barrier spit is completely overtopped in the 500-year RI event with extreme inundation occurring with the 2500-year RI event.

4.3 Discussion of Inundation Results: Maketu and Pukehina

At Maketu, again we see that the eastern end of the sand spit is overtopped in the 500-year RI event. This effect is increased as for the larger scenarios and higher water levels. The steep cliffs along the west-facing shore of the peninsula stop any significant inundation from happening there. There is also significant inundation predicted at the eastern end of the estuary and extending well inland.

Perhaps the most vulnerable area is along the Pukehina spit and the entrance to the Little Waihi estuary lying to the east of the Maketu Peninsula. In the 500-year MHWS scenario the spit is overtopped along the southern and central sections. As the source recurrence interval is increased, the degree of overtopping also increases causing flooding in the farmlands on the inland side. In the MCE scenario the farmland is nearly completely over run but the flow is restricted from flowing further inland by the presence of the road and canal embankments.

In the MHWS+SLR scenario, the entire area is flooded prior to any tsunami activity due to the low lying topography. The narrow strip of land remaining along the Pukehina Spit is overtopped in several places by the 500-year RI event and completely over run in the 2500-year and MCE scenarios. The modelled tsunami surge penetrates across the flooded farmland producing additional inundation along the margins of this area.

Figure 4.1 (following page top) Maximum computed tsunami height in the A grid for Waihi Beach sources at 500-year, 1000-year (top L, R), 2500-year and MCE (bottom L, R).

Figure 4.2 (following page, bottom) Maximum computed tsunami height in the B grid for Waihi Beach sources at 500-year, 1000-year (top L, R), 2500-year and MCE (bottom L, R).

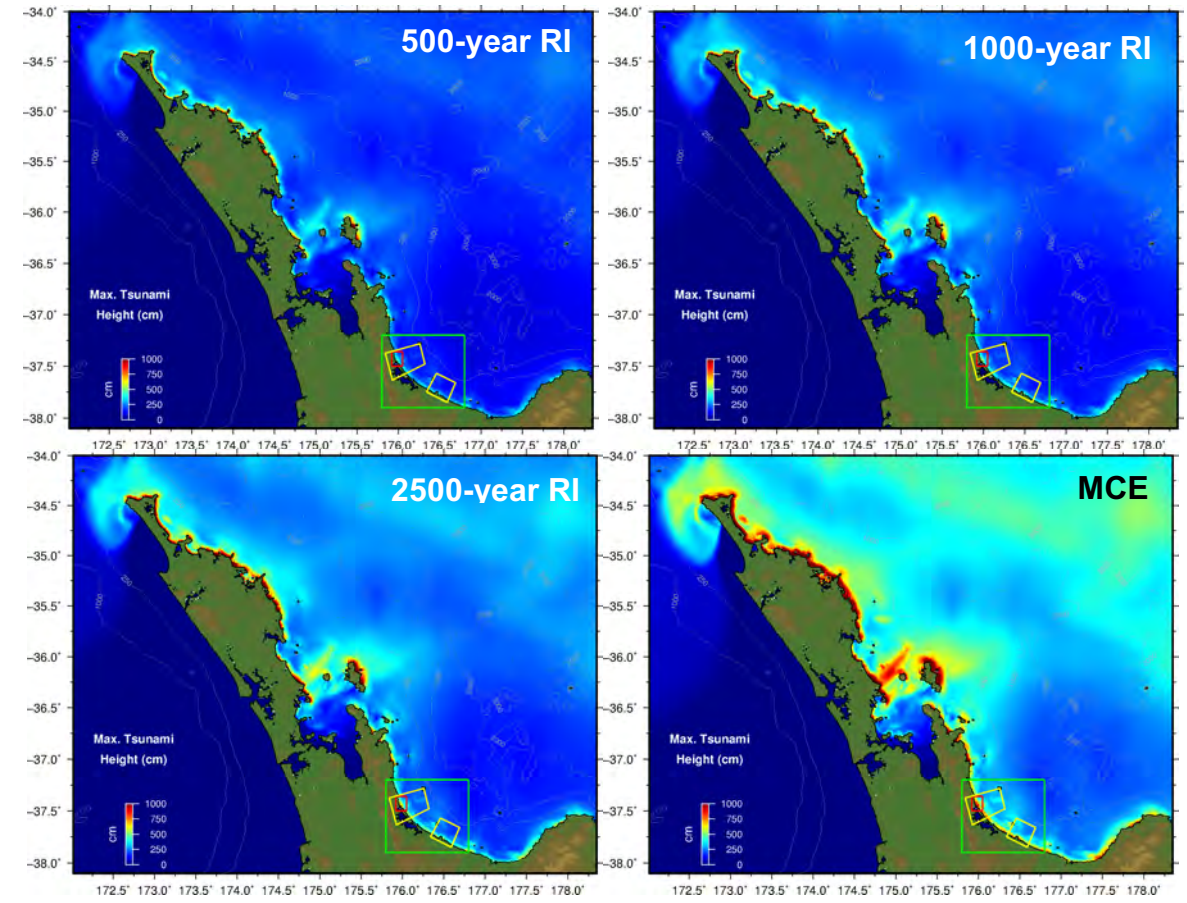
500-year RI
1000-year RI
2500-year RI
MCE
Max. Tsunami Height (cm)
cm
1000
750
500
250
0

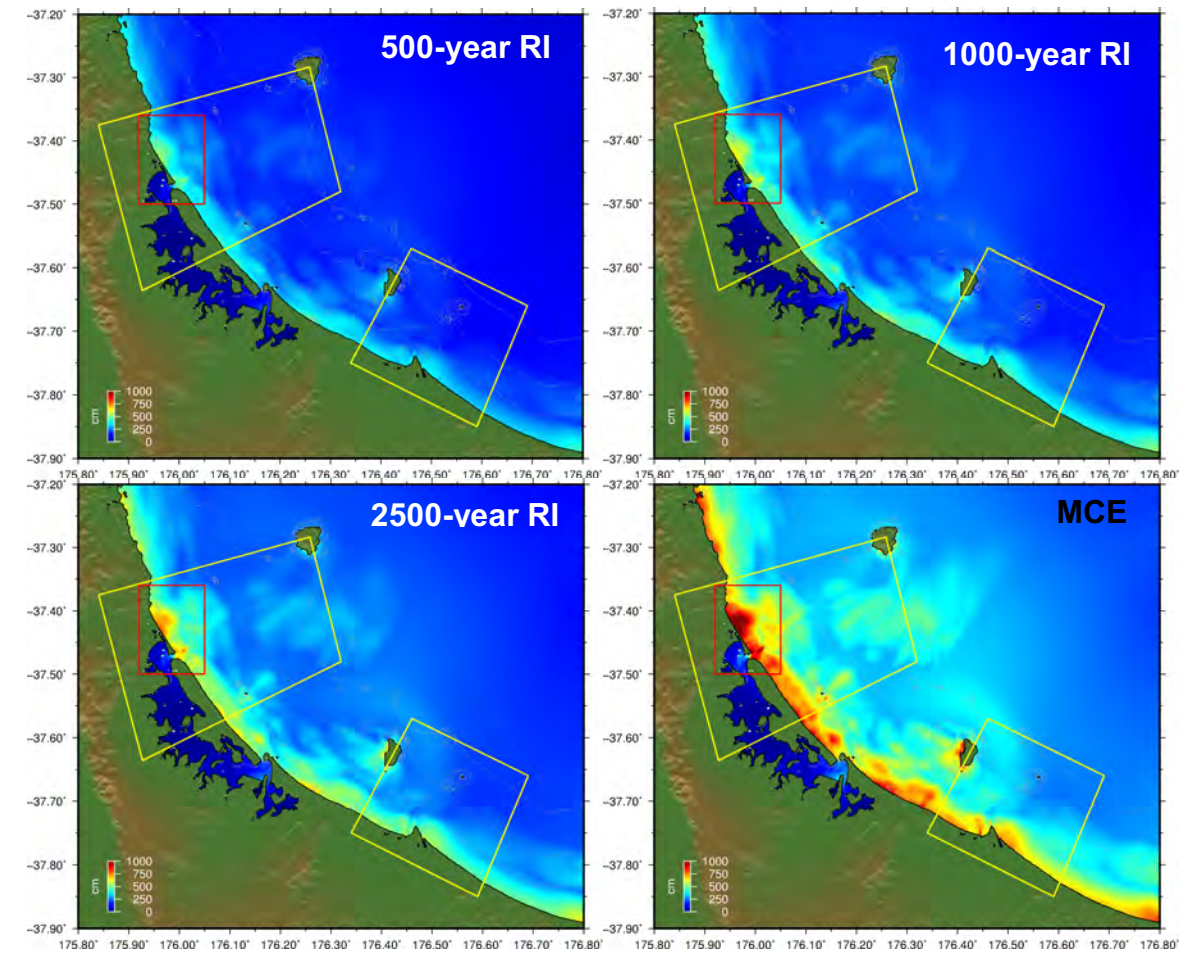
500-year RI
1000-year RI
2500-year RI
MCE
cm
1000
750
500
250
0

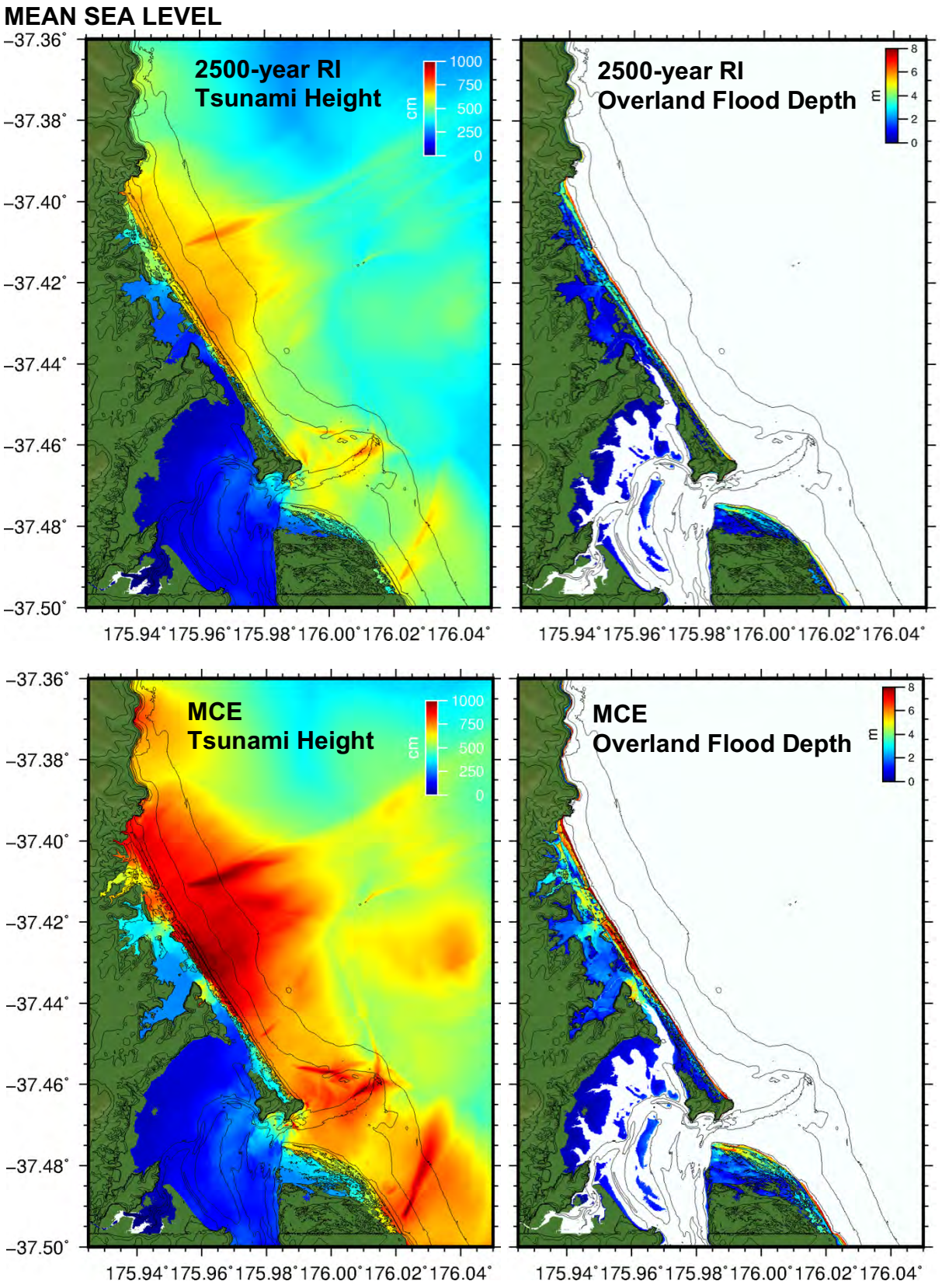

Figure 4.3 Maximum computed tsunami height (left) and overland flow depth (right) for the 2500-year event (top) and the maximum credible event (bottom) at Waihi Beach at mean sea level.

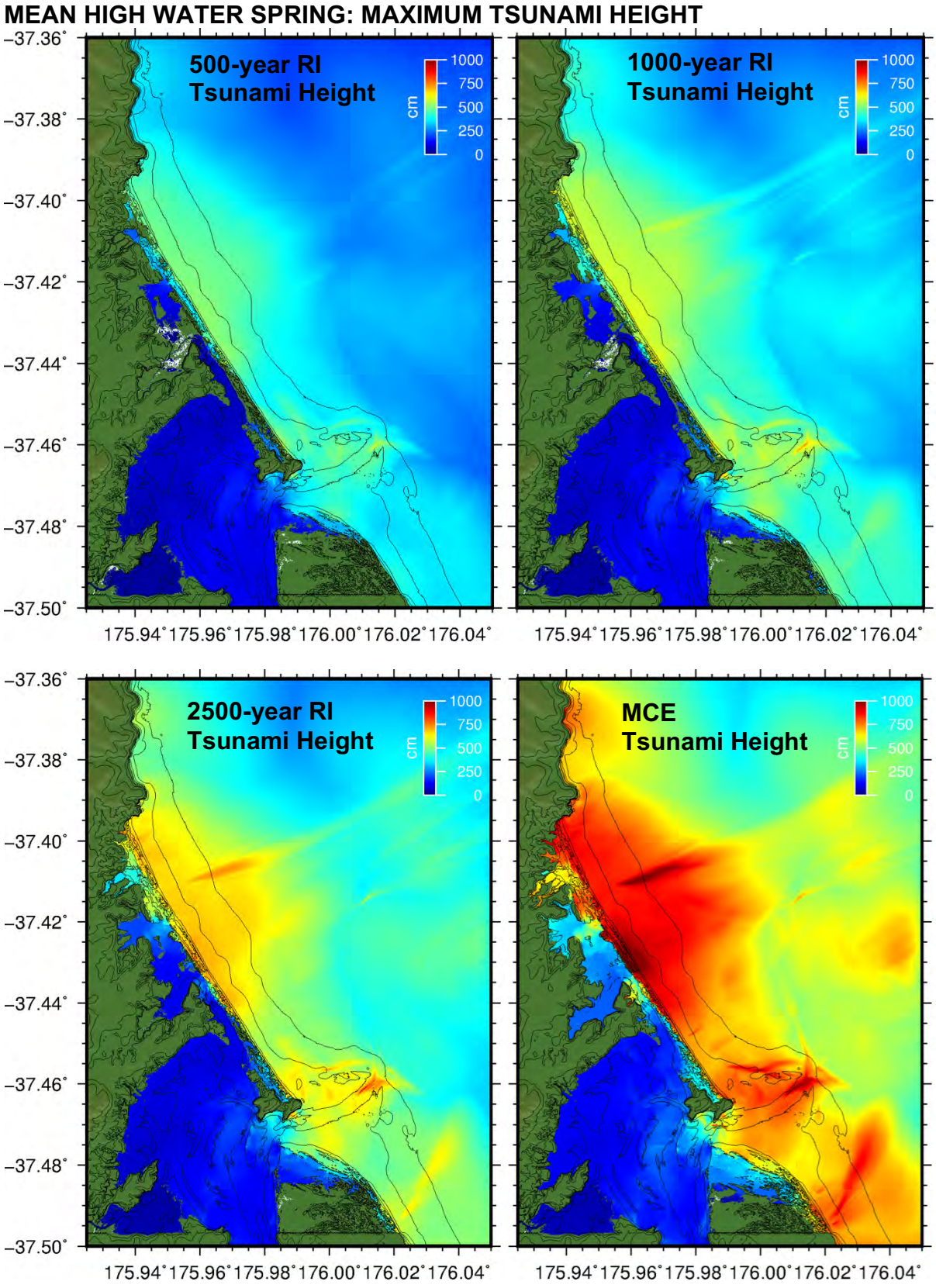

Figure 4.4 Maximum computed tsunami heights at Waihi for the 500-year, 1000-year (top L, R) 2500-year and maximum credible events (bottom L, R) at MHWS.

MEAN HIGH WATER SPRING + SLR: MAXIMUM TSUNAMI HEIGHT

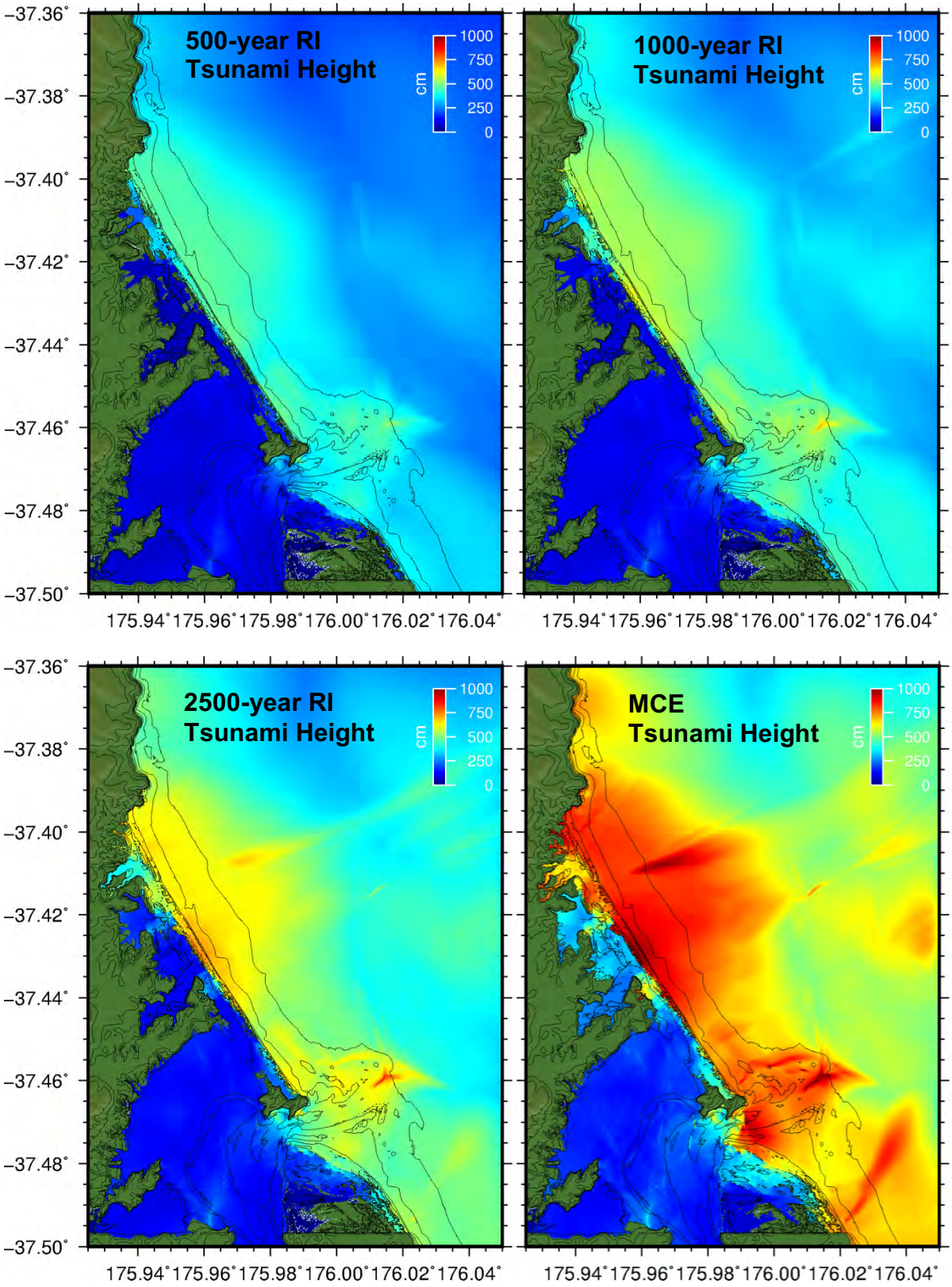

Figure 4.5 Maximum computed tsunami height at Waihi for the 500-year, 1000-year (top L, R) 2500-year and maximum credible events (bottom L, R) at MHWS + SLR.

Figure 4.6 (following page top) Maximum computed tsunami height in the A grid for Maketu/Pukehina area sources at 500-year, 1000-year (top L, R), 2500-year and MCE (bottom L, R).

Figure 4.7 (following page bottom) Maximum computed tsunami height in the B grid for Maketu/Pukehina area sources at 500-year, 1000-year (top L, R), 2500-year and MCE (bottom L, R).

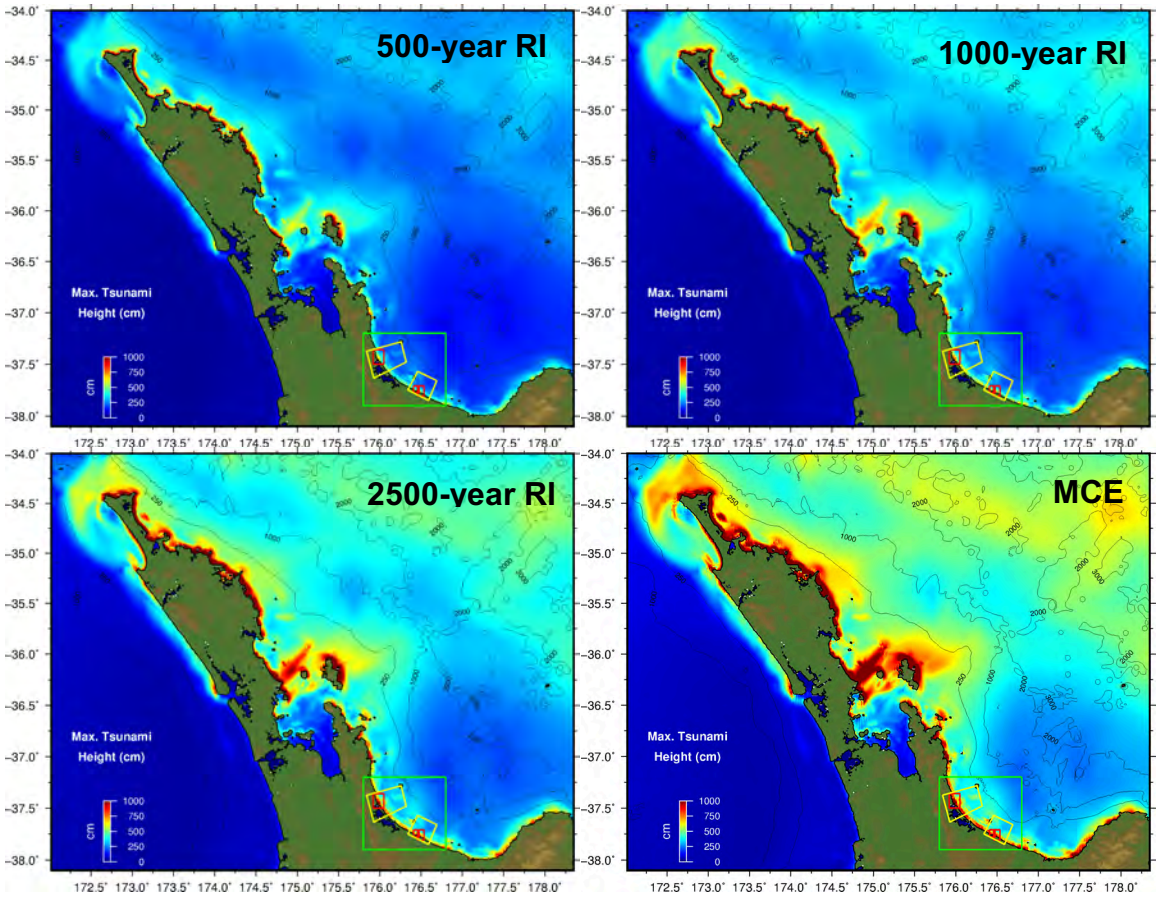
500-year RI
1000-year RI
2500-year RI
MCE
Max. Tsunami
Height (cm)
cm
1000
750
500
250
0

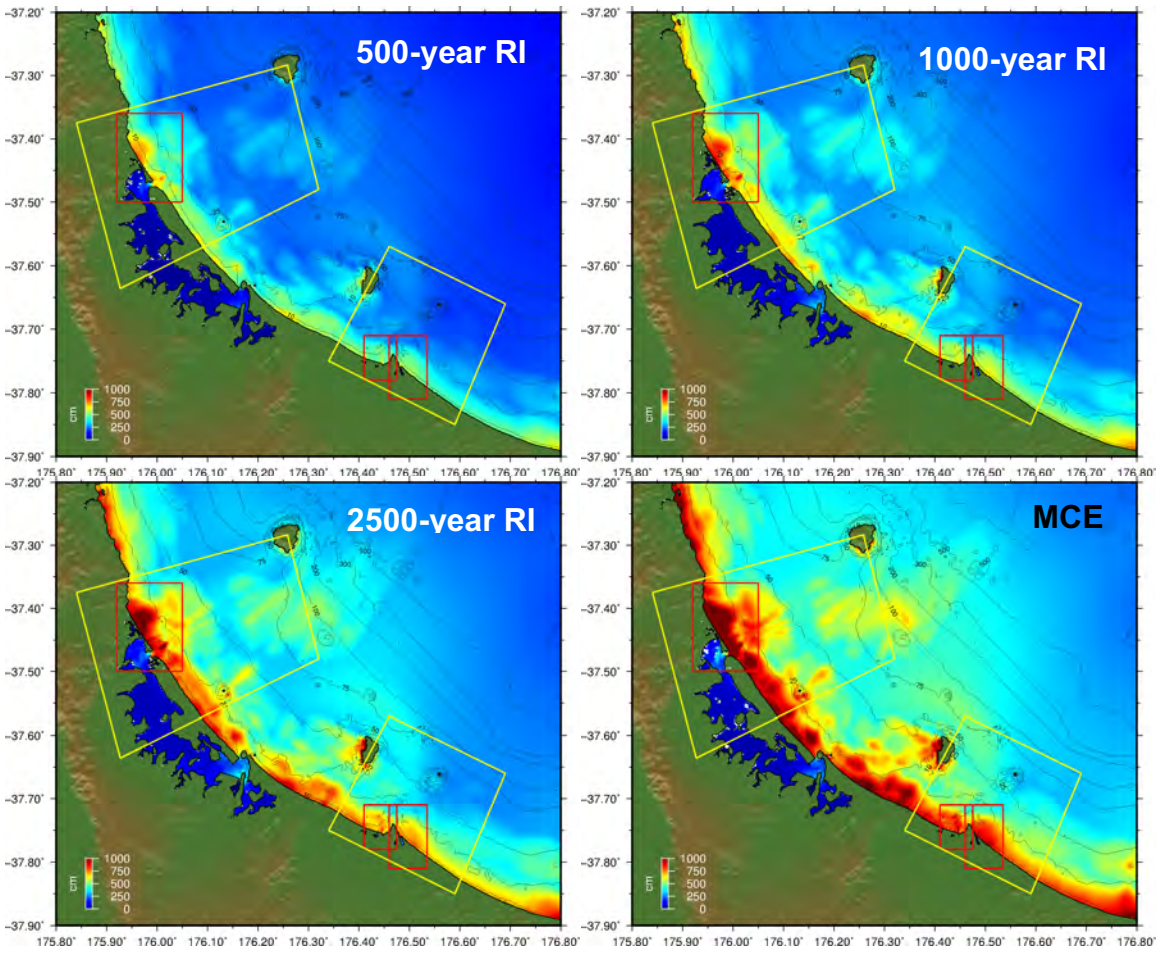
500-year RI
1000-year RI
2500-year RI
MCE
cm
1000
750
500
250
0

MEAN SEA LEVEL

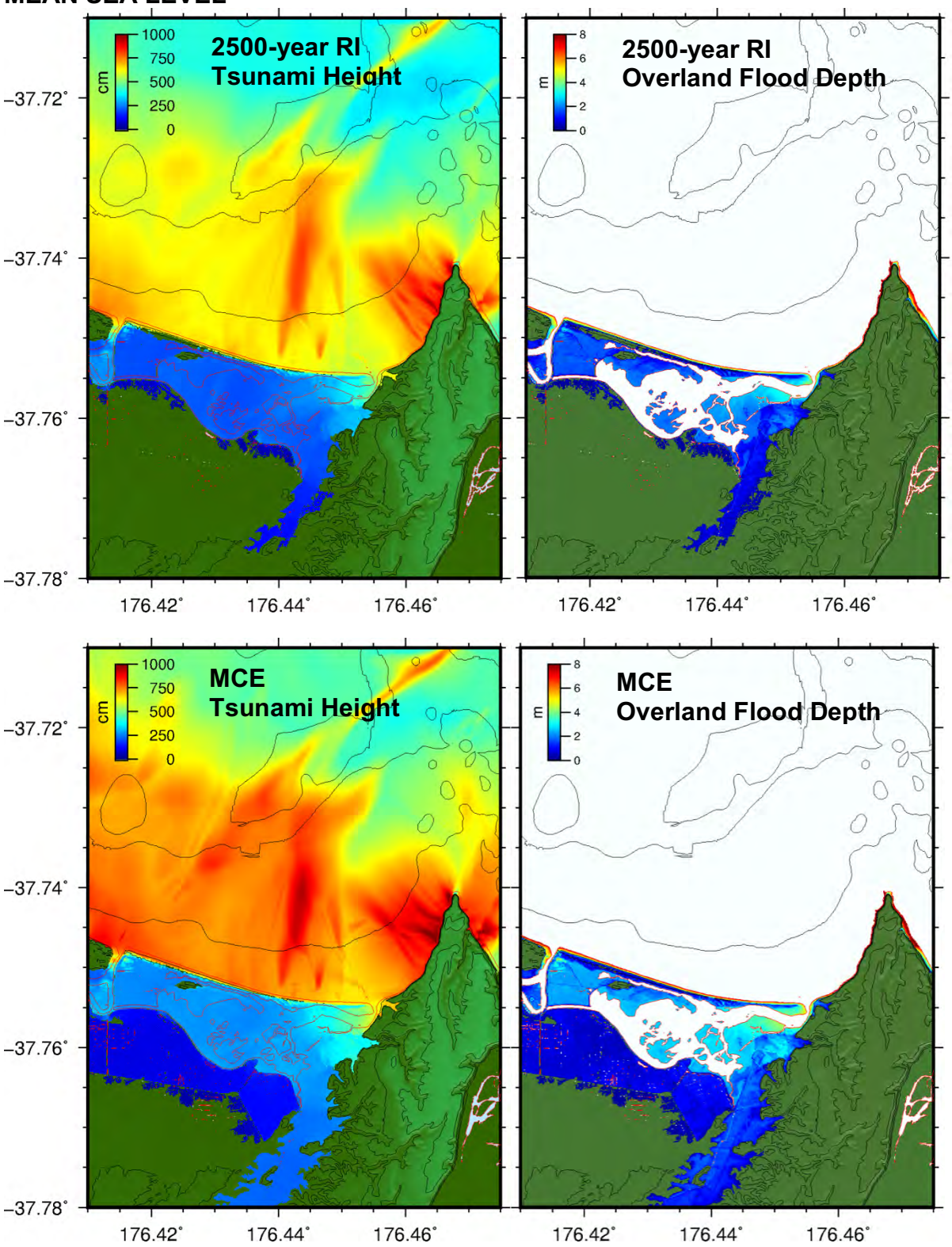

Figure 4.8 Maximum computed tsunami height (left) and overland flow depth (right) for the 2500-year event (top) and the maximum credible event (bottom) at Maketu at MSL.

MEAN HIGH WATER SPRING: MAXIMUM TSUNAMI HEIGHT

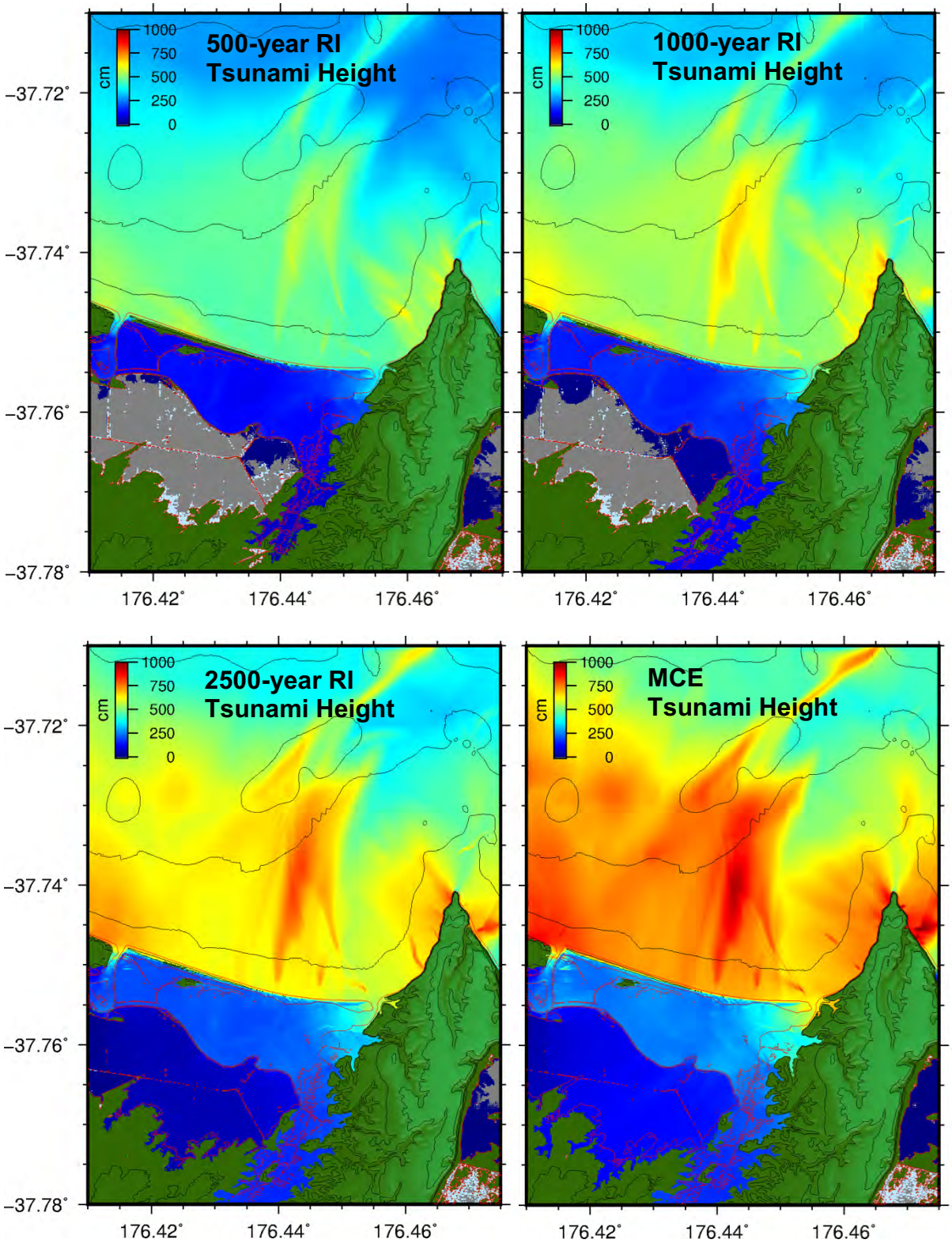

Figure 4.9 Maximum computed tsunami height at Maketu for the 500-year, 1000-year (top L, R) 2500-year and maximum credible events (bottom L, R) at MHWS.

MEAN HIGH WATER SPRING + SLR: MAXIMUM TSUNAMI HEIGHT

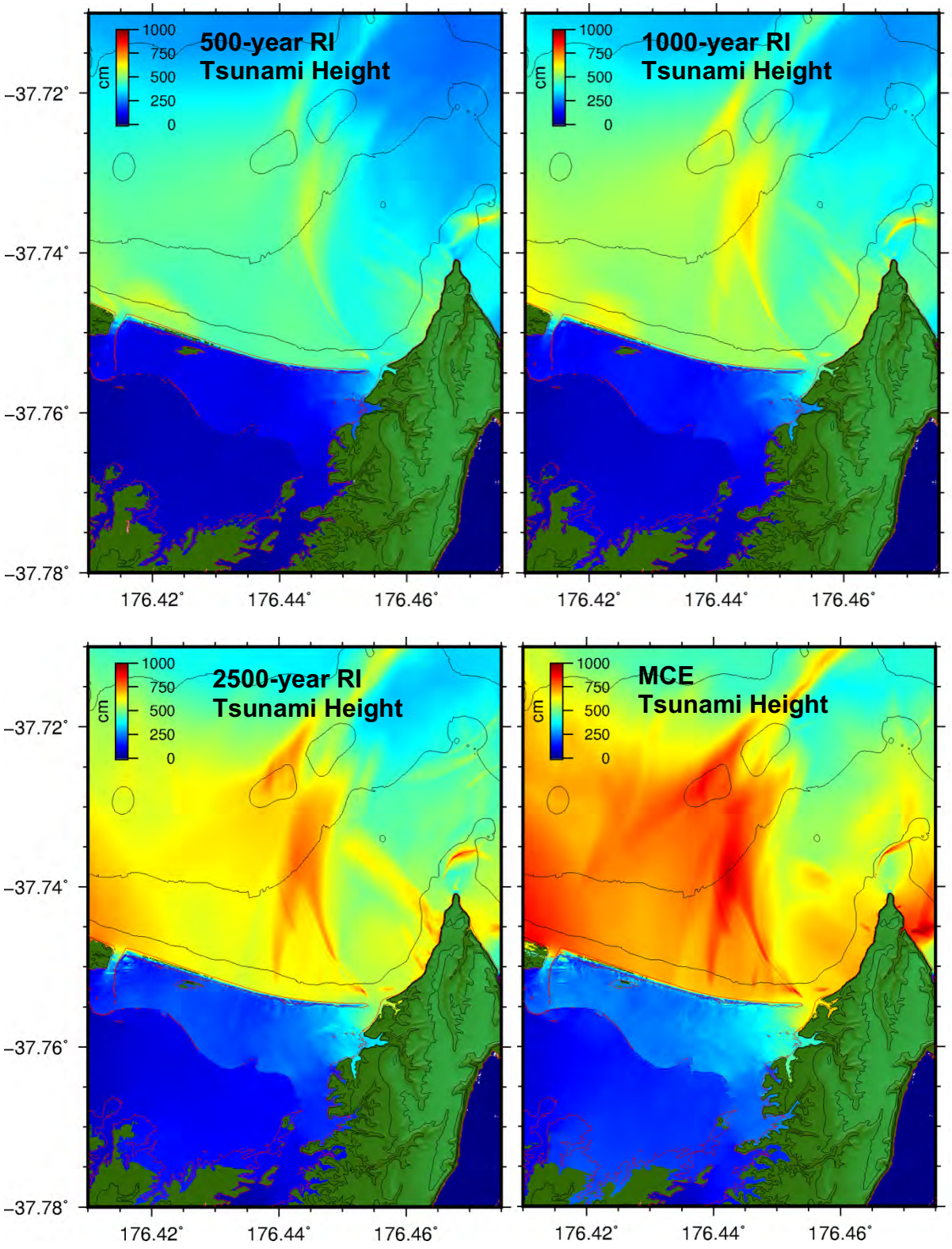

Figure 4.10 Maximum computed tsunami height at Maketu for the 500-year, 1000-year (top L, R) 2500-year and maximum credible events (bottom L, R) at MHWS + SLR.

MEAN SEA LEVEL

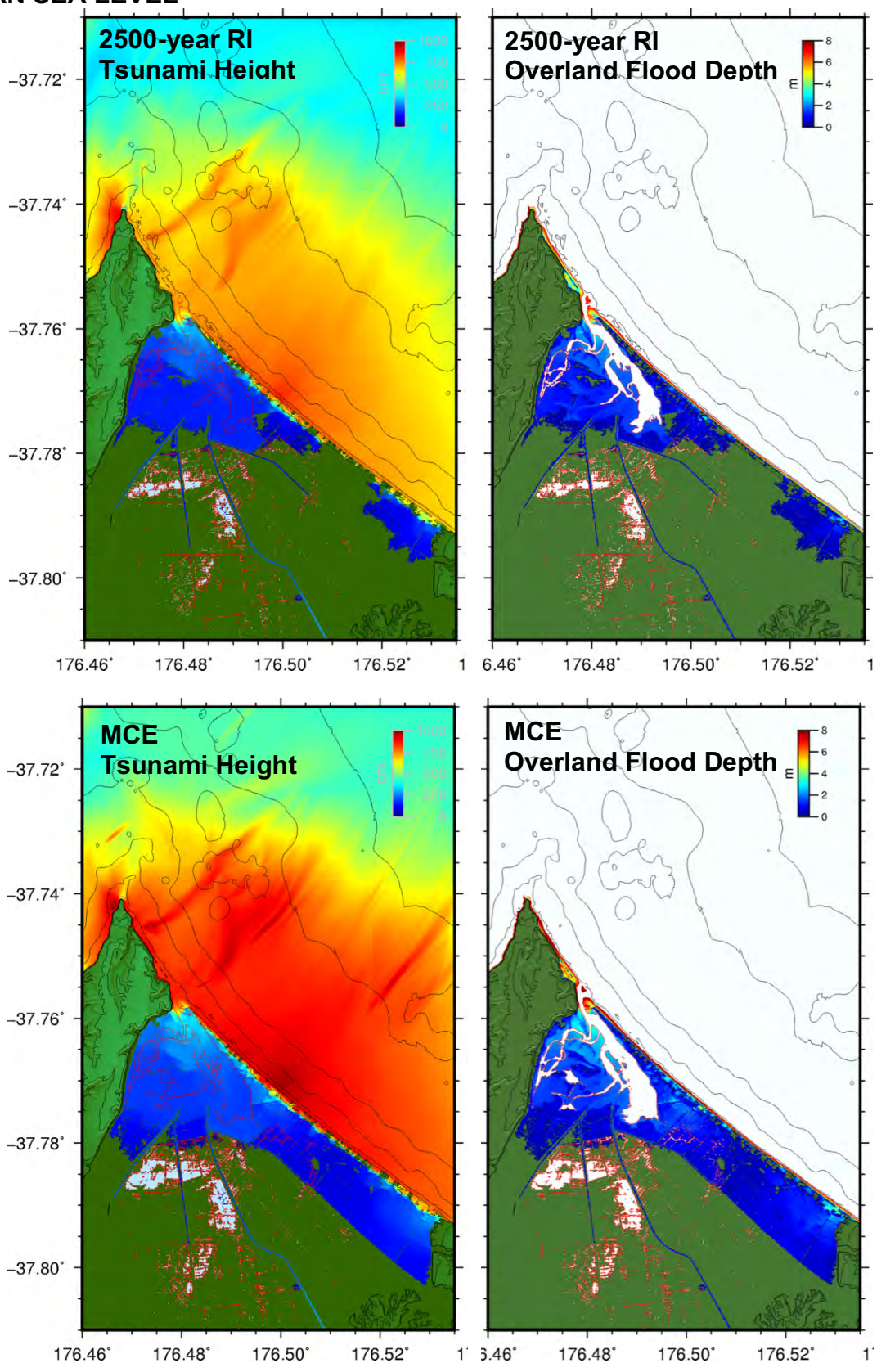

Figure 4.11 Maximum computed tsunami height (left) and overland flow depth (right) for the 2500-year event (top) and the maximum credible event (bottom) at Pukehina at MSL.

MEAN HIGH WATER SPRING

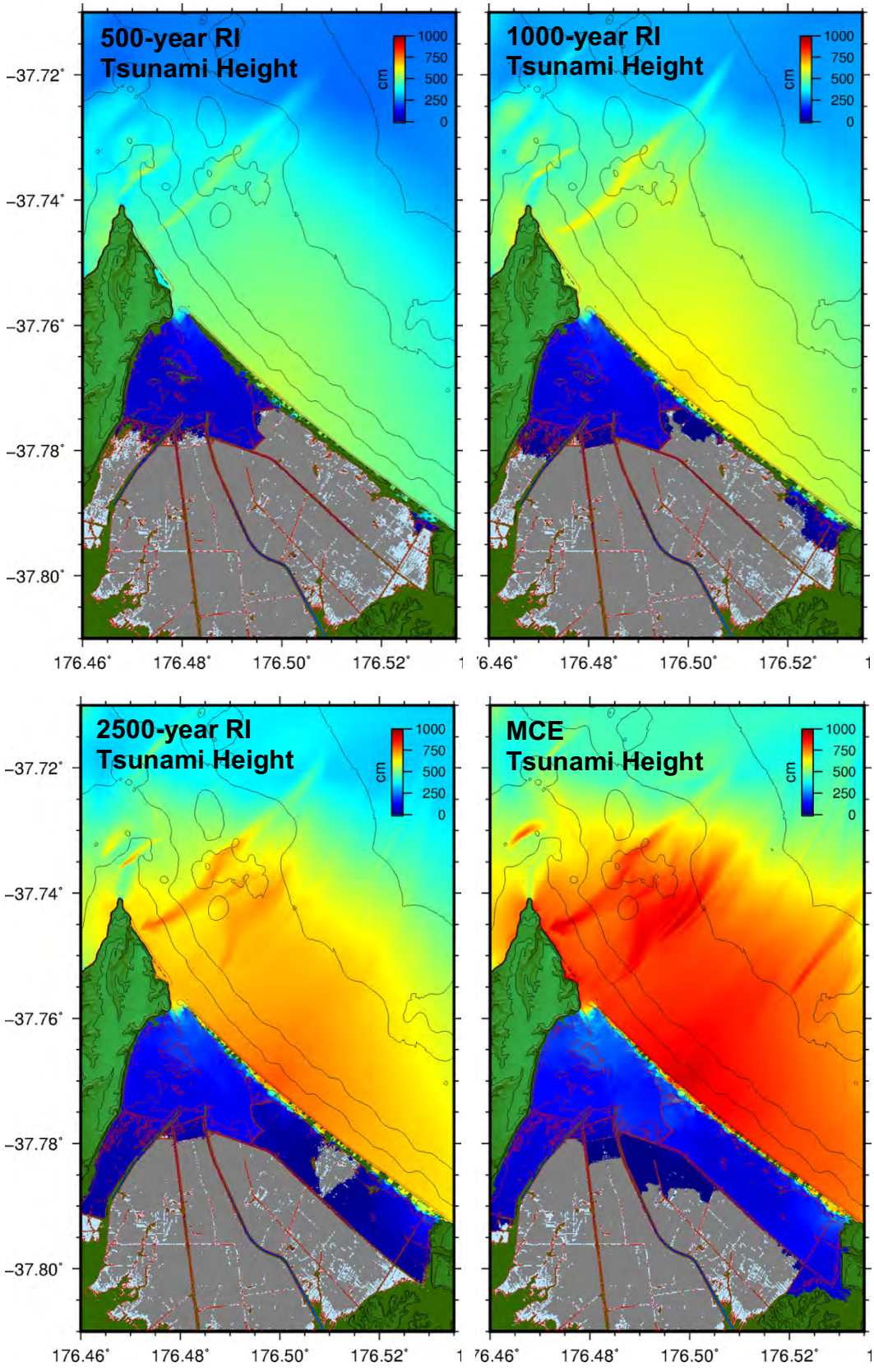

Figure 4.12 Maximum computed tsunami height at Pukehina for the 500-year, 1000-year (top L, R) 2500-year and maximum credible events (bottom L, R) at MHWS.

MEAN HIGH WATER SPRING + SLR

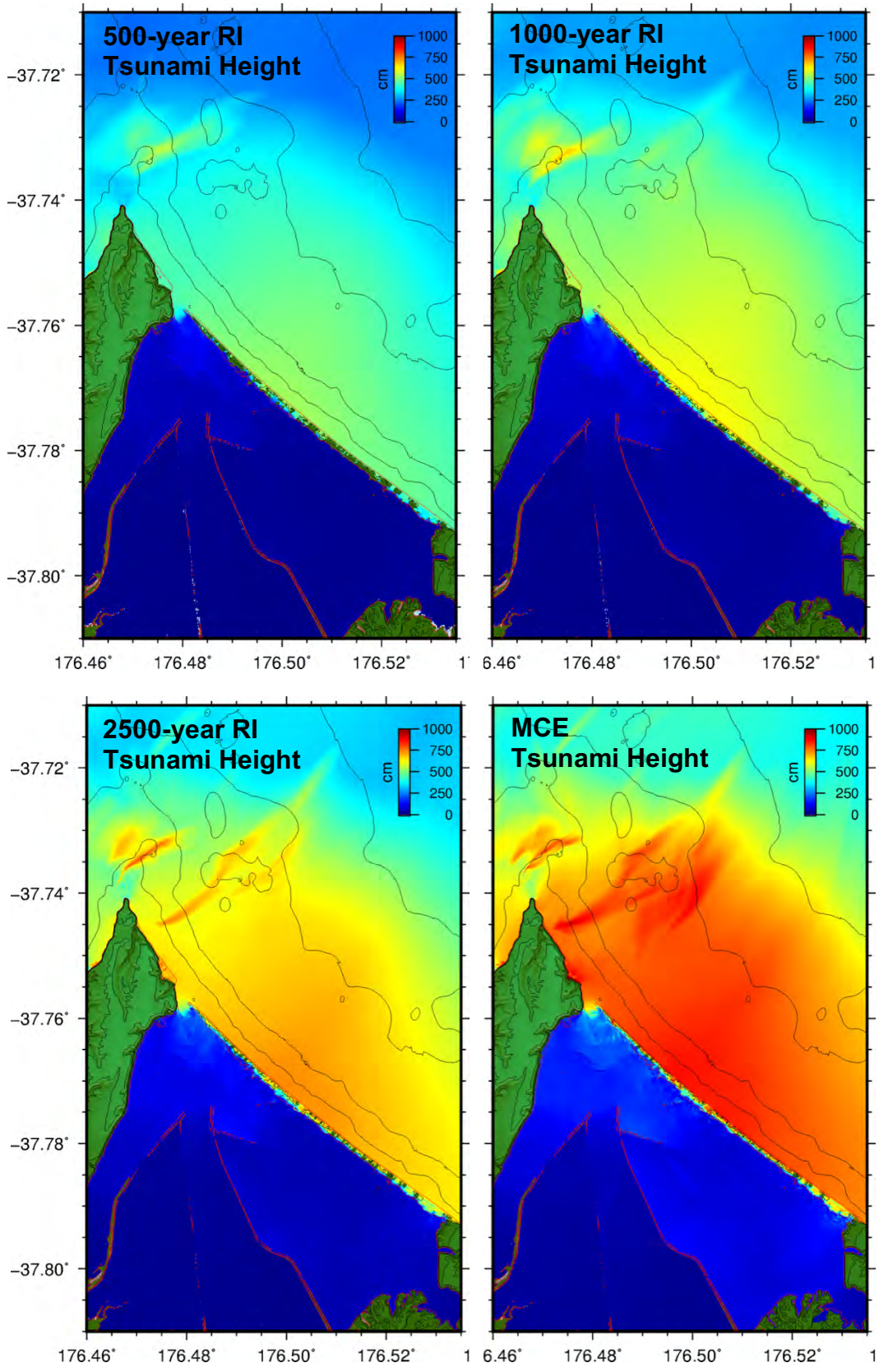

Figure 4.13 Maximum computed tsunami height at Pukehina for the 500-year, 1000-year (top L, R) 2500-year and maximum credible events (bottom L, R) at MHWS + SLR.

5 SUMMARY AND CONCLUSIONS

This study has used an existing probabilistic tsunami hazard analysis for New Zealand (Power 2013, 2014) to evaluate the tsunami inundation hazard along the coast of the western Bay of Plenty. The study used a deterministic modelling approach to match probabilistic estimates of offshore tsunami wave amplitudes.

Tsunami sources were devised to match 50th percentile offshore tsunami amplitudes at recurrence intervals of 500, 1000 and 2500-years. An additional tsunami source corresponding to the 84th percentile wave heights at 2500-year recurrence interval was also included and deemed the Maximum Credible Event.

Detailed tsunami inundation results were modelled using the ComMIT tsunami tool. Inundation assessments were run over detailed bathymetry and topography grids with 10 m resolution. From the model results estimates of the total tsunami height, tsunami overland flow depth, offshore current speeds and onshore flow speeds were provided.

These results are intended to be used by the Bay of Plenty Regional Council for detailed tsunami risk assessments within the region.

6 REFERENCES

Borrero, J., Bell, R., Csato, C., DeLange, W., Greer, D., Goring, D., Pickett, V. and Power, W. (2012). Observations, Effects and Real Time Assessment of the March 11, 2011 Tohoku-oki Tsunami in New Zealand, Pure and Applied Geophys., 170, 1229-1248, DOI 10.1007/s00024-012-0492-6

Borrero, J.C. and Greer, S.D. (2012) Comparison of the 2010 Chile and 2010 Japan tsunamis in the Far-field, *Pure and Applied Geophysics*, 170, 1249-1274, DOI 10.1007/s00024-012-0559-4.

Borrero, J.C., LeVeque, R.J., S. Dougal Greer, Sam O'Neill and Brisa N. Davis (2015) Observations and Modelling of Tsunami Currents at the Port of Tauranga, New Zealand, Proceedings of Coasts and Ports Conference, Auckland, New Zealand, September, 2015.

deLange, W.P. and Healy, T.R. (1986). New Zealand tsunamis 1840–1982. *New Zealand Journal of Geology and Geophysics*, *29*(1), 115–134. doi:10.1080/00288306.1986.10427527

GeoNet (2017), M 7.1 East Cape Fri, Sep 2 2016 http://www.geonet.org.nz/earthquake/2016p661332 Accessed June 22, 2017.

Lynett, P., Borrero, J., Weiss, R., Son, S., Greer, D., Renteria, W. (2012) Observations and Modeling of Tsunami-Induced Currents in Ports and Harbors, Earth and Planetary Science Letters, 327-328 (68-74).

New Zealand Palaeotsunami Database (2017). https://ptdb.niwa.co.nz, Accessed June 2017.

Percival, D, Denbo, D, Eble, M, Gica, E, Mofjeld, H, Spillane, M, Tang, L, and Titov, V (2010). Extraction of tsunami source coefficients via inversion of DART buoy data, Nat. Haz. doi:10.1007/s11069-010-9688-1.

Power, W. L. (2013). Review of Tsunami Hazard in New Zealand (2013 Update) GNS Science Consultancy Report No. 2013/131, 238 pages.

Power, W. L. (2014). Tsunami hazard curves and deaggregation plots for 20km coastal sections, derived from the 2013 National Tsunami Hazard Model GNS Science Consultancy Report No. 2013/59, 558 pages.

Titov, V. V., & González, Frank, I. (1997). *Implementation and testing of the Method of Splitting Tsunami (MOST) model* (No. ERL PMEL-112) (p. 14). Retrieved from http://www.pmel.noaa.gov/pubs/PDF/tito1927/tito1927.pdf

Titov, V. V., Moore, C. W., Greenslade, D. J. M., Pattiaratchi, C., Badal, R., Synolakis, C. E., & Kânoğlu, U. (2011). A New Tool for Inundation Modeling: Community Modeling Interface for Tsunamis (ComMIT). *Pure and Applied Geophysics*, *168*(11), 2121–2131. doi:10.1007/s00024-011-0292-4

Titov, V.V., and C.E. Synolakis (1995): Modeling of breaking and nonbreaking long wave evolution and runup using VTCS-2. *J. Waterways, Ports, Coastal and Ocean Engineering*, 121(6), 308–316.

USGS (2017) M 7.0 - 175km NE of Gisborne, New Zealand https://earthquake.usgs.gov/earthquakes/eventpage/us10006jb, accessed on June 22, 2017.

Wei, Y., Chamberlin, C., Titov, V. V., Tang, L., & Bernard, E. N. (2012). Modeling of the 2011 Japan Tsunami: Lessons for Near-Field Forecast. *Pure and Applied Geophysics*, *170*(6–8), 1309–1331. http://doi.org/10.1007/s00024-012-0519-z

Wei, Y, Newman, A, Hayes, G, Titov, V, Tang, L (2014). Tsunami Forecast by Joint Inversion of Real-Time Tsunami Waveforms and Seismic or GPS Data: Application to the Tohoku 2011 Tsunami. Pure Appl. Geophys. doi:10.1007/s00024-014-0777-z

7 APPENDIX 1: WAIHI BEACH: GRID SIZE SENSITIVITY STUDY

Although not part of the project scope, a sensitivity study on the inundation and overland flow depths as a function of model grid resolution was conducted. For this analysis, the 2500-year RI event was run over three model set ups each using the same outer A and B level grids. The innermost C-level grids were run for three different resolutions 50-m, 20-m and 10-m. The model grid details are presented in Table 7.1. The model was run over the mean sea level bathymetry.

Table 7.1 Grid resolutions, time steps and model run-times for the sensitivity study.

Grid	nx	ny	dx	dt	Run time
	(nodes)	(nodes)	(m)	(sec)	(min)
A	458	365	1254.8	6.71	n/a
B	443	389	199.7	2.27	n/a
Waihi Beach					
C: 50 m	222	312	50.0	2.49	26
C: 20 m	554	778	20.1	1.0	86
C: 10 m	1107	1555	10.0	0.5	534

The raw model results are presented in Figure 7.1 showing the computed flow depths over each of the three grid resolutions. In Figure 7.2 we plot the model results along a shore normal transect both for both the original grid spacing (i.e. 10, 20 or 50 m) as well as for grids interpolated to 10 m resolution.

To assess the differences, the results from the coarser (20 and 50-meter grids) were interpolated to a 10 m grid. Then a difference plots were made by subtracting the interpolated gird results from the original 10 m grid, i.e.:

- 10 m results MINUS interpolated 20 m results and
- 10 m results MINUS interpolated 50 m results.

The resulting data set would produce positive numbers where the 10 m flow depths are greater and negative numbers where the 20 or 50 m results were larger. These difference plots are presented in Figure 7.3 and Figure 7.4 for the full grid extents and close-up regions respectively.

The difference plots show that at the shoreline, the model produce higher flow depths on the finer scale grids, but that as the flow proceeds inland, the coarser grids produce greater flow depths

The full set of model results are presented in Figure 7.5 through Figure 7.7 with plots for maximum computed tsunami height, tsunami current speed, overland flow depth and overland flow speed.

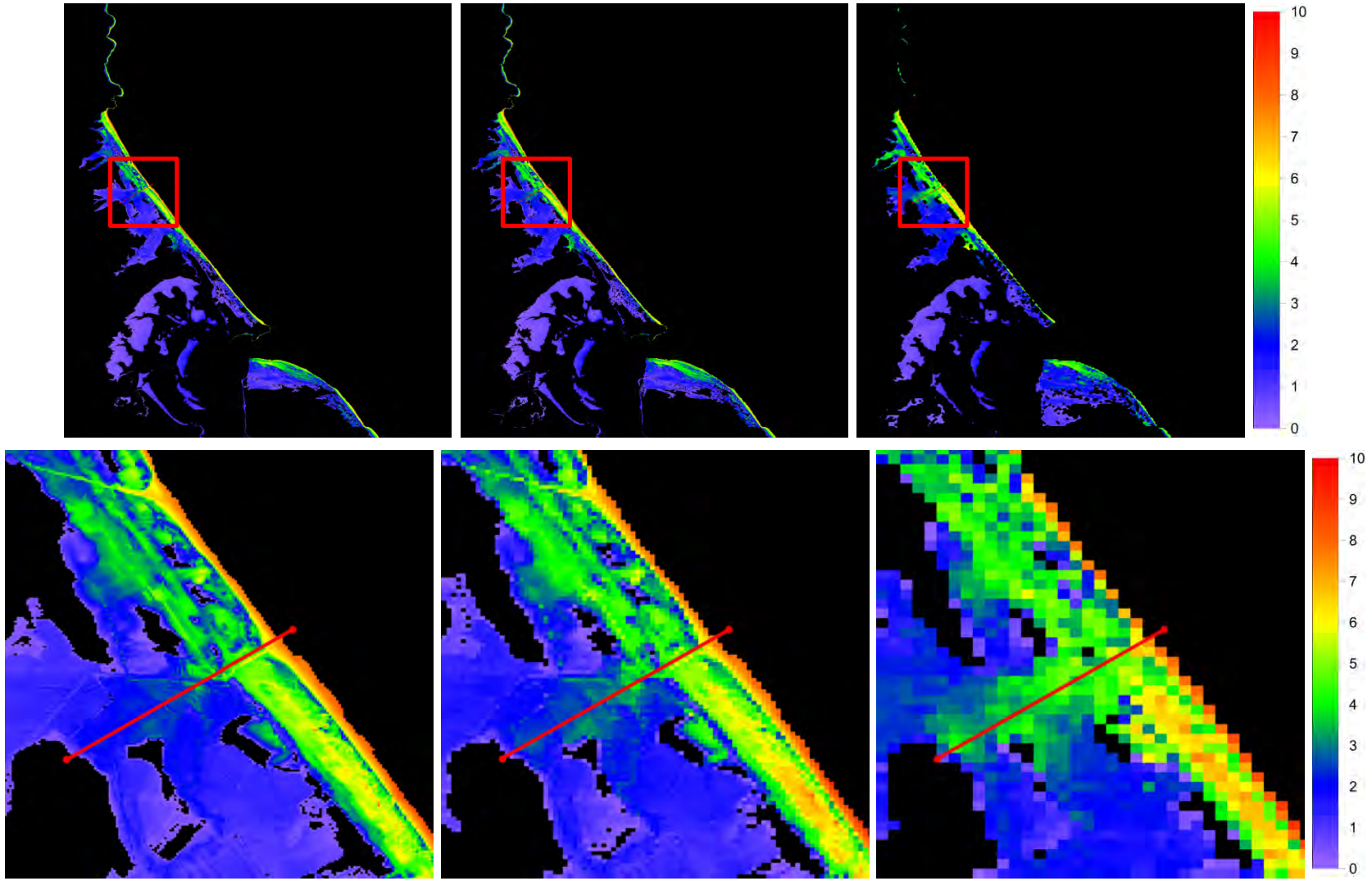

Figure 7.1 Flow depth over the 10 m (left) 20 m (middle) and 50 m (right) grids. Zoomed area is indicated by the red rectangle.

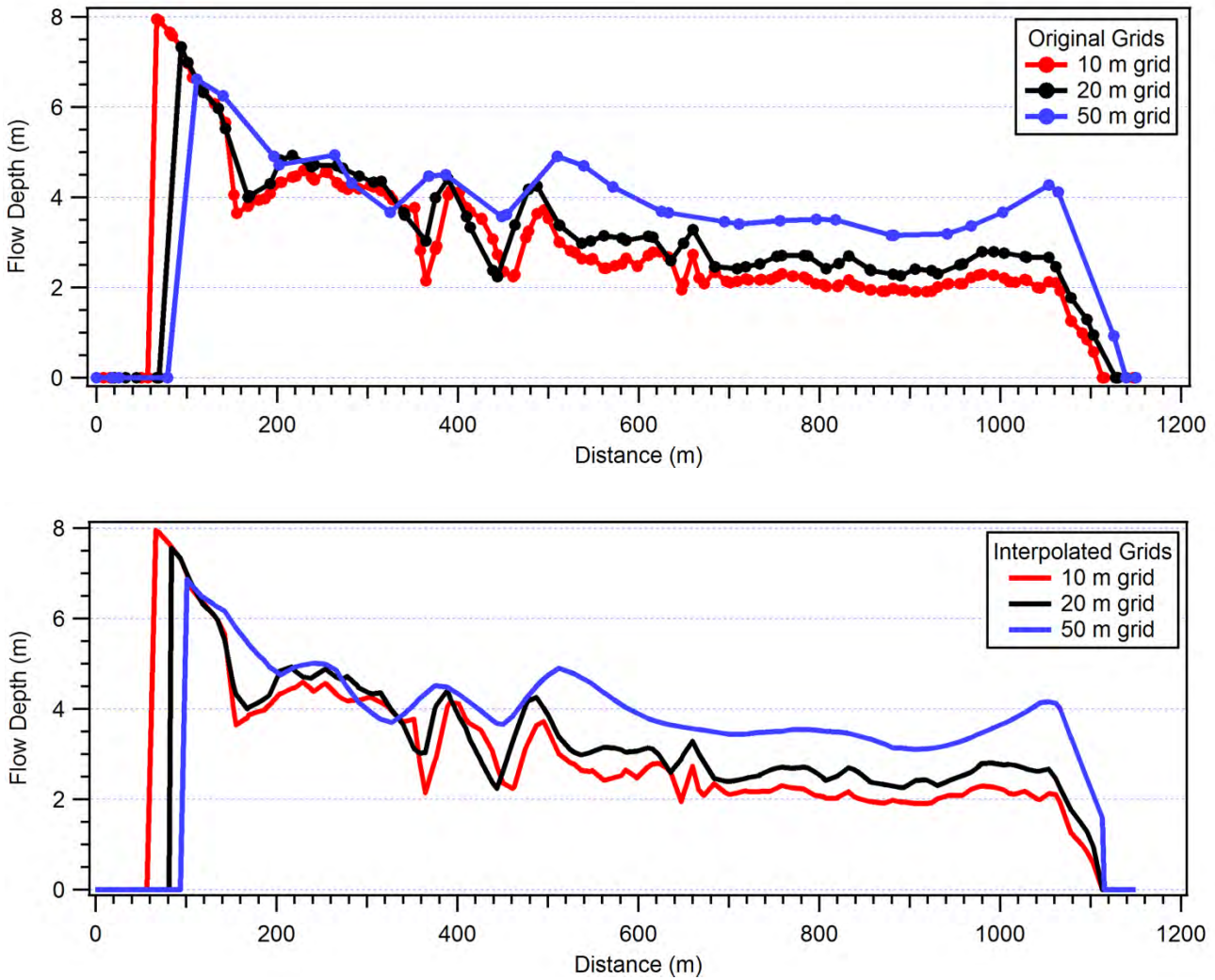

Figure 7.2 Computed maximum flow depths along the transects indicated in Figure 7.1 above.

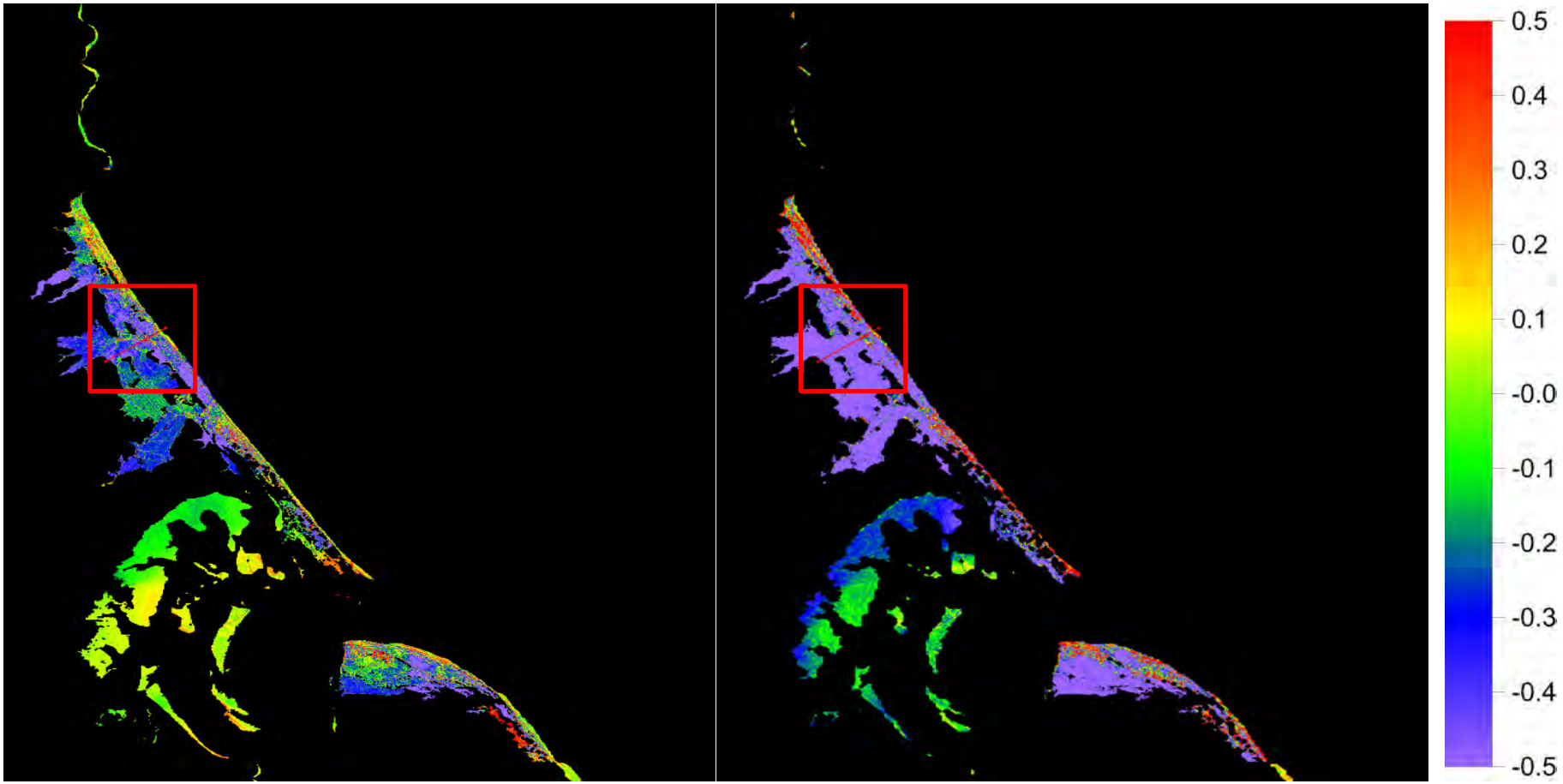

Figure 7.3 Difference in computed flow depth. 10 m results MINUS 20 m results (left) and 10 m results MINUS 50 m results (right). Colour scale is in meters.

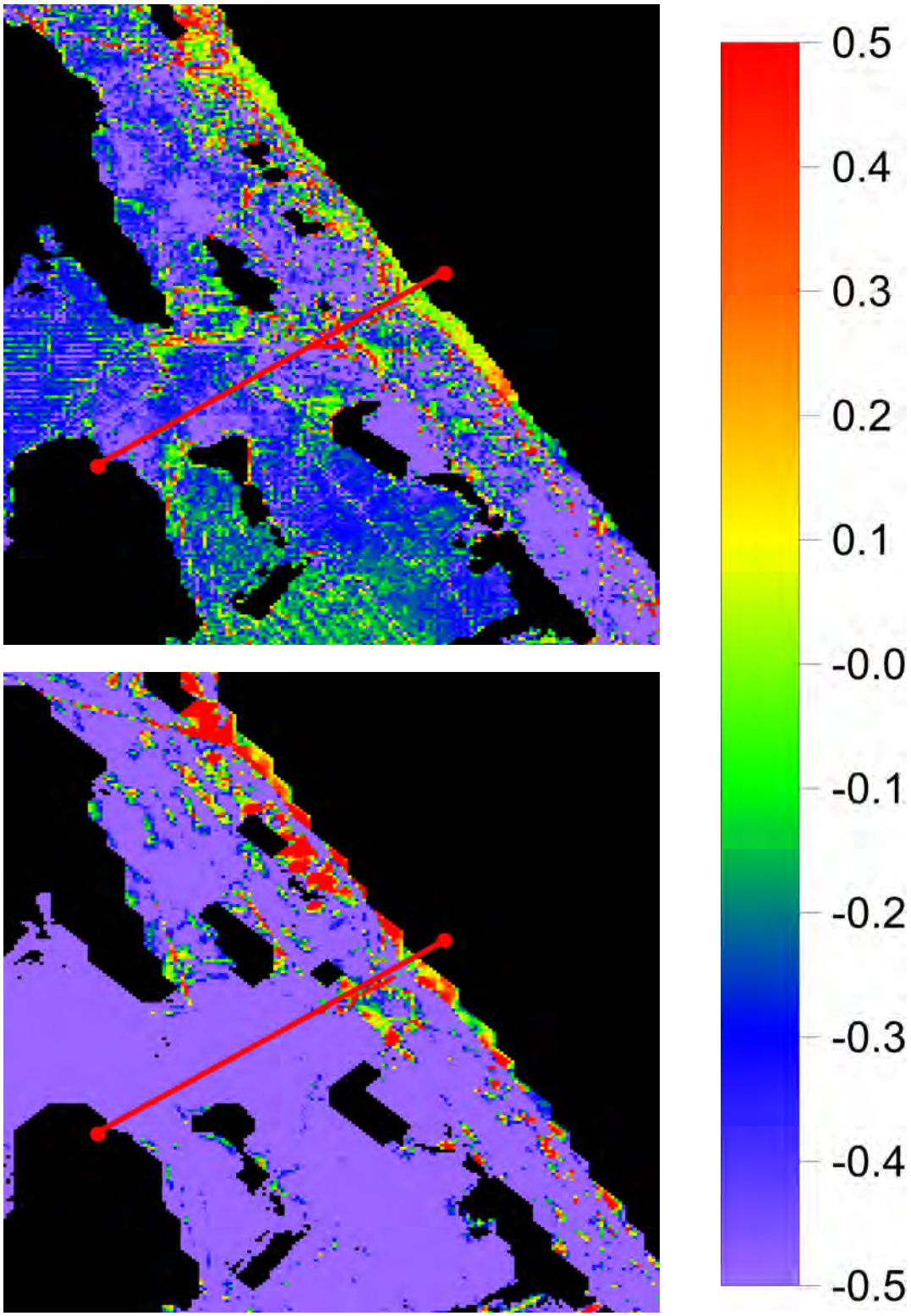

Figure 7.4 Difference in computed flow depth. 10 m results MINUS 20 m results (top) and 10 m results MINUS 50 m results (bottom). Colour scale is in meters.

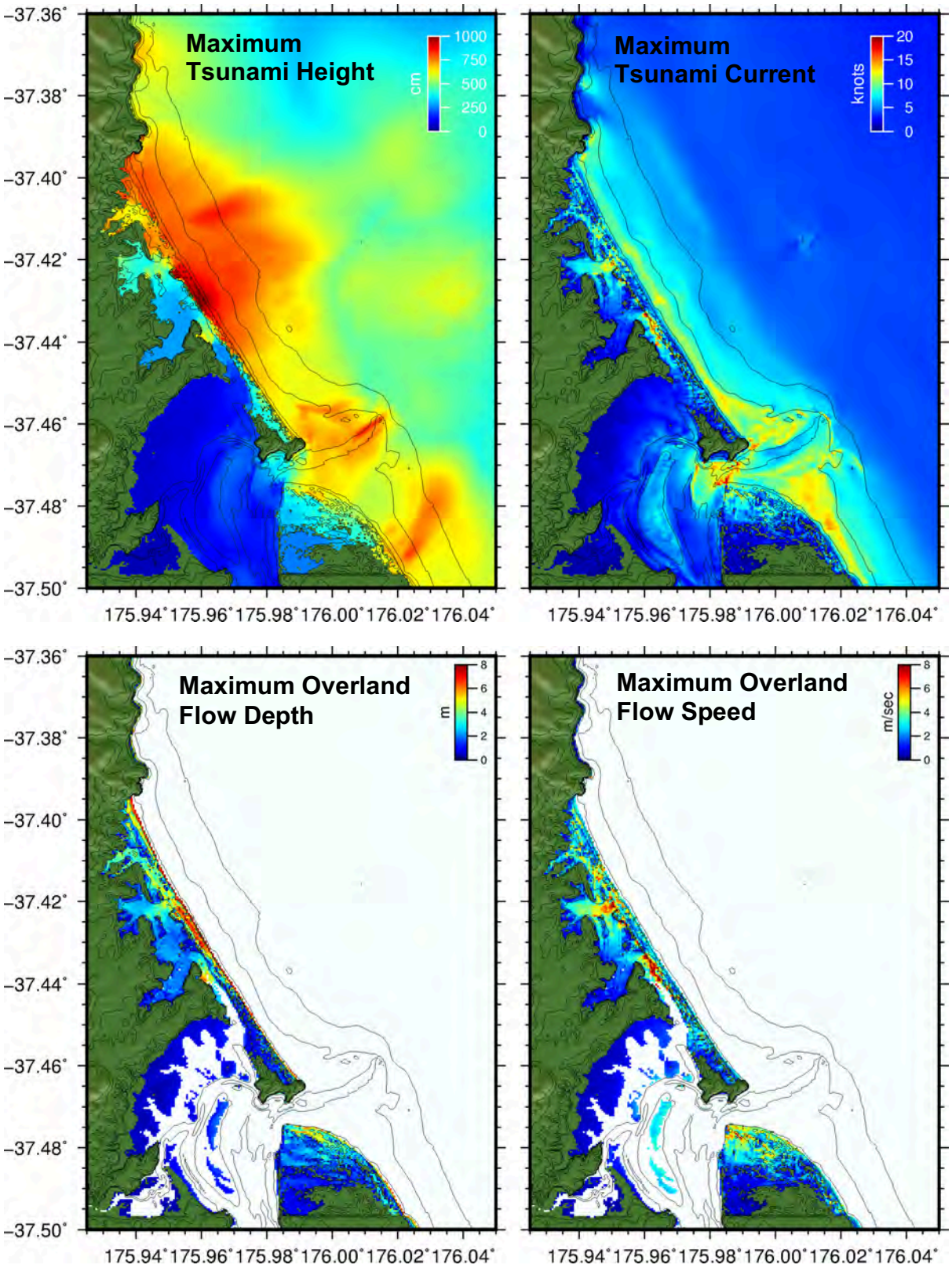

Figure 7.5 Model results for the 50-m C grid

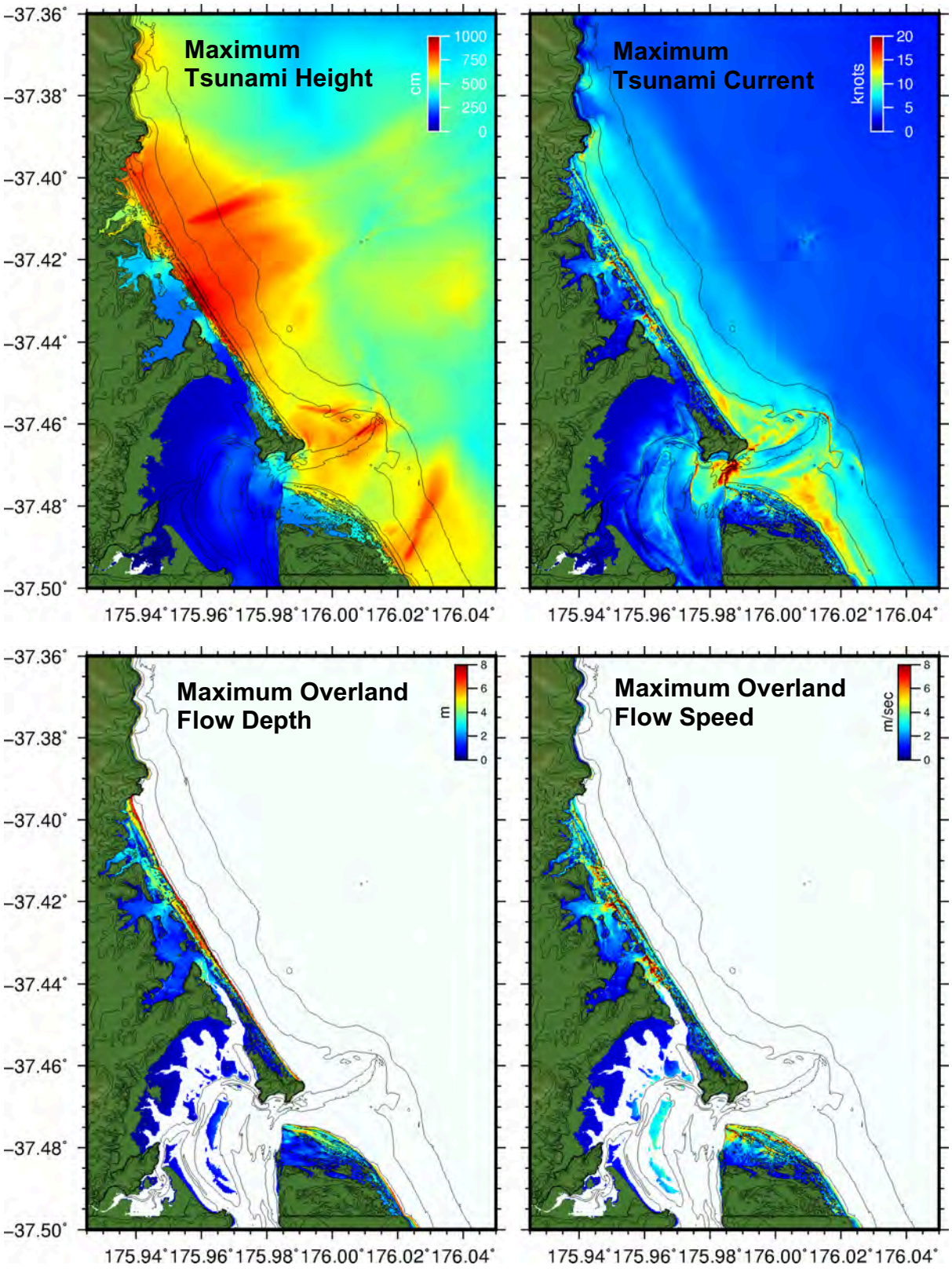

Figure 7.6 Model results for the 20-m C grid

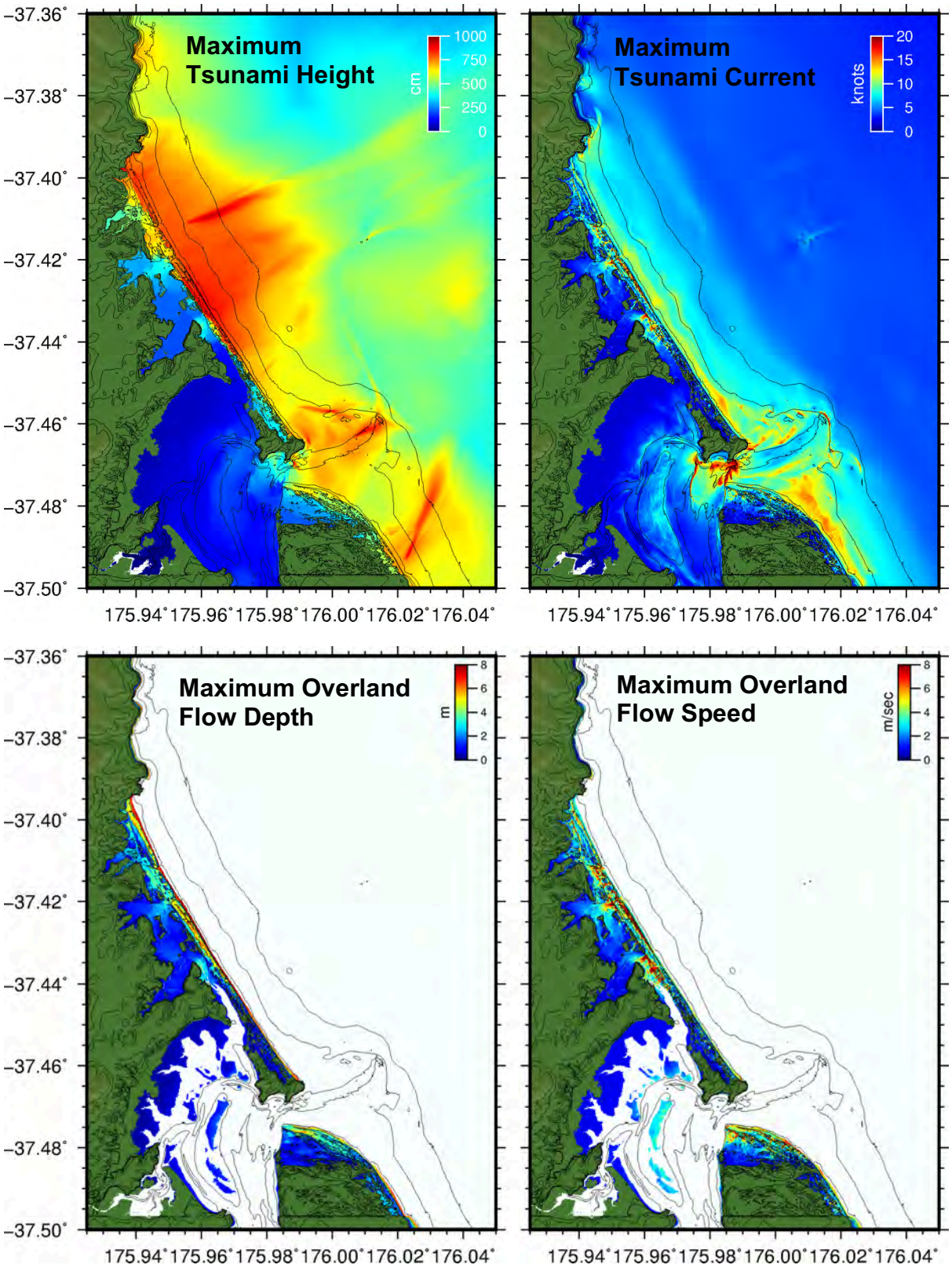

Figure 7.7 Model results for the 10-m C grid

8 APPENDIX 2: PUKEHINA AND LITTLE WAIHI ESTUARY: FLOODED AREAS SENSITIVITY STUDY

Due to the fact that large expanses of the inland areas sit just at or below sea level, raising the water level datum from MSL to MHWS results in these areas being located below the static water level at the initialization of the model run. In reality, these areas remain 'dry' because they are separated from the open ocean by elevated levees, stop banks or road beds. However, in the a numerical model, there is no practical way for the model to differentiate between areas that are truly 'wet' because they are below the static water level and are hydraulically connected to the sea and areas that lie below sea level but are actually 'dry'. In these situations, the model see these areas essentially as 'inland lakes'.

This problem was particularly evident for the Pukehina model domain. The model grid bathymetry for this region at MHWS is shown in Figure 8.1. It is evident that the area inland of the Little Waihi estuary lies largely between 0.0 and 0.8 m below the MHWS water level.

Because this regions would contain a thin layer of numerical 'water', we conducted a model sensitivity study to explore the effect of this on the model results. For this analysis we used the 2500-m RI source. The first model run was conducted over the MSL bathymetry as this water level does not present the issue with large expanses of grid nodes situated below the static water level. The results from this run are presented in Figure 8.2 where we see that the tsunami surge is largely stopped by the dykes and stop banks located along the inland extents of the Little Waihi estuary. The tsunami surge overtops the western and eastern ends of the Pukehina Beach sand spit. The central section is not overtopped.

Next in Figure 8.3, we present the model results for the 2500-year RI event over the MHWS topography. The grey regions in the plots are areas that were below sea level (i.e. 'wet') at the start of the model run and were subsequently never inundated during the model run. Problems arise in the plotting of the 'flow depth' for this case. This is because 'flow depth' is defined as the depth of the tsunami surge over grid nodes that started the model run as 'dry' and were subsequently inundated. This is calculated by subtracting the topographic height from the tsunami height, i.e. if a tsunami surge with a height of 8 m flows over ground with a topographic height of 2 m, the resulting flow depth is 6 m. Hence, since these nodes started the model run as 'wet' they are masked out of the flow depth computation and no flow depth can be calculated at these points resulting in the large expanses of white in the lower panels of Figure 8.3.

In an effort to improve the graphical output for these cases, we investigated the effect of raising these areas to be above the static water level. This is shown in Figure 8.4 for the case with the topography raised to 0.15 m above MHWS. The resulting inundation pattern is markedly different from the previous cases and extends well inland, completely covering large expanses of the agricultural lands inland from the Little Waihi estuary. This extensive inundation can be attributed to the fact that the topography is perfectly smooth. Although there is friction in the model, it does not significantly retard the flow and the inundation extents are largely governed by the presence of high topographical relief in the form of a stop bank or elevated road way.

Thinking that small-scale topographic irregularities contributed to the reduction in the inundation extents, we next tried a case where the areas that were set to +0.15 m above MHWS were seeded with random noise following a Gaussian distribution having a standard deviation of +/- 0.1 m. These results are shown in Figure 8.5 where it can be seen that the added topographic variability does indeed reduce the inundation extents, however the results still seem unrealistic. Another case was trialled with the standard deviation of the topographic roughness increased to +/- 0.25 m and these results are presented in Figure 8.6. Here it can be seen that the increased magnitude of the topographic roughness further reduces the inland extent of the inundation, with the inundation pattern approaching that of the un-modified MHWS topography. Ultimately due to the lack of compelling calibration evidence, it was decided that running the model on the unmodified bathymetry was the best approach.

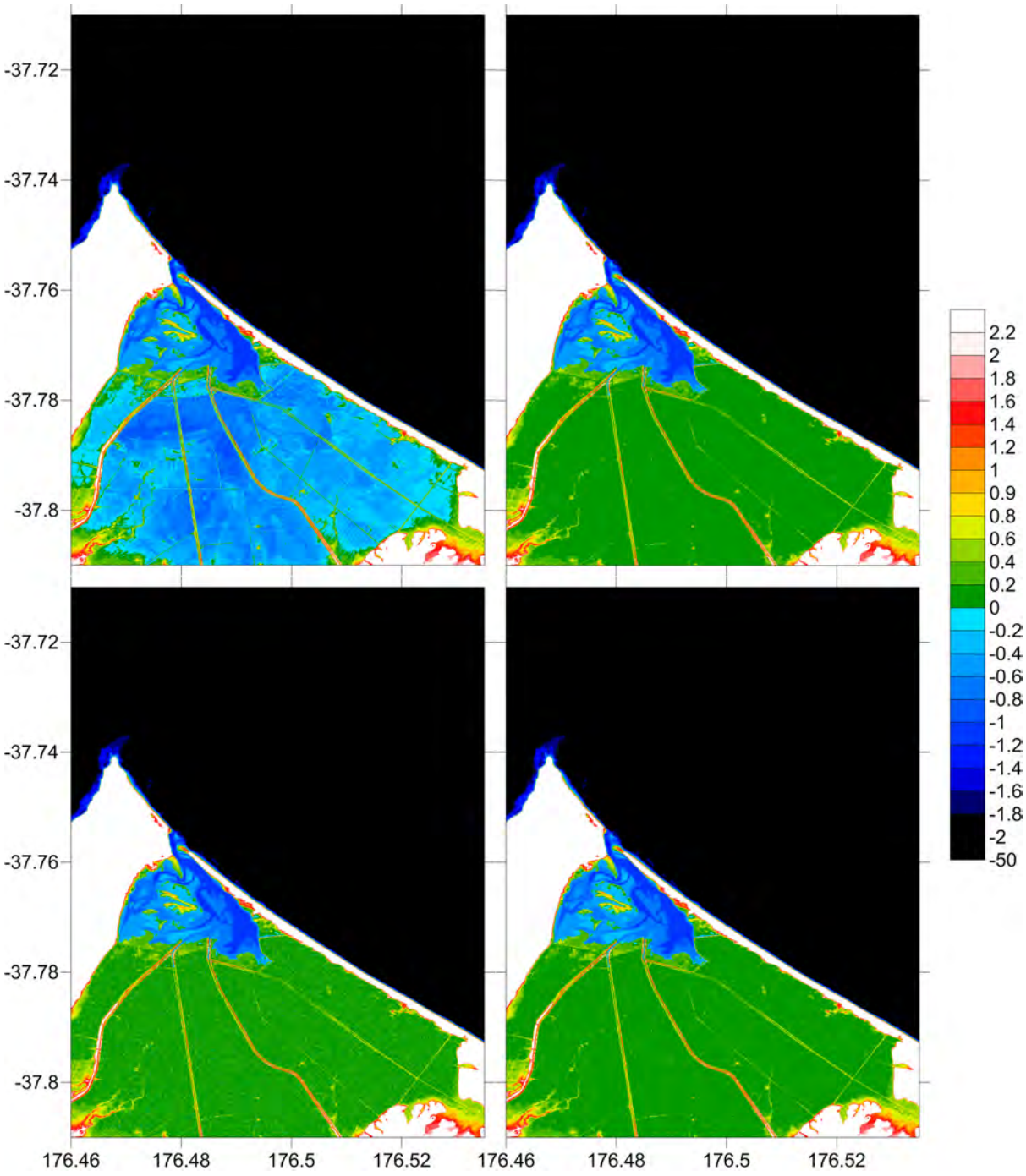

Figure 8.1 Topography of the different grids trialled. Top left: the original MHWS topography. Top right: the MHWS topography with inland areas raised up to +0.15 m MHWS. Bottom left: inland areas seeded with random noise SD = 0.25 m. Bottom right: inland areas seeded with random noise SD = 0.1 m. Regions above 2 m height and below 2 m depth are coloured white and black respectively.

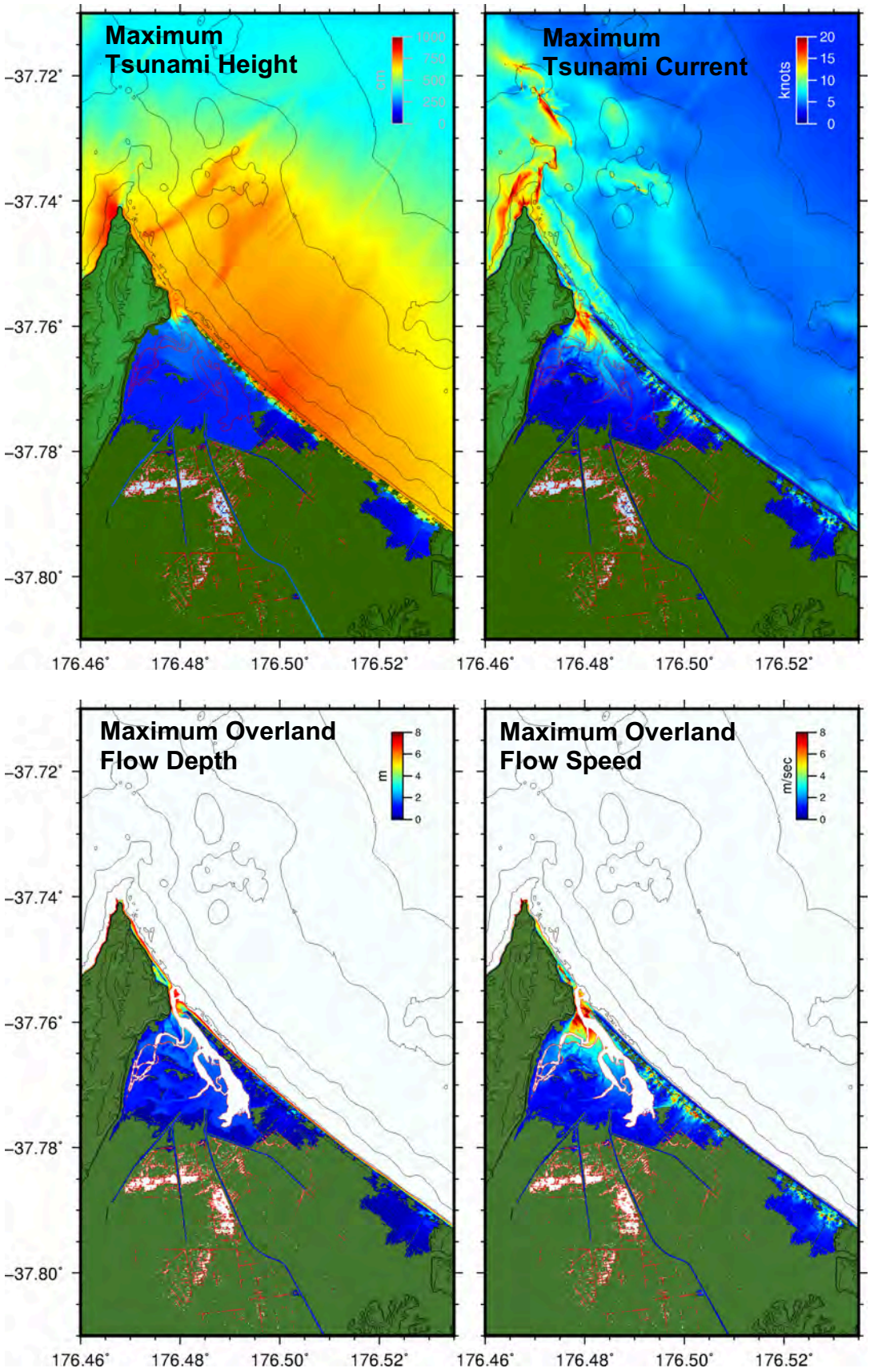

Figure 8.2 2500 year RI event over MSL topography.

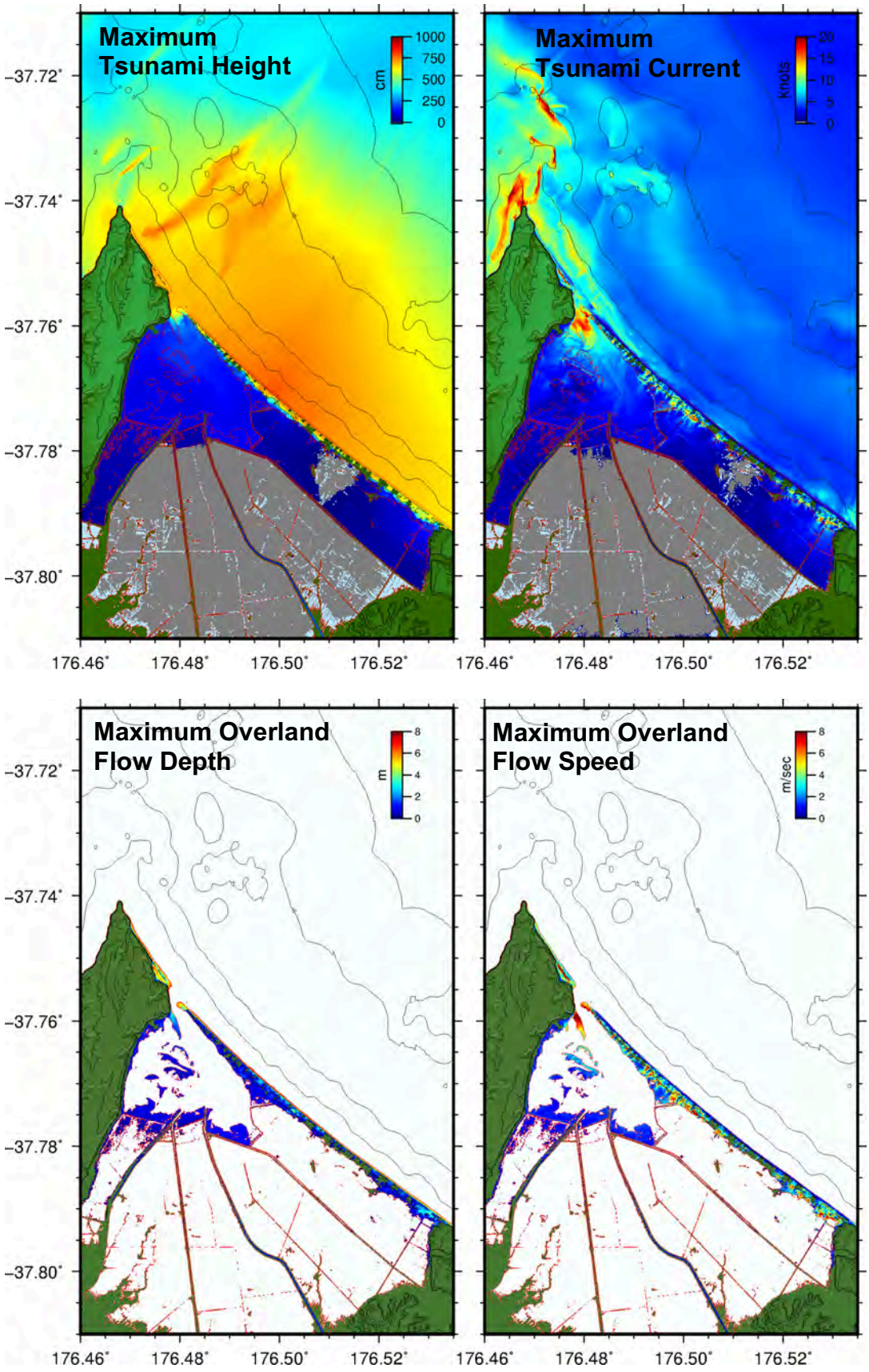

Figure 8.3 2500 year RI over unmodified MHWS topography.

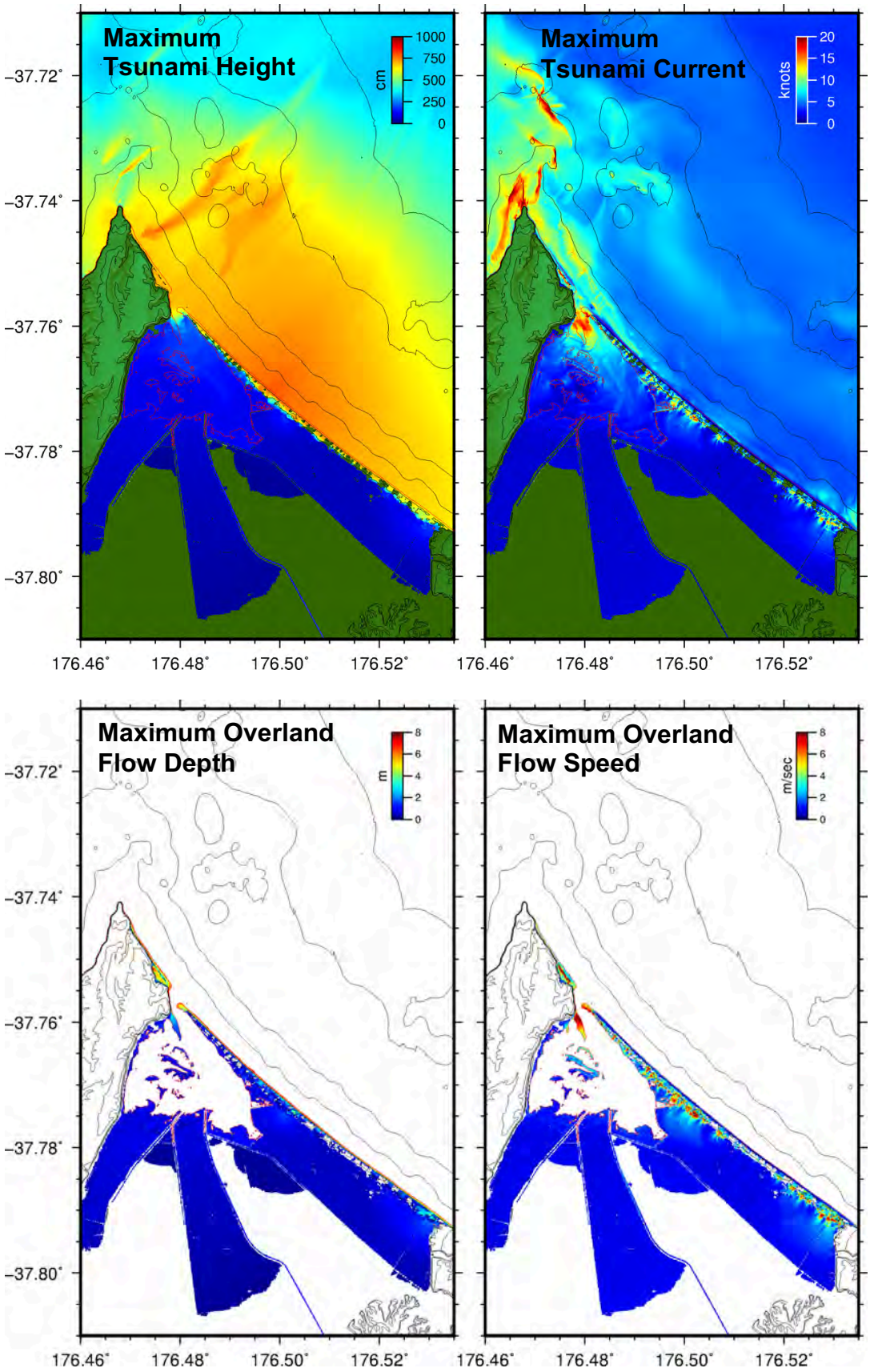

Figure 8.4 2500 year RI over MHWS topography. Land uniformly filled to +0.15 m above MHWS.

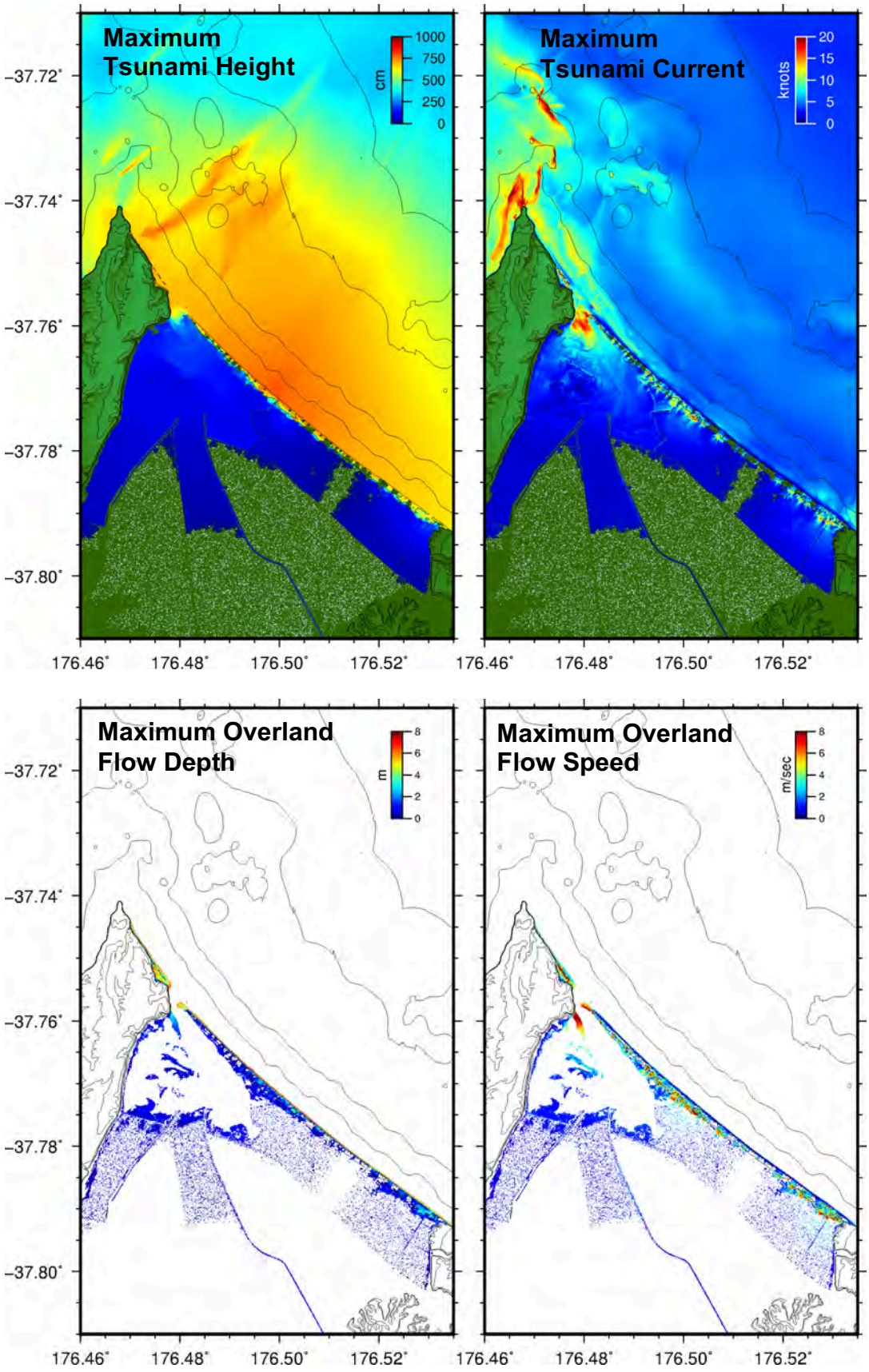

Figure 8.5 2500 year RI over MHWS topography. Land uniformly filled to +0.15 m above MHWS. Random 'noise' added to flat land areas, SD = 0.1.

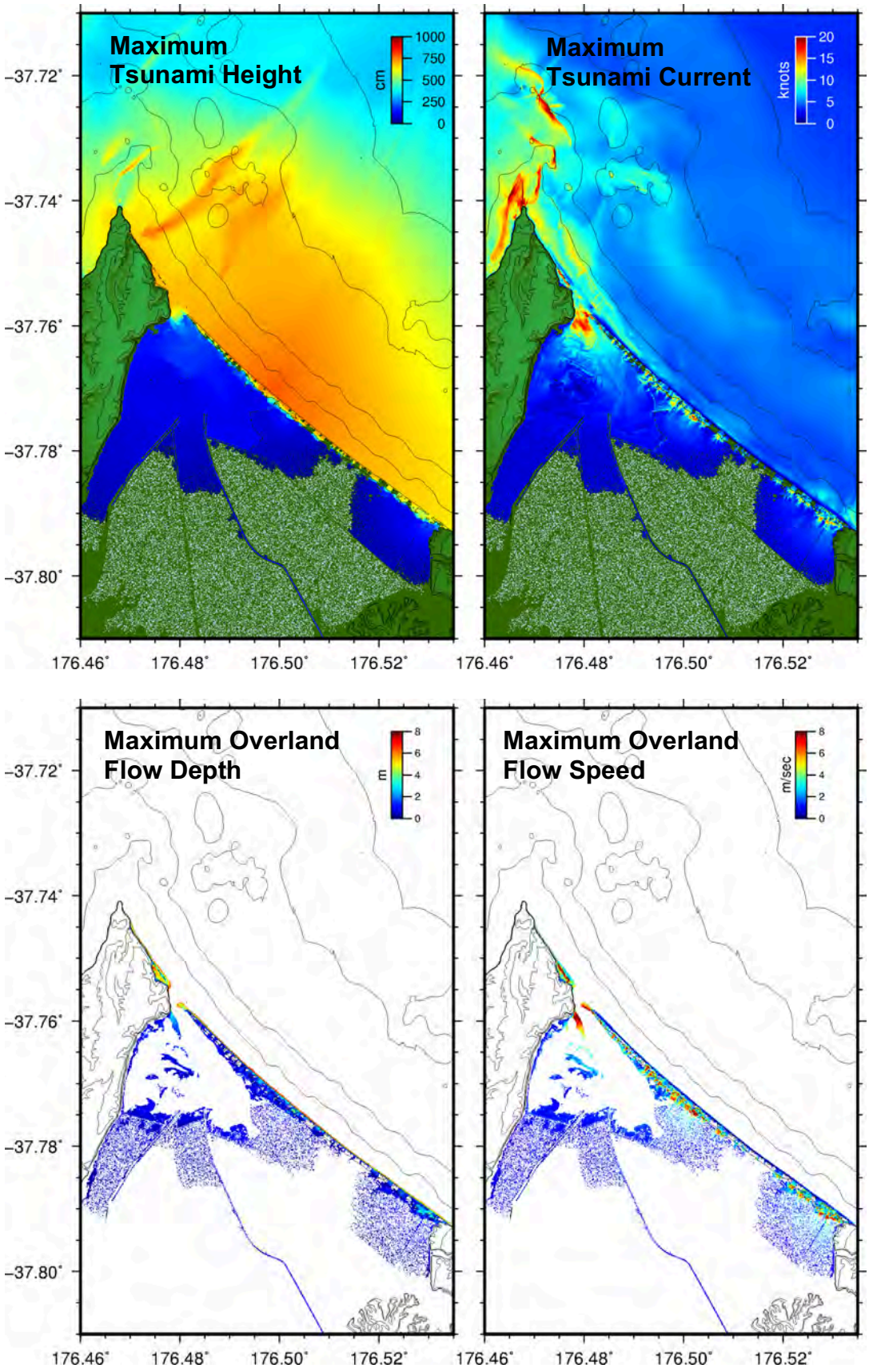

Figure 8.6 2500 year RI over MHWS topography. Land uniformly filled to +0.15 m above MHWS. Random 'noise' added to flat land areas, SD = 0.25.